THE HONG KONG POLYTECHNIC UNIVERSITY

INSTITUTE OF TEXTILES AND CLOTHING

COUPLED MECHANICAL AND LIQUID MOISTURE TRANSFER BEHAVIOUR OF TEXTILE MATERIALS

LIU Tao

A thesis submitted in partial fulfillment of the requirements for the degree of Doctor of Philosophy

Under the Supervision of

Dr. CHOI Ka Fai and Prof. LI Yi

January 2008

CERTIFICATE OF ORIGINALITY

I hereby declare that this thesis is my own work and that, to the best of my knowledge and belief, it reproduces no material previous published or written, nor material that has been accepted for the award of any other degree or diploma, except where due to acknowledgement has been made in the text.

LIU Tao

January 2008

Abstract

The mechanical properties of yarns have a considerable effect on the processing behavior and performance characteristics of yarns and fabrics. The absorbency and transportation of liquids by textile yarns are important factors in the dyeing and finishing of yams and fabrics. The wicking mechanism in a yarn is coupled with the mechanical behavior of the yarn and constituent fibers with presence of diffusion of the wicking liquid into fibers. Therefore, the mathematical modeling of mechanical behavior of yarn, liquid transport behavior of yarn and the coupled mechanism were the subjects of this research. Knowledge of mechanical and liquid transfer behavior of yarn is fundamental to examine the coupled mechanism.

A comprehensive mechanical model of yarn to predict tensile as well as torsional behavior of singles yarn was developed. On the basis of a discrete modeling principle, the yarn was treated as an assembly of discrete fibers whose shapes followed perfect helices. Migration of fibers and interfiber slippage were not investigated in this research. An energy method was employed to calculate applied external forces, and nonlinearities of tensile, bending and torsional behavior of fibrous material were considered in the calculation. Experimental validation showed that the prediction agreed well with the experimental results under limited conditions of small strain.

Many textile fibers, especially synthetic fibers, have a circular section. Fibers inside a yarn are more or less parallel to each other. Therefore, an investigation of the wicking mechanism in the gap between cylinders may provide a basic understanding of capillary rise in twisted yarn. A mathematical model to simulate the capillary rise between cylinders was developed for this purpose. Using an interfacial analysis, wicking height of the liquid at equilibrium was derived in terms of interfacial features and characteristics of the liquid. An experimental apparatus was designed and a series of experiments was conducted using this apparatus.

On the basis of the model of wicking between cylinders, a mathematical description of the capillary rise in twisted yarn was presented. Uniform packing of fibers was assumed. The governing equation of the wicking liquid was derived from a macroscopic force balance analysis of the liquid, and the wicking time was obtained in the form of the capillary rise by solving the governing equation. Then the theory was extended to investigate non-uniformly packing yarn, and swelling and change of mechanical properties of fibers after absorption were also considered. The wicking mechanism was coupled with the mechanical behavior of yarn and fiber in a manner that absorption of the wicking liquid of fibers during wicking caused the fibers to swell and change their mechanical properties; on the other hand, change of mechanical properties and geometric features of fibers altered pore structures between fibers and capillary pathways, thus affected the wicking process. A mechanical model of yarn and a model of wicking in yarn were combined to study the coupled mechanism, and a basic understanding of the coupled mechanism was developed.

Publications arising from the thesis

Refereed journals:

1. **Liu, T.**, Choi, K. F., Capillary rise between cylinders, ***Surface and Interface Analysis***, 40, 368-370 (2008)

2. **Liu, T.**, Choi, K. F. and Li, Y., Wicking in twisted yarns, ***Journal of Colloid and Interface Science***, 318, 134-139 (2008)

3. **Liu, T.**, Choi, K. F. and Li, Y., Mechanical modeling of singles yarn, ***Textile Research Journal***, 77(3), 123-130 (2007)

4. **Liu, T.**, Choi, K. F. and Li, Y., Capillary rise between cylinders, ***J. Phys. D: Appl. Phys.***, 40, 5006-5012 (2007)

5. **Liu, T.**, Choi, K. F. and Li, Y., Coupled mechanical and liquid transfer behavior of textile yarns, ***Polymer***, (submitted)

Conference publications:

1. **Liu, T.**, Choi, K. F. and Li, Y., Mechanical behavior of wool yarns, International conference on textile and clothing, Lahore, Pakistan, 2006

2. **Liu, T.**, Choi, K. F. and Li, Y., Wicking between cylinders, 12th European conference on application of surface and interface analysis, Brussels, Belgium, 2007

Acknowledgements

First and foremost, I would like to express my sincere thanks to my chief supervisor, Dr. Choi Ka-fai, for giving me the opportunity to work on this interesting and rewarding project. I was fortune to have been a student of Dr. Choi. He is such a wonderful supervisor, and always gave me valuable advices, patient guidance and continuous encouragement throughout the years of work. Dr. Choi's help was not limited to my research field, but also extended to my living in this metropolitan city. I still remember the warm and kind helps given by Dr. Choi when I first came to HK.

I am also very grateful to my co-supervisor, Professor LI Yi, for his critical comments and helpful discussion. His enthusiasm in scientific pursuit and indefatigable dedication to research study always inspired me.

My special thanks are due to Ms Gail Taylor, for her proofreading of the whole thesis. Her comments on the writing of this thesis are highly appreciated.

Gratitude and thanks are also extended to Ms M. N. Sun and K. O. Choi (technical staff in the testing laboratory, ITC) for their assistance in the experimental work.

Many individuals and colleagues should be thanked for the completion of this thesis. They always stood by me with numerous words of encouragement and support. They are: Dr. YU Jianming, Dr. GAO Xiaoping, Dr. SHAO Sijie, Ms

SONG Qingwen, Ms LV Ru, Mr. YANG An, Ms CHAN Man Hin Eve, Mr. SAKAR Manas, Ms LAU Mei Mei, Ms WONG Carrie, Ms YOU Sophie.

The financial support from the Hong Kong Polytechnic University is gratefully acknowledged.

Finally, I wish to thank my parents and brother for their never-ending love and support.

Table of contents

List of figures

List of tables

Chapter 1. Introduction

1.1 General introduction

There is a wide range of structures to be considered in textile research, including fiber structures, yarn structures, fabrics, and finished goods or garments. Among them yarns form an important intermediate stage in many methods of textile production. They may be defined as long, fine structures capable of being assembled or interlaced into textile products as woven and knitted fabrics, braids, ropes and cords. Despite the growing use of several forms of nonwoven fabrics directly assembled from fibers, fabrics composed of interlaced yarns will continue to be important for many years. The study of yarn is thus a necessary part of textile technology, and therefore this project focuses mainly on textile yarns.

The mechanical properties of yarns have a considerable effect on the processing behavior and performance characteristics of yarns and fabrics. They directly influence the strength of the yarns, their knittability, twist distribution, yarn-twist instability and the tendency of yarns to snarl, all of which are important to the final appearance and aesthetics of fabric. The strength of the yarn is greatly determined by the tensile behavior of the fibers and yarn geometry, and it is one of the important factors that should be considered in the processing of fabrics. When we move from one-dimensional yarn state into the two-dimensional fabric state, we must bend or coil the yarn to fit the interlaced structure of a woven material or a knitted fabric. Then the bending and torsional behaviors of the yarn become a matter of considerable importance, and study on such behaviors is of great values. With the speedy development of computer technology CAD/CAM techniques are widely used in the textile industry today. On the basis of yarn modeling the configuration and deformation of yarn/fabric can be dynamically visualized, and this can offers illustrious reference to textile design.

There have also been important technological developments such as the introduction of new yarn types, the use of new spinning methods, and the availability of new fibers for incorporation in yarns. All these innovations make it important to have a sound understanding of the basic features of yarn structure and properties.

Liquid flow is one of the most frequently observed phenomena in the processing and use of fibrous materials. Water or other liquid may be transported through fibrous structures driven by external pressure or capillary force. Capillary flow, also termed wicking, was one of the subjects of this research. Study of capillary flow in textile media is of great interest for two main reasons. Firstly, it allows a better understanding of liquid/fiber contact in order to characterize any liquid flow of spin finishes, dyeing, or coating of either fabrics or yarns. Secondly, it enables the characterization of textile structures, their heterogeneity, and more precisely their porosity resulting from the capillaries formed by the inter-filament spaces in which the liquid flows.

Many textile fibers, especially natural fibers, absorb the wicking liquid during wicking due to their internal chemical compositions and structural features. The property of absorption is a valuable feature of clothing materials. Apart from its direct utility in keeping the skin dry, the absorption of water causes the fabric to act as a heat reservoir, protecting the body from sudden changes of external conditions. The absorption changes the properties of fibers. It causes swelling to occur which alters the geometry, dimension and mechanical properties of fibers. For example, wool fibers and cotton fibers can increase their cross section area by 30% from dry to wet. The modulus and tensile strength of viscose fibers can change by 50% from dry to wet. The swelling of fibers also greatly changes the internal structure of yarn, such as shape and dimension of pores which directly influence the liquid flow process through the yarn. In this respect, the study of the coupled mechanism is of great practical importance.

With these considerations, the research of this project focus mainly on three parts, i.e. mechanical properties of textile yarns, liquid flow through parallel cylinders and twisted yarns, and coupled mechanical and liquid transfer behavior of textile yarns. Knowledge of the first two parts is fundamental and necessary to investigate the coupled mechanism. In order to derive a good mathematical description of the coupled mechanism, highly accurate outputs from mechanical modeling and liquid transport simulation of textile yarns are required.

1.2 Research background

Study on mechanical properties of textile yarns can be dated back to 1907 (Gegauff, 1907). In Gegauff's model, a continuous filament yarn was assumed to be composed of a series of coaxial helices, and all such helices had a pitch equal to the reciprocal of the twist of the yarn. Gegauff's basic model forms a foundation of the subsequent modeling of yarn structure. In the middle of the twentieth century, based on Gegauff's model many research have been carried out to study the tensile properties (Hearle, 1959, 1960, 1969; Platt, 1950a; Platt *et al.*, 1958) as well as the bending and torsional behaviors of continuous filament yarn using the force method (Leaf, 1995; Postle *et al.*, 1964). In these models, good agreement was found between the prediction and the experimental investigation.

The force method is a traditional and commonly used method to study yarn mechanics. Using the force method, we can obtain a whole force-deformation relationship of yarn, stress distribution within the yarn or fiber, interaction between fibers, and so on, from the characteristics of fibers. However, because stress is a tensor, it is very complex to implement the stress analysis when all stress components are considered. Furthermore, if large deformation and deviation of fiber material from Hooke's law are considered, the analysis becomes more complicated.

Besides the force method, the finite element method (FEM) (Van Luijk, 1981) and the energy method (Treloar and Riding, 1963) have also been employed to examine yarn mechanics. The FEM has been confirmed to be successful in solving engineering problems. However, the derivation of final FE equations of fibrous elements is very complicated due to the complexity of the deformation modes of fibrous elements. On the other hand, the assumption that the yarn is a continuum medium, that makes the discretization of yarn possible, is dubious because of the non-uniformity, discontinuity and high porosity of the fibrous assemblies. The energy method was first proposed by Treloar and Riding to study the tensile properties of singles yarn (Treloar and Riding, 1963). The popularity of the energy method in recent years is possibly due to the fact that the energy is a scalar and the calculation of the energy is quite simple. Besides, the energy method is logically self-consistent, and therefore the effect of any stresses needed to maintain a specified state of strain can be included.

The most important phenomenon in fabric wicking is the motion of liquid in void spaces between fibers in a yarn (Hollies *et al.*, 1956). The larger pores between yarns are not as important in long-range motion of liquid. Thus, a study of wicking in yarns should provide a way to understand the role of geometric and material parameters in fabric wicking. One of the aims of this study was to construct a basic understanding of the mechanism of liquid flow through fiber bundles and textile yarns.

Extensive publications on liquid flow through porous medium as well as fibrous materials have been reported. The models of wicking through fibrous assemblies can always be grouped into two categories. The first one is to model the fibrous assembly as a bundle of parallel capillary tubes through which the fluid flow follows the Lucas-Washburn equation (Lucas, 1918; Washburn, 1921). The second one is to treat the fibrous assembly as porous media through which the liquid flow is characterized by Darcy’s law (Chatterjee, 1985; Kissa, 1996; Rahli *et al.*, 1997). However, the equivalent capillary radius and the equivalent contact angle needed in the LW equation are difficult to quantify. If the fibrous assemblies are considered as porous media, then the characteristic parameters such as permeability, porosity, must also be obtained from experiments. When compared with typical porous media, fibrous assemblies, for example continuous filament yarns, have a regular and ordered structure. Therefore, a mathematical wicking model based on the geometric parameters of yarns as well as the fluid properties with less fitting parameters is possible.

Due to complex structures and molecular compositions, the mechanical and transport behavior of textile assemblies are very complicated and traditionally studied separately. In practice, however, they are highly coupled, especially with the presence of diffusion of liquid into fibers. The changes in fiber geometric dimensions and mechanical properties after a fiber has absorbed the wicking liquid will significantly change the structural features of the textile yarns such as pore distributions and capillary pathways, which will in turn influence the liquid transport processes in the yarns. Therefore, it was necessary to study the liquid transport processes together with the mechanical deformation of the yarn and fibers simultaneously. Neglect of either effect of one process on the other would have led to inaccurate simulation of the entire coupled system. However, such a model to investigate the coupled mechanism is still not available in the literatures.

1.3 Research objectives

Extensive research has been reported on yarn mechanics as well as experimental investigation of capillary flow through textile assemblies. However, there are still several gaps in the research:

- Although much work has been carried out on yarn modeling using the energy method, results of the prediction from those models are far from satisfactory. A comprehensive yarn model which can give quite accurate predictions of mechanical responses of yarn to external forces is still lacking. When a yarn is subject to external forces, how fibers move, how the jammed region develop, and to what extent fiber tension, fiber bending and fiber torsion contribute to external force are unclear.
- Most previous investigations on the wicking process in textile assemblies were based on a capillary tube model or Darcy's law. For either method, at least two parameters were unknown, and they were always determined by fitting the experimental data. A model to predict the final capillary rise of a liquid in a yarn is not available.
- To date, the mechanical and wicking behaviors of textile yarns have always been examined separately. However, in practice they are closely coupled.

Publications on the analysis of the coupled system are quite limited. Interaction between fibers and the wicking fluid; influences of twist, movement of fibers and swelling of fibers on the coupled system are still not clear.

In order to fill these gaps, this study aimed:

- To establish a mathematical model to accurately predict the mechanical responses, i.e., tensile as well as torsional behavior of yarns, and validate the mathematical model by conducting a series of experiments. The whole stress-strain curve of the fiber material was taken into account in the calculation. Nonlinearities of tensile, bending and torsional behavior of fiber material, which were always treated using linear approximation by other researchers, were considered in the model. The contributions of fiber tension, fiber torsion as well as fiber bending to the external force were calculated and compared. The torsional buckling was investigated and the buckling area was identified.
- To develop a sound scientific understanding of the mechanism of liquid transport through parallel cylinders as well as twisted yarns. As fibers inside a yarn are more or less parallel to each other, it is desirable to study wicking in the gap between cylinders. This may provide a better understanding of the mechanism of the interaction between fibers and liquid. On the basis of the investigation on capillary rise between cylinders, the wicking flow of a liquid

through fiber bundles and twist yarns was numerically simulated. The model was based on a macroscopic force balance analysis.

- To develop a basic mathematical model to describe the coupled mechanism between mechanical properties and wicking behavior of yarns. The mechanical model of the yarn and the wicking model were incorporated to study the coupled mechanism. The final capillary rise was predicted using the model, and a series of experiments was conducted to verify the model. Factors influencing the coupled system, such as twist level of yarn, were examined.

1.4 Significance of research

Mechanical properties of yarns greatly affect the processing behavior and performance characteristics of yarns and fabrics. They directly influence the performance of yarns in spinning, knitting, weaving, etc. The flexibility, wearing durability and comfort of fabrics also rely to some extent on the mechanical behavior of constituent yarns. Mechanical analysis of yarns provides a better understanding of yarn deformation and failure mechanism.

Many researchers have revealed that it is the wicking flow inside yarns rather than between yarns, which contributes most to the wicking flow of a liquid through fabrics. A better understanding of wicking behavior of a fluid through yarns can provide a first approximation of the wicking properties of the fluid through resultant fabrics.

Most textile fibers used in clothing are hygroscopic and absorb liquid/moisture water during wear. The absorption keeps the skin dry and sustains a comfortable microclimate between the skin and the clothing layer. Therefore, research on how fabric/yarn behaves after absorbing water, and how the changes of mechanical properties affect the liquid flow through textile materials has both theoretical and practical value. Such a study will enrich the knowledge of textile mechanics, liquid flow through textile materials and the coupled system.

Chapter 2. Literature review

2.1 Introduction

As stated in Chapter 1, this research focused mainly on three topics: mechanical properties of textile yarns, liquid flow through yarns and the coupled mechanism. Therefore, literature on the structural mechanics of textile yarns and liquid flow through fibrous assemblies were surveyed respectively. The three commonly used methods to investigate yarn mechanics, i.e., the force method, the finite element method (FEM) as well as the energy method were discussed. Then the research on capillary flow through tube, porous media and fibrous assemblies were reviewed.

2.2 Structural mechanics of textile yarns

2.2.1 Introduction

There are many publications on the subject of yarn mechanics. Generally, the method used in the study of yarn mechanics can be classified into three categories: force method, finite element method (FEM) and energy method. They are discussed respectively.

2.2.2 Force method

Yarns may be made directly from man-made continuous filaments or they may be spun from short staple fibers. This leads to two categories of singles yarn, namely, continuous-filament yarn and staple fiber yarn. Continuous filament yarns are the simplest in structure, but they are now subjected to many modifying processes designed to change their bulk, texture, extensibility and other properties. Spun yarns have an additional complexity of discontinuities at fiber ends which may induce partial slippage of fibers. If two or more singles yarns are twisted together, we can get ply yarns which have a much more complicated structure. Ply yarns are more commonly used because of their twist stability. As the top textile structure in terms of complexity, fabric can be made from textile yarns by many methods, including weaving, knitting, etc. Studies on these fibrous structures using force method have been critically reviewed (Pan and Brookstein, 2002; Treloar, 1977), and they are introduced in a hierarchical order.

2.2.2.1 Continuous filament yarns

Extensive work has been conducted to study continuous filament yarns using the force method. Research on mechanical properties of textile yarns can be dated back to 100 years ago. In 1907, Gegauff (Gegauff, 1907) set down the basic mathematics of a yarn model. In his model, yarn was assumed to be composed of a series of coaxial helices, and all such helices had a pitch equal to the reciprocal of the twist of the yarn. Only forces acting parallel to the fiber axes were considered, and any change in yarn diameter during extension was neglected. These assumptions can be applied to continuous filament yarns directly. Gegauff’s model was elaborated by Gurney (Gurney, 1925) in a study of the distribution of stresses in cotton yarns in which inter-fiber friction was very high and single fiber was considered to exhibit linear stress-strain behavior.

In order to relate yarn strength to the geometrical parameters of yarn as well as constituent fibers, many efforts were made in Gregory's series of papers on cotton yarn (Gregory, 1950a, 1950b, 1950c, 1953a, 1953b). Unfortunately, no detailed yarn structure modeling is given. The theory is inadequate in that it cannot predict the whole stress-strain curve of yarn.

To fill this gap Platt conducted a pioneering work on yarn mechanics in his series of papers (Platt, 1950a, 1950b; Platt *et al.*, 1958, 1959). His definition of yarn geometry was the foundation of the following research on yarn mechanics. In his yarn model, the following assumptions were made:

1. The yarn is uniform along its length, and its cross-sectional outline is circular.
2. All fibers within a yarn possess the same properties and are circular in cross section.
3. The centerline of each fiber lies in a perfect helix, with the center of the helix located at the center of the yarn cross section.
4. The fibers fall into a rotationally symmetric array in cross-sectional view.
5. The diameter of the yarn is large compared with the diameter of the fiber.

On the basis of Platt's work, the mechanics of twisted continuous-filament yarns was systematically analyzed in the middle of the twentieth century (Hearle, 1958, 1959, 1960; Hearle *et al.*, 1961; Hearle *et al.*, 1969; Riding, 1959; Sullivan, 1942). Among those studies Hearle's work (Hearle *et al.*, 1969) is significant. He obtained stresses applied on a yarn using a unit element analysis with consideration of yarn contraction in diameter and contribution of transverse stress. Considering the yarn as a continuum solid, yarn stress was obtained using structural mechanics analysis. Recently, a model based on composite theory was developed to study the mechanical properties of high-performance fiber yarns (Rao and Farris, 2000).

In addition to the tensile behavior of yarn, bending and torsional properties of yarn are also important. They greatly influence the hand feel and appearance of fabric. As a consequence, research on the bending and torsional behavior of yarn has elicited much interests. Yarn bending and torsional properties have been studied and characterized according to flexural rigidity and torsional rigidity (Leaf, 1995). The hysteresis loops for multifilament yarn showed somewhat different shape from the corresponding loops for the monofilament yarn, which indicated the importance of friction in the former case.

Torque in a twisted yarn consists of three components due to fiber tension, fiber bending and fiber torsion. Expressions for yarn torque due to fiber torsion and fiber bending were derived by Platt *et al* (Platt *et al.*, 1958) where helical yarn geometry and linear elasticity were assumed. Based on Platt's theory, Postle *et al*. (Postle *et al.*, 1964) and Dhingra *et al*. (Dhingra and Postle, 1974a, 1974b) derived a general equation of yarn torque arising from fiber tension. The yarn was considered as a solid continuous homogeneous medium rather than a group of discrete fibers. However, Postle's theory is limited in the sense that it does not consider lateral compression between fibers, and the radial contraction of fibers is neglected.

2.2.2.2 Staple fiber yarns

It is more difficult to model staple fiber yarns due to discontinuities at fiber ends and the fact that fibers will partly slip. Twist and fiber migration in spun yarns are not merely secondary factors as they are in continuous filament yarns. They are the only reason why an assembly of short fibers holds together as a yarn. Taking into account fiber migration and friction between fibers, the tensile behavior of staple fiber yarns has been investigated (Cybulska and Goswami, 2001; Hearle, 1965; Hearle and Bose, 1965; Hearle *et al.*, 1969; Hearle and Gupta, 1965; Hearle *et al.*, 1965; Hearle *et al.*, 1972) and reviewed by Ghosh *et al* (Ghosh *et al.*, 2005). Most of the work was based on a discrete fiber principle in which the yarn was treated as an assembly of a large quantity of discrete fibers. Fiber material was assumed to obey the Hooke's law. Nonlinearity of fiber material was not considered.

An attempt to develop a general constitutive theory governing the mechanical behavior of twisted short fiber structures has been reported by Pan *et al* (Pan, 1992, 1993; Pan and Brookstein, 2002). The yarn was treated as a transversely isotropic material. Based on the similarity of the stress transfer mechanism between two structures, a staple yarn was considered analogous to a short fiber composite; a fiber was viewed as embedded in a matrix made of neighboring fibers. Hence the composite material theory (Christensen, 1979) was adopted to derive the tensile stress distribution as well as the transverse stress distribution of individual filaments. The author concluded that the tensile and transverse stresses on each individual fiber were by no means constant along its length which were also qualitatively described by Hearle *et al* (Hearle *et al.*, 1969). Unfortunately, the fiber matrix theory based on composite material knowledge which is valid for a straight fiber bundle is questionable for twisted yarn. Furthermore, inter-fiber slippage which may occur in low twist yarn was neglected

Taking account of inter-fiber slippage a theoretical model to predict the entire load-extension response of low twist staple yarns has been proposed (Shao, 2002; Shao *et al.*, 2005a, 2005b). The model was also used to study the response of such yarns subjected to cyclic tensile loading. A stress analysis was performed on a fiber in a staple yarn subjected to tensile loading based on short-fiber composite theory. The model gave a reasonably accurate prediction of the stress-strain curve of the yarn. In the model, the author indirectly presumed that the deformation of the fiber obeyed Hooke's law. However, this may not be true when the yarn is subject to high extension. In such a case, tensile stress in a typical fiber may exceed the proportional limit, and fiber may deform nonlinearly.

Besides tensile properties, bending and torsional characteristics of yarn are also important, and study on bending and torsional behaviors of yarn have both theoretical and practical value. The bending rigidity of wool worsted yarn has been estimated by Ly and Denby (Ly and Denby, 1984). The first approximation to yarn bending rigidity was based on the bending rigidity of a single fiber in yarn. The approximation was then corrected by four factors due to fiber diameter distribution, yarn twist, fiber ellipticity and mean fiber length.

The torsional and recovery properties of single worsted yarn were studied using a torsion-balance apparatus designed to obtain the torsional hysteresis curve of the yarn under conditions of constant tension (Dhingra and Postle, 1975). A stress-analysis method was employed to derive an expression for the yarn torque resulting from the fiber tensile stress in the yarn. A hexagonal packing of fibers was assumed in the yarn cross-section. For staple fiber yarns, however, the packing of fiber is far from uniform. Fibers at different radial positions take different displacement modes which makes the equation developed above invalid.

2.2.2.3 Ply yarns

The geometry of multi-ply yarns was first examined by Treloar (Treloar, 1956, 1977). Filament path was defined through a principal plane and an osculating plane. It was assumed that the path of a filament in the ply was generated by means of a rotating vector of length r advancing at constant rate along the helical ply axis (Figure 2.1).

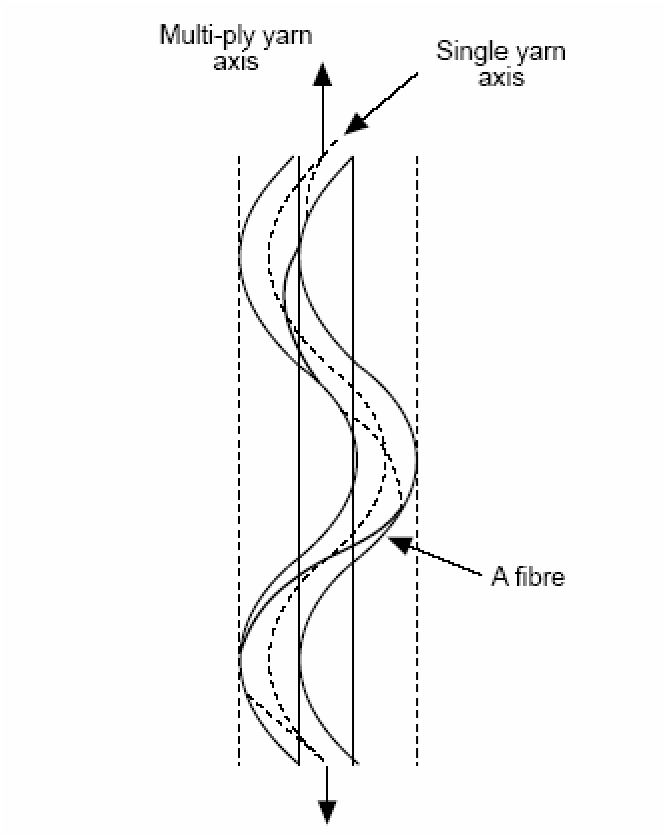

Figure 2.1 Path of a fiber in multi-ply yarn (Treloar, 1977)

The cording process was then investigated and cord retraction was modeled. A general agreement in form between the calculated and observed quantities justified the provisional acceptance of the theory as a working model for further investigation of cord properties.

Stansfield (Stansfield, 1958) proposed a self-consistent geometry of cords made from multi-filament yarns. The path of a single filament was assumed to follow an epi-helix. The vector used for defining ply twist is perpendicular to the cord axis rather than to the ply axis. On basis of the epihelical path of filament, the cord was modeled and the cord retraction formulae were derived. The formulae developed were a good fit to the experimental data of yarn retraction and the cord retraction for both simple and compound twisting.

Tao (Tao, 1994) investigated the effect of multi-ply structure on yarn bending properties. The discrete fiber approach was adopted and the geometry of fiber in the yarn followed the doubly wound helix developed by Treloar (Treloar, 1956). The first approximation of bending rigidity of multi-ply yarn was assumed to be the summation of the bending rigidity of all the constituent coaxial doubly wound helices. The interaction of fibers was ignored. However, for wool worsted yarn, four corrections were required to assure more accurate approximation. They are fiber diameter distribution, fiber length distribution, fiber cross-sectional shape and fiber path. The curvature components in the principal directions of the cross section of fiber were calculated based on Love's deviation (Love, 1944). Although the theory proposed by the author was easy to follow, it involves quite a lot of tedious formulae which make it very complicated to solve. Furthermore, the inter-fiber friction was not taken into account. Thus, the model may be used to predict the minimum bending rigidity of yarn.

2.2.2.4 Conclusion

The force method is a traditional and commonly used method to analyze yarn mechanics. By the force method we can easily obtain a whole force-deformation relationship of yarn, stress distribution within the yarn or fiber, interaction between fibers, and so on, from the characteristics of fibers. Inter-fiber slippage can be conveniently taken into account by means of force method. However, because stress is a tensor, it is very complex to implement the stress analysis when all stress components are considered. Furthermore, if large deformation and deviation of fiber material from Hooke’s law are considered, the analysis becomes more complicated.

2.2.3 Finite element method (FEM)

2.2.3.1 Introduction

The finite element method (FEM) is a prevailing numerical method in structural analysis due to its robusticity in dealing with complex structures and irregular boundary conditions. The behavior of textile yarns under tensile loading has been analyzed with the aid of finite element method (FEM), with particular emphasis on wool yarns (Djaja, 1989; Postle *et al.*, 1988; Van Luijk, 1981; Van Luijk *et al.*, 1984, 1985). The yarn was treated as an axisymmetric cylindrical continuous element and homogeneous in length. The physical region occupied by the undeformed yarn was divided into concentric annular zones or finite elements. Only tensile stress and transverse stress were considered when the yarn was stretched. All other continuum stresses due to shear were ignored although this might limit the accuracy of the model at high strain. The migrating helical paths, a V-shaped migration envelope of individual fibers were accommodated within the finite element. Both ends of fiber lay at the surface and the envelope surrounding the migrating helix decreased monotonically from the outside to the center and then increased again, finishing back at the surface of the yarn. An incremental method with Newton-Raphson iteration was used to solve the equilibrium equations (Van Luijk, 1981).

A finite element model to predict stress-strain and torque-tensile strain curves of a yarn was presented by Van Langenhove (VanLangenhove, 1997a, 1997b, 1997c). The ideal yarn was considered as an axisymmetric cylindrical continuous element and homogeneous in length, but anisotropic. The yarn was divided into concentric elements along the yarn radius direction. The displacement field was obtained as the sum of a global field and a disturbance field that arose from anisotropy and nonlinear material behavior. In order to reach a continuous function for the global displacement field, displacements in cylindrical coordinates were linearly interpolated between nodal values using the linear interpolation shape functions. The Green-Lagrange deformation tensor was then calculated from the displacement field and the constitutive equations were deduced. The nonlinear element problem was iteratively solved using the method of dynamic relaxation (Underwood, 1983).

A two-dimensional element model as well as a three-dimensional element model were developed (Munro *et al.*, 1997a, 1997b) to model aligned fiber assemblies. Difficulties with nonlinear material properties and large-scale deformations were overcome by defining the element stiffness matrix in a co-ordinate system based on the energy modes of the element deformation. The same modal decomposition approach can be applied to the three-dimensional aligned fiber assemblies.

2.2.3.2 Conclusion

It is novel to investigate yarn mechanics by FEM which has been confirmed to be successful in solving engineering problems. The systematically theory of FEM can be readily adopted with modifications. Moreover, there are many FEM software packages available which facilitate the process of analysis. However, the derivation of final FE equations of fibrous elements is very complicated due to the complexity of the deformation modes of fibrous elements. On the other hand, the assumption that the yarn is a continuum medium, that makes the discretization of yarn possible, is dubious because of the non-uniformity, discontinuity and high porosity of the fibrous assemblies.

2.2.4 Energy method

2.2.4.1 Introduction

The energy method in yarn mechanics was first proposed by Treloar and Riding (Treloar and Riding, 1963) to predict the whole load-extension curve of continuous-filament yarns. The theory was re-examined by Hearle (Hearle, 1969) and further developed to study tensile properties of staple-fiber yarns (Carnaby and Grosberg, 1976) and rotor spun yarn (Jiang *et al.*, 2002), bending of singles yarn (Choi and Tandon, 2005), torsional behavior of staple-fiber yarns (Tandon *et* *al.*, 1995a; Tandon *et al.*, 1995b), ply yarns (Choi *et al.*, 1998; Choi and Wong, 1999; Riding, 1965; Treloar, 1965) and fabric mechanics (Choi and Lo, 2003; Griesser and Taylor, 1996; Hearle *et al.*, 2001; Hearle and Shanahan, 1978; Komori and Itoh, 1991; Sagar and Potluri, 2004; Shanahan and Hearle, 1978). The main idea of the energy method is that analysis of the mechanics of the system is carried out by making use of the principle of energy. External forces applied on the textile structure are obtained by partially differentiating the total energy of the system with respect to corresponding equivalent strain.

Analysis by the energy method is much simpler than that of the direct stress analysis in that energy is a scalar quantity, permitting numerical summation, whereas stress is a tensor, which must be summed vectorially. The energy method, however, gives less information than the stress method, yielding only the total yarn tension but not the distribution of stresses through the yarn. Furthermore, the energy method is only applicable to the case of an incompressible material.

In staple fiber yarns, the packing density is not only low, but also variable. Therefore, the large and non-uniform lateral movements of fibers must be considered when the strain distribution in the yarn is estimated. The tensile behavior of staple-fiber yarns at small strain was studied using a discrete-fiber modeling principle with the consideration of lateral movement of fibers Carnaby and Grosberg (Carnaby and Grosberg, 1976). The energy method was adopted to deduce the applied tension on the yarn in which yarn extension was increased in small steps, and the force on the yarn was found from the corresponding increase in stored energy. The yarn cross section was divided into 25 zones of equal thickness and the total energy of yarn was derived from the summation of energy of fibers in each zone.

The same fundamental approach to predict the tensile behavior of singles yarn was used and extended to model yarn torsion (Tandon *et al.*, 1995a; Tandon *et al.*, 1995b). The theoretical analysis was based on a discrete-fiber-modeling principle, an energy method and a shortest-path hypothesis. The yarn torque with different pre-tension level was predicted by taking partial derivative of the total yarn energy with respect to yarn twist. However, the accuracy of the prediction was far from satisfactory. If a more accurate fiber packing density function is obtained and the full stress-strain constitution of fiber is used in the yarn energy calculation, a more accurate prediction can be expected.

The tensile properties of rotor spun yarns were modeled by Jiang *et al*. (Jiang *et al.*, 2002). The study was based on a coaxial-helix structure, taking account of the non-uniform fiber packing density. A changing-pitch system was introduced to replace the constant-pitch system treatment which turned out to be an oversight used to model rotor spun yarn, whose twist insertion was operated layer by layer. The pitch function was determined with the aid of a nonlinear regression method and a curve-fitting approach using images obtained from a tracer fiber technique.

The model was found to be successful in explaining the experimental observations.

The tensile behavior of multi-ply cords was investigated by Riding and Treloar (Riding, 1965; Treloar, 1965) based on a doubly wound helix geometry of fiber path developed by Treloar (Treloar, 1956, 1977). The theory enabled the whole stress-strain curve of the twisted yarn to be predicted from knowledge of the stress-strain curve of the filament material. The applied force were obtained in terms of the strain energy of the filaments, and of the whole assembly, with a consequent simplification of the mathematical treatment compared with theories involving the analysis of the system of internal stresses. The corresponding equations of two-ply, three-ply and seven-ply cords were obtained with experimental data to verify the theory. The results showed that the theory gave quite a good prediction. However, for high cord twists and low strains, the experimental values of cord stresses were lower than the calculated values. This may partly be attributed to the initial crimp of the singles yarn as well as the filament. A uniform fiber packing density was assumed which was invalid for bulky yarns. A non-uniform fiber packing density is more realistic in practice.

The mechanism of bending of ply yarns was discussed by Park *et al*. (Park and Oh, 2003). During bending, a coercive couple was defined as the bending hysteresis, which was the non-recovery moment that overcame friction. After geometrical development, the energy method was adopted to derive the coercive couple. The coercive couple could be estimated from structural factors such as twist angle, characteristics of constituent fibers. Good agreement was found between the theoretical and experimental data.

Recently a computer model was constructed to predict the properties of flat yarns, twisted yarns and ply-cords from single-filament data (Zimliki *et al.*, 2000a, 2000b). The modulus of the fiber assembly was obtained by taking the derivative of the average stress-strain curve from single-filament tensile tests. The distribution of elongation to break was fitted to a Gaussian curve and a relationship was derived between the filament elongation and elongation of twisted structures.

2.2.4.2 Conclusion

Analysis of yarn mechanics using the energy method is simple because energy is scalar quantity which can be summed numerically, whereas in the force method stress is a tensor, which must be summed vectorially. Besides, the energy method is logically self-consistent, and therefore the effect of any stresses needed to maintain a specified state of strain can be included. The energy method, however, gives less information than the force method, yielding only total yarn force and not the distribution of stresses through the yarn. Although the energy method cannot calculate the energy loss due to inter-fiber slippage which may lead to inaccuracy at large deformation, it was found to be successful in predicting the mechanical response of yarn at small deformation. With these considerations, the energy method was adopted in this research to analyze yarn mechanics.

2.2.5 Summary of literature survey on yarn mechanics

Extensive research has been carried out on yarn mechanics using the force method, the FEM and energy method. The traditional stress analysis method has been developed for more than one century and was proved to be successful in studying mechanics of simple structures, for example continuous filament yarns. However, analysis of complex structures using the force method becomes too complicated due to the tensor analysis of stress when all constitutive stresses must be considered if a high accuracy is required.

The FEM has been applied to examine yarn mechanics by some researchers. The existence of a great deal of FEM software makes the analysis of yarn mechanics by the FEM easy to carry out. However, the complexity of the deformation modes of fibrous elements limits the popularity of the FEM. If a 3-D structure is considered, freedom of the system will be huge and calculation of solving the FE equation will be very time-consuming.

The energy method has a much simpler form compared with the force method and the FEM. It derives the external forces acting on the yarn by the energy variation of the whole yarn, which is obtained by summation of contributions of all individual fibers. The energy method has been employed by many researchers to analyze continuous-filament yarns as well as staple-fiber yarns. However, most of the predictions, within the author's knowledge, are unsatisfactory. A comprehensive mechanical model of yarns which can give a reasonably accurate prediction of mechanical response of yarns is still unavailable.

2.3 Liquid flow through fibrous assemblies

2.3.1 Introduction

Liquid flow is one of the most frequently observed phenomena in the processing and use of fibrous materials. Among the liquid flow modes driven by different forces, capillary flow which is driven only by capillary force has drawn much attention. Owing to its simple form, the capillary tube flow model has been broadly used to simulate capillary flow through fibrous assemblies. As an alternative, fibrous structures are also always treated as porous media due to their high porosity. Therefore, research on capillary flow through a capillary tube and porous media were surveyed first. This is followed by a literature survey on capillary flow through fibrous assemblies.

2.3.2 Capillary flow through capillary tube and porous media

A liquid moves into a capillary tube when it is subject to capillary pressure, i.e., the differential pressure across the liquid-air interface due to curvature of meniscus in the narrow confines of the capillary. The magnitude of the capillary pressure is commonly given by the Laplace equation (Adamson, 1967):Equation Chapter 2 Section 1

$$p = \frac{2\gamma \cos\theta}{r_c} \tag{2.1}$$

where r_c is capillary radius, γ is surface tension of the advancing liquid and θ is the contact angle at the liquid-solid-air interface. The dynamics of capillary flow originated from the pioneering work of Washburn (Washburn, 1921) and Lucas (Lucas, 1918). The distance penetrated by a liquid flowing under capillary pressure alone into a horizontal capillary or one with small internal surface was found to be proportional to the square root of time. If a porous body behaved as an assembly of very small cylindrical capillaries, the volume which penetrated into the porous media was also found proportional to the square root of time. Experiments with mercury, water and other liquids verified the theoretical deduction. Washburn's work has laid a foundation for the investigation of liquid transport in textile assemblies driven by capillary pressure only. However, the LW equation has many limitations. Firstly, it only investigates wicking flow in horizontal tubes or the case where gravity of penetrating liquid is negligible. This is apparently limited in practice. Secondly, inertia of the liquid, which may be important at the beginning of the flow, is not considered. Thirdly, the contact angle used in LW equation is a static advancing contact angle, while the dynamic advancing contact angle may change during the kinetic process. Finally, it is difficult to separately estimate the influences of capillary radius and contact angle on the liquid flow. These discrepancies were partly overcome by many researchers (Hamraoui and Nylander, 2002; Ichikawa and Satoda, 1994; Joos *et al.*, 1990; Levine *et al.*, 1980; Reed and Wilson, 1993; Siebold *et al.*, 2000; Stange *et al.*, 2003; van Mourik *et al.*, 2005; Zhmud *et al.*, 2000).

In practice, intercapillaries in pore structure are neither round nor uniform along the fiber length. Therefore, capillary flow in irregular channels has attracted considerable interest, and extensive research has been carried out to study the wicking in a generalized channel (Xiao *et al.*, 2006), nesting cylinders (Brady *et al.*, 2003), capillaries with curved sides (Lago and Araujo, 2003), interior corner (Weislogel and Lichter, 1998), cylindrical containers of arbitrary cross-section (deLazzer *et al.*, 1996), non-uniform cross-sectional capillaries (Erickson *et al.*, 2002; Staples and Shaffer, 2002; Young, 2004a), angular capillary tubes (Bico and Quere, 2002), square capillary tubes (Dong and Chatzis, 1995; Ichikawa *et al.*, 2004; Kim and Whitesides, 1997), triangular tubes (Mason and Morrow, 1991) and some other noncircular tubes (Patzek and Silin, 2001; Turian and Kessler, 2000).

Understanding the kinetics of capillary penetration of liquids into porous media is essential for their characterization as well as for the development of imibibition processes. However, the structure of most real porous media is extremely complex; therefore detailed modeling of capillary penetration into them is yet unrealistic. The simplest possible approach to model penetration into porous medium is to consider it in terms of an equivalent, cylindrical capillary or an assembly of parallel capillary tubes. With such an idealized tube structure, the Hagen Poiseuille law for laminar flow through pipes can be employed. The law states that the volumetric flow rate is proportional to the pressure drop gradient along the tube (Hagen, 1839; Poiseuille, 1840):

$$q = \left(\frac{r_c^{\ 2}}{8\eta} \right) \frac{\Delta p}{L} \tag{2.2}$$

where q is volume flux, r_c is equivalent capillary radius, η is fluid viscosity, L is wicking length, and ΔP is net driving pressure. At the early stage of wicking where L is small compared to L_{eq}, the gravity of wicking fluid is negligible and the following approximation can be used which is commonly known as the Washburn equation (Washburn, 1921):

$$L = \sqrt{\frac{r_c \gamma \cos\theta}{2\eta}} t^{1/2} = k_0 t^{1/2} \tag{2.3}$$

where θ is contact angle, t time and k_0 constant. This proportionality has been confirmed experimentally in the movement of liquid front during liquid imbibition into wood pulp fibers (Aberson, 1970), building materials (Karoglou *et al.*, 2005), filter paper (Hyvaluoma *et al.*, 2006; Marmur and Cohen, 1997), carton liquid packaging (Lin and Jorge, 2005) and paper chromatography (Ackerman and Cassidy, 1954).

Another popular approach to model wicking in porous media is to employ Darcy's law (Chatterjee, 1985; Kissa, 1996; Rahli *et al.*, 1997) which is applicable to a homogeneous porous medium. The one-dimensional Darcy's law equation can be expressed as:

$$u = -\frac{\kappa}{\mu}\frac{dP}{dx} \tag{2.4}$$

where u is superficial velocity, κ is permeability, μ is viscosity , dP/dx is fluid pressure gradient and x is length in the streamwise direction. The empirical Carman-Kozeny equation (Carman, 1937; Kozeny, 1927) is often employed to predict permeability, although it is used only for uniform packing of fibers (Griffin *et al.*, 1995). The Carman-Kozeny equation is given by:

$$\kappa = \frac{{D_f}^2}{16K_0}\frac{\varepsilon^2}{(1-\varepsilon)^2} \tag{2.5}$$

where D_f is average fiber diameter, K_0 is the Kozeny constant and ε is porosity. Although the Carman-Kozeny equation is usually applied to predict permeability, discrepancies are often reported. The Kozeny constant for a specific fibrous structure, which has to be determined experimentally, is always inconsistent for different authors.

Besides the two approaches discussed above, there are also many other pore space models for transport phenomena in porous media, such as discrete particle models (Bear, 1972; Gauvin and Katta, 1973; Masliyah and Epstein, 1970), continuum models (Bear, 1972; Scheidegger, 1974), statistical dynamics (Liao and Scheideg.Ae, 1970).

2.3.3 Capillary flow through fibrous assemblies

Capillary phenomena in fibrous media are of great importance in wetting and wicking in textiles. In textiles, especially woven textiles, the fibers are more or less parallel inside a yarn, and most synthetic fibers are close to cylindrical in shape. Therefore, a study on capillary rise between cylinders may lead to a better understanding of the behavior of liquids in textile materials. Although extensive research has been reported in this area (Lukas and Chaloupek, 2003; Lukas *et al.*, 2006; Princen, 1968; Princen, 1969, 1970), most of those studies only considered cylinders of equal size, and the packing of cylinders was assumed to be uniform and regular. Few experimental data were reported.

As discussed by Hollies *et al*. (Hollies *et al.*, 1956; Hollies *et al.*, 1957), during wicking of a liquid in fabrics the constitute yarns are responsible for the main portion of the wicking action. Therefore, considerable research has been conducted to study the wicking behavior in textile yarns. Similar to liquid transport in porous media, most models to simulate the capillary flow in yarns can be classified into two main categories: one is to treat the yarn as an equivalent capillary tube in which the flow can be characterized by the LW equation, and the other is to consider the yarn as a homogenous porous media in which the flow can be described by Darcy's law. With modifications to the LW equation, models of the first category were successfully applied to study Nylon yarns (Hollies *et al.*, 1956; Hollies *et al.*, 1957; Minor *et al.*, 1959; Nyoni and Brook, 2006), cotton and viscose yarns (Hamdaoui *et al.*, 2007), PET yarns (Perwuelz *et al.*, 2001; Perwuelz *et al.*, 2000) and carbon fiber bundles (Bayramli and Powell, 1991). However, the equivalent capillary radius and the equivalent contact angle in the LW equation are difficult to quantify, and they are always derived experimentally. Although most models of the second category are used to study axial impregnation (Amico and Lekakou, 2000, 2002a, 2002b; Deng *et al.*, 2003), they can be easily extended to investigate transverse flow normal to the axis of yarn (Bayramli and Powell, 1990; Pillai and Advani, 1996; Young, 2004b). However, characteristic parameters of pore structure, such as permeability, porosity, are also difficult to quantify, and they are always obtained by experiments. Besides these two categories, there are also some other available models to analyze liquid wetting in fibrous assemblies, such as the Ising model (Lukas and Pan, 2003; Lukas *et al.*, 2004; Zhong *et al.*, 2001, 2002; Zhong and Xing, 2004).

There are several methods to measure wicking in yarn. The first was based on visual observations of dye-liquid penetration (Ansari and Haghighat, 1995; Hollies *et al.*, 1956; Minor *et al.*, 1959). The second technique is to set liquid sensitive sensors along yarn and measure the electrical capacitance/resistance (Hollies *et al.*, 1957; Kamath *et al.*, 1994). The third method is to measure weight variation with a Wilhemy balance (Hsieh and Yu, 1992; Hsieh *et al.*, 1992; Pezron *et al.*, 1995).

The research on wetting and wicking behaviors in fabric were reviewed by Kissa and Patnaik *et al*. (Kissa, 1996; Patnaik *et al.*, 2006). On the basis of different wicking processes, the wicking of a liquid into fabric could be divided into four categories:

- Immersion. When the fabric was completely immersed into a liquid, this kind of wicking occurred. The liquid entered the fabric from all directions.
- Transplanar wicking. The transport of a liquid in a fabric perpendicular to the plane of the fabric.
- Longitudinal wicking. The transport of a liquid in a fabric plane was termed "longitudinal wicking".
- Wicking from a limited reservoir. This kind of wicking was epitomized by the spreading of a liquid droplet into a fabric.

Of all the research on these four wicking patterns, longitudinal wicking has been the subject of numerous studies (Amico and Lekakou, 2000; Hamdaoui *et al.*, 2006; Hsieh, 1995; Pezron *et al.*, 1995). The distance covered by a liquid flowing under capillary pressure is described either by a modified LW equation (Hamdaoui *et al.*, 2006; Hsieh, 1995; Pezron *et al.*, 1995) or by Darcy's law (Amico and Lekakou, 2000). If Darcy's law is used to describe liquid transport in fibrous assemblies for the wide range of conditions associated with what is traditionally referred to as wetting and wicking, then capillary pressure and permeability values must be known for conditions ranging from a textile structure with no liquid in it to a textile structure where all void spaces are filled with liquid. Although many attempts have been made to characterize the pore spaces in fabric (Gooijer *et al.*, 2003a, 2003b; Neckar and Ibrahim, 2003; Rebenfeld and Miller, 1995), it is still unrealistic to model the detailed pore structure due to its extreme complexity. Therefore examining the parameters experimentally seems to be a more practical method. The capillary pressure and permeability were examined experimentally by Ghali *et al*. (Ghali *et al.*, 1994). Capillary pressure head was measured as a function of saturation, which is commonly used to define the liquid content of a porous medium, using the column test (Ghali, 1992). Permeability was measured as a function of saturation using the siphon test (Nguyen and Durso, 1983). Cotton and polypropylene fabrics were the test materials. The former was considered to be hydrophilic material (small contact angle), whereas the latter was always considered hydrophobic (large contact angle). The results showed that the capillary pressure decreased while the permeability increased with the increasing of saturation for both fabrics. At the same time, the cotton fabric had a higher capillary pressure than the polypropylene at a given saturation.

When a droplet of wetting liquid is deposited on a yarn, it spontaneously wicks into the yarn due to the capillary forces associated with the given structures and geometry of the void spaces between the filaments. The kinetics of wicking of liquid droplets into yarns was studied using a computer imaging system by Dr. Neimark's group (Chen *et al.*, 2001).

2.3.4 Summary

Extensive publications on liquid flow through porous medium as well as fibrous materials are available. The fibrous assemblies are always treated either as a bundle of parallel capillary tubes through which the fluid flow follows the Lucas-Washburn equation (Lucas, 1918; Washburn, 1921), or as porous media through which the liquid flow is characterized by Darcy's law (Chatterjee, 1985; Kissa, 1996; Rahli *et al.*, 1997). However, the effective capillary radius and the effective contact angle needed in the LW equation are difficult to quantify. They are always approximated by experimental values, namely empirical. If the fibrous assemblies are considered as porous media, then the characteristic parameters such as permeability, porosity, must also be obtained from experiments. When compared with typical porous media, fibrous assemblies, for example continuous filament yarns, have a regular and ordered structure. Therefore, a mathematical wicking model based on the geometric parameters of yarns as well as the fluid properties is expected to give a more accurate predictive result of the wicking process of yarns.

This extensive literature review shows that although broad research has been carried out on wicking in fibrous structures, most studies focused mainly on the wicking mechanism without considering influence of the mechanical properties of yarn. However, during wear fabric/yarn always undergoes deformation. Such deformation, which is determined by mechanical properties of fibers and yarn, will greatly alter the radial positions of fibers and the porous structure of the yarn, and hence affect the wicking mechanism. Furthermore, many natural fibers, such as wool, take up water during wicking. Absorption of water will greatly change the mechanical properties of fiber (Abbott *et al.*, 1968; Ahumada *et al.*, 2004) and cause fibers to swell (Jenkins and Donald, 2000; Pierlot, 1999), hence it significantly affects the wicking process. Therefore, a comprehensive model to investigate the coupled mechanism is needed. However, such a model is still lacking in this research area.

Chapter 3. Mechanical modeling of singles yarn

3.1 Introduction

This chapter presents the mechanical modeling of singles yarn. A comprehensive model to predict the tensile behavior as well as torsional behavior of singles yarn was developed. The model was based on a discrete fiber modeling principle. An energy method was adopted to calculate the applied force on the yarn. Contributions to the applied force arising from fiber tension, fiber bending and fiber torsion were computed and compared. Taking into account the nonlinear behavior of fiber material, the entire force-deformation curve of singles yarn can be predicted. Bulky wool singles yarns were used to evaluate the model. The prediction agreed very well with the experimental data.

3.2 Model development

3.2.1 Assumptions

To predict the mechanical response of singles yarn, the following assumptions were made:

1. The yarn is cylindrical in shape and has a well-defined surface. According to the discrete-fiber-modeling principle (Postle *et al.*, 1988), the yarn is made up of a large number of discrete fibers. Each fiber is a discrete component of the

yarn structure and the aggregate response of the assembly is obtained simply by adding the separate contributions of individual fibers.

2. All fibers have an ideal geometry of coaxial helices which are identical and uniform along their lengths. All such helices have the same pitch with the helix angle being zero at the yarn center and a maximum at the yarn surface. Under tension/twist, all the helices undergo the same amount of extension/rotation.

3. The fibers are assumed to deform without changing their volume, that is, they are postulated to be incompressible under hydrostatic pressure with a Poisson’s ratio equal to 0.5. Under this circumstance, tensile energy is only a function of axial strain. However, the yarn as a whole is unnecessary to deform without change of volume, i.e. the density of packing may be variant.

4. Stress-strain properties of fibers in the yarn are assumed to be the same as they are tested individually. Time effect is ignored.

5. Test gauge length is short so that fiber migration and inter-fiber slippage are negligible, and the system is postulated to be conservative thus all the work done on the yarn is converted into stored internal energy of fibers.

3.2.2 Notation

The following notations are used in this chapter. Subscripts 0 and 1 denote initial state and deformed state, and subscripts f and y refer to fiber and yarn respectively.

ρ_f	fiber density
A	fiber cross-sectional area
L_f	fiber length
H	pitch length of fiber helix
κ, τ	curvature and torsion of fiber helix
σ_f	fiber tensile stress
σ_{bf}, σ_{tf}	fiber shear stress due to bending and torsion
ξ_f	fiber tensile strain
γ_{bf}, γ_{tf}	fiber bending and torsional strain
r	radial position of an arbitrary fiber
r_A	initial radial position of fibers that will be the outer boundary of a jammed region in the strained state
r_{Ajam}	radius of the outer boundary of the jammed region in the strained state
$\phi(r_0)$	initial fiber packing density
ϕ_{jam}	fiber packing density in a jammed region
r_y	yarn radius

ξ_y, ξ_θ, ξ_{ymax}, $\xi_{\theta max}$ yarn tensile and torsional strain, and the prescribed maximum

T_{ten}, T_{tor} tension and torque act on the yarn

T_y pre-tension acting on the yarn when the yarn is twisted

U_{ften}, U_{fben}, U_{ftor} fiber tensile, bending and torsional energy

U_{ten}, U_{ben}, U_{tor}, U_{tot} yarn tensile, bending, torsional and total energy

ε error tolerance

3.2.3 Tensile model

In their natural state, the fibers in a yarn are loose and unstrained. When the yarn is under a tension, according to the shortest-path hypothesis (Postle *et al.*, 1988), the fibers will move freely in the lateral direction to avoid being extended until they are prevented from doing so by preoccupied fibers. Those fibers that cannot move further laterally are referred to being jammed. If the yarn is not wholly jammed, the deformed yarn can be divided into two parts, a jammed region which is located at the center and an unstrained region which is out of the jammed region (Figure 3.1).

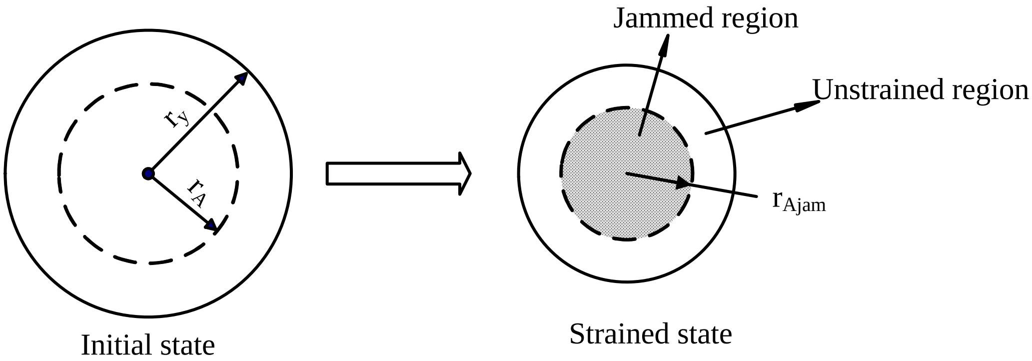

Figure 3.1 Yarn cross section before and after deformation

Without losing generality, only one pitch of the yarn is considered. According to the theory developed by Choi (Choi, 1998), r_{Ajam} can be given by:Equation Chapter 3 Section 1

$$r_{Ajam} = \sqrt{\frac{2}{\phi_{jam}\lambda_y}\int_0^{r_A} r_0\phi\left(r_0\right)dr_0} \tag{3.1}$$

r_A can be obtained by solving Equation (3.2):

$$\int_0^{r_A} r_0\phi\left(r_0\right)dr_0 = \frac{\left(4\pi^2 r_A{}^2 + H_0{}^2 - H_0{}^2\left(1+\xi_y\right)^2\right)\left(1+\xi_y\right)\phi_{jam}}{8\pi^2} \tag{3.2}$$

The internal energy of yarn, which is made up of tensile energy, bending energy and torsional energy, can be obtained by adding up the energy of individual fibers which is composed of the three kinds of energy as well. With a given initial fiber packing density the energy of yarn was calculated based on the initial state, and calculations of the three-component energy are discussed successively.

3.2.3.1 Tensile energy

Since unstrained fibers do not develop tensile strain, only those fibers in the jammed region were considered in the calculation of yarn tensile energy. For an arbitrary fiber the tensile energy is given by:

$$U_{ften} = W_{ften}\left(\xi_f\right) \cdot AL_{f0} \tag{3.3}$$

where W_{ften} is the tensile energy stored in unit volume of fiber. It can be calculated by:

$$W_{ften}\left(\xi_f\right) = \int_0^{\xi_f} \sigma_f\left(\xi\right) \cdot \xi d\xi \tag{3.4}$$

where

$$\xi_f = \frac{L_{f1}}{L_{f0}} - 1 \tag{3.5}$$

$$L_{f0} = \sqrt{{H_0}^2 + \left(2\pi r_0\right)^2} \tag{3.6}$$

$$L_{f1} = \sqrt{{H_0}^2\left(1+\xi_y\right)^2 + \left(2\pi r_1\right)^2} \tag{3.7}$$

r_1 can be calculated in the same way as r_A (Equation (3.1)):

$$r_1 = \sqrt{\frac{2}{\phi_{jam}\lambda_y}\int_0^{r_{f0}} r\phi\left(r\right)dr} \tag{3.8}$$

For most metal materials, during a stretch test they obey the Hooke’s law until proportional limit. The whole deformation will recover upon unloading. If the strain exceeds the yield point, the stress does not change significantly with increase of the strain, and the strain will partly recover upon unloading. The residual strain is called plastic strain. After the yield region increase of strain will lead to a remarkable increase of stress again, and this is called strain-hardening. A typical stress-strain curve of metal material (steel) is shown in Figure 3.2.

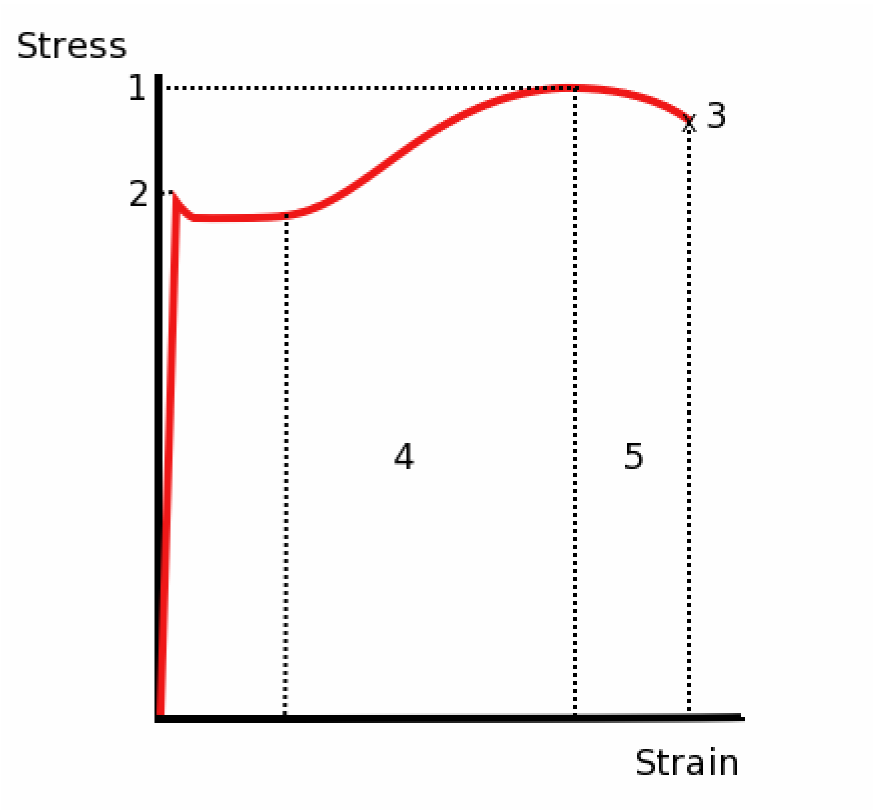

Figure 3.2 Stress-strain curve for low-carbon steel

1. Ultimate strength.

2. Yield strength-corresponds to yield point.

3. Rupture.

4. Strain hardening region.

5. Necking region.

Wool fibers under tension behave differently with metal materials due to their molecular structures and morphologies. A schematic diagram of a typical stress-strain curve of wool fiber is shown in Figure 3.3.

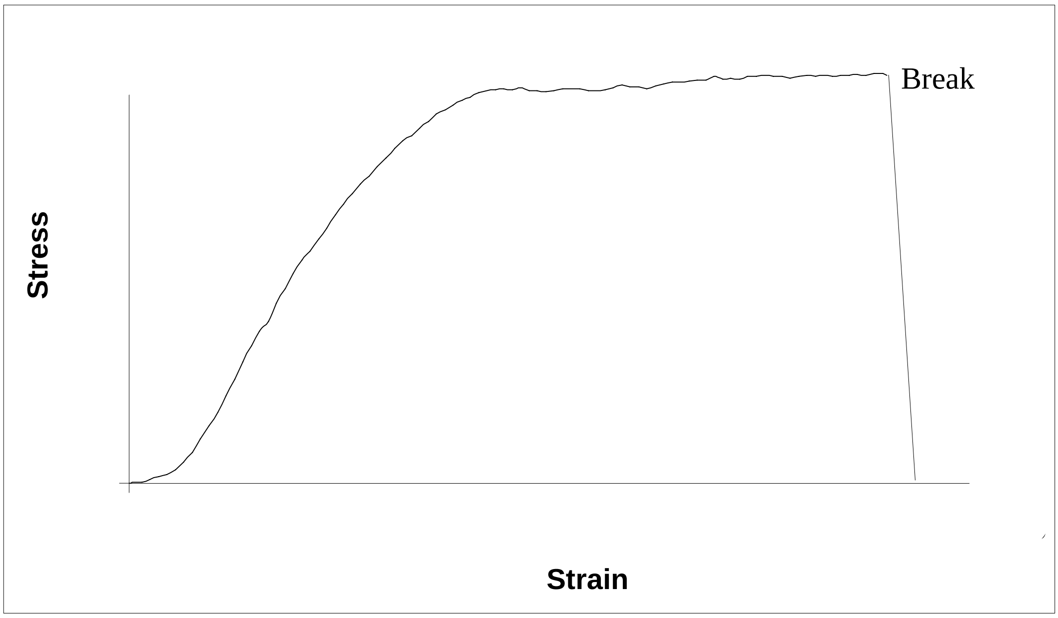

Figure 3.3 Stress-strain curve of a wool fiber

It is observed from Figure 3.3 that there exists a small nearly linear-elastic region just before the Hookean region. In this region, the elastic rigidity is very small. This may be attributed to the natural crimp of wool fiber. Figure 3.3 also shows that there is no obvious yield region. In this regard it is desirable to simplify the real stress-strain curve by piecewise straight lines in calculation, and W_{ften} in Equation (3.4) is just the area of the shade in Figure 3.4.

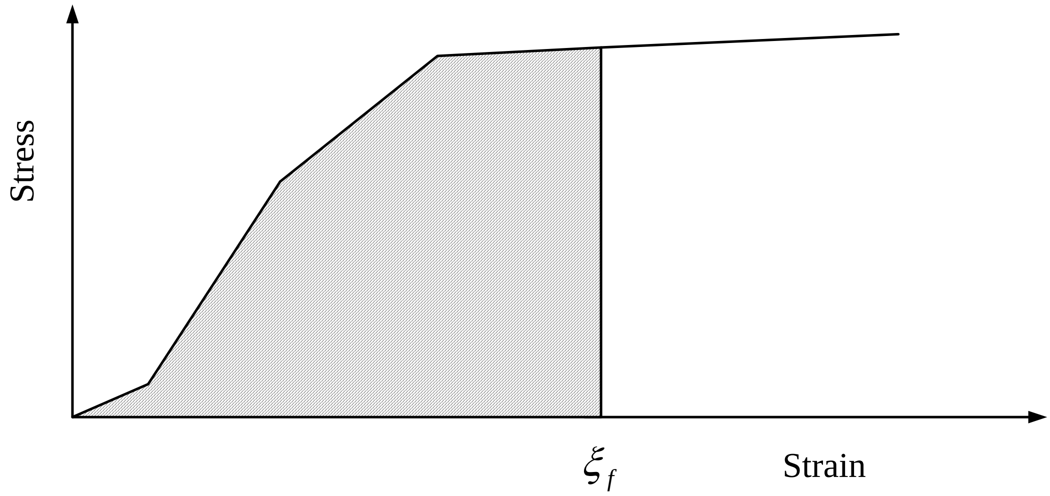

Figure 3.4 Simplified stress-strain curve of wool fiber

Since only fibers in jammed region develop tensile strain, the total tensile energy of yarn can be obtained by:

$$U_{ten} = \frac{2\pi H_0}{\rho_f} \int_0^{r_A} \phi(r_0) r_0 \cdot W_{ften}\left(\xi_f\right) dr_0 \tag{3.9}$$

3.2.3.2 Bending energy

When strained, the bending energy of yarn is stored in the jammed region as well as the unstrained region. Therefore, all fibers within the initial yarn cross-sectional area should be considered. The bending energy of one individual fiber is given by:

$$U_{fben} = W_{fben}\left(\gamma_{bf}\right) \cdot L_{f0} \tag{3.10}$$

where W_{fben} is the bending energy stored in unit length of fiber. It can be calculated by:

$$W_{fben}\left(\gamma_{bf}\right)=\int_{0}^{\gamma_{bf}}\sigma_{bf}\left(\gamma\right)\cdot\gamma d\gamma \tag{3.11}$$

where

$$\gamma_{bf}=\frac{\kappa_1-\kappa_0}{\kappa_0} \tag{3.12}$$

Referring to differential geometry theory, curvatures of fiber simple helix before (κ_0) and after deformation (κ_1) can be calculated by:

$$\kappa_0=\frac{\sin^2\alpha_0}{r_0},\quad \kappa_1=\frac{\sin^2\alpha_1}{r_1} \tag{3.13}$$

where

$$\alpha_0=\arctan\left(2\pi r_0/H_0\right),\quad \alpha_1=\arctan\left(\frac{2\pi r_1}{H_1}\right) \tag{3.14}$$

$$H_1=H_0\left(1+\xi_y\right) \tag{3.15}$$

r_1 can be obtained in the same way as Equation (3.8):

$$r_1=\begin{cases}\sqrt{\dfrac{2}{\phi_{jam}\left(1+\xi_y\right)}\int_0^{r_0}r\phi\left(r\right)dr} & r_0\le r_A\\ \sqrt{\dfrac{4\pi^2r_0^{\,2}+H_0^{\,2}\left(1-\left(1+\xi_y\right)^2\right)}{4\pi^2}} & r_0>r_A\end{cases} \tag{3.16}$$

The total bending energy of yarn is obtained in a similar way to U_{ten}:

$$U_{ben}=\frac{2\pi H_0}{\rho_f A}\int_0^{r_y}\phi\left(r_0\right)r_0\cdot W_{fben}\left(\gamma_{bf}\right)dr_0 \tag{3.17}$$

3.2.3.3 Torsional energy

In the same way as the calculation of bending energy, total torsional energy of yarn can be obtained by:

$$U_{tor} = \frac{2\pi H_0}{\rho_f A} \int_0^{r_y} \phi(r_0) r_0 \cdot W_{ftor}\left(\gamma_{tf}\right) dr_0 \tag{3.18}$$

where W_{ftor} is torsional energy stored in unit length of fiber which can be given by:

$$W_{ftor}\left(\gamma_{tf}\right) = \int_0^{\gamma_{tf}} \sigma_{tf}\left(\gamma\right) \cdot \gamma d\gamma \tag{3.19}$$

where

$$\gamma_{tf} = \frac{\tau_1 - \tau_0}{\tau_0} \tag{3.20}$$

The torsions of one fiber helix before (τ_0) and after deformation (τ_1) are given by:

$$\tau_0 = \frac{\sin\alpha_0 \cos\alpha_0}{r_0}, \quad \tau_1 = \frac{\sin\alpha_1 \cos\alpha_1}{r_1} \tag{3.21}$$

3.2.3.4 Energy method

According to the energy method (Treloar and Riding, 1963), the generalized resultant forces applied on the yarn can be derived by partial derivative of total energy with respect to corresponding generalized strains:

$$T_{ten} = \frac{\partial U_{tot}}{\partial \xi_y} / H_0 \tag{3.22}$$

where

$$U_{tot} = U_{ten} + U_{ben} + U_{tor} \tag{3.23}$$

3.2.4 Torsional model

When the yarn is twisted, tension must be applied on the yarn before further twist in order to avoid torsional buckling (Hearle *et al.*, 1969). Therefore, the degrees of freedom of the yarn are two, these being elongation freedom and rotational freedom, while there is only elongate freedom when the yarn is stretched. Therefore, the torsional model can be considered as a generalization of the tensile model. In the calculation of structural parameters, Equation (3.2) becomes:

$$\int_0^{r_A} r_0 \phi(r_0) dr_0 = \frac{\left(4\pi^2 r_A{}^2 + H_0{}^2 - H_0{}^2 \left(1+\xi_y\right)^2\right)\left(1+\xi_y\right)\phi_{jam}}{8\pi^2 \left(1+\xi_\theta\right)^2} \tag{3.24}$$

In the calculation of energy, equations derived in the tensile model still apply except that Equation (3.16) becomes:

$$r_1 = \begin{cases} \sqrt{\dfrac{2}{\phi_{jam}\left(1+\xi_y\right)} \displaystyle\int_0^{r_0} r\phi(r)\, dr} & r_0 \le r_A \\ \sqrt{\dfrac{4\pi^2 r_0{}^2 + H_0{}^2 \left(1-\left(1+\xi_y\right)^2\right)}{4\pi^2 \left(1+\xi_\theta\right)^2}} & r_0 > r_A \end{cases} \tag{3.25}$$

According to the energy method, the pre-tension and the torque applied on the yarn can be obtained by:

$$T_{ten} = \frac{\partial U_{tot}}{\partial \xi_y} / H_0 \tag{3.26}$$

$$T_{tor} = \frac{\partial U_{tot}}{\partial \xi_\theta} / 2\pi \tag{3.27}$$

The flow chart for the computer program in Matlab language is shown in Figure 3.5:

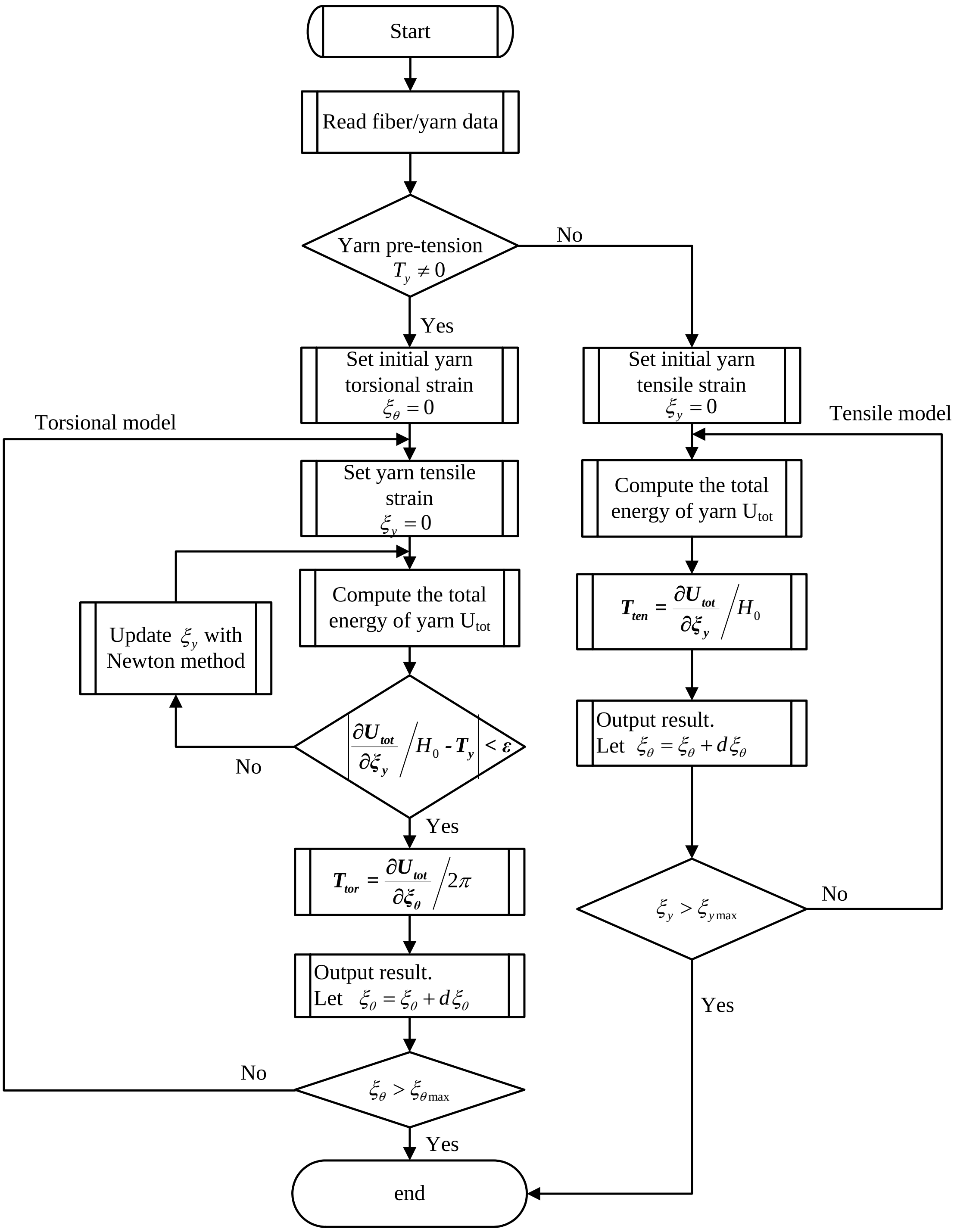

Figure 3.5 Flow chart for computer program for mechanical model of singles yarn

As an example, the parameters needed in the input file are listed in the following and the output from the program is given.

Input file:

```
2.278;       //phia,phia-phid:  yarn  packing  density
distribution parameters in cubic curve
-4.069;  //phib
1.372;   //phic
0.4436;  //phid
1.0;    //phijam, maximum yarn density,g/cm^3
0.0018;  //rf, fiber radius, cm
0.0000035279; //rfsq, mean fiber radius square, cm^2
191;    //twist, ture per meter
0.06;   //ry, yarn radius, cm
4500000; //E1, E1-E4: modulus of four straight lines
45100000;//E2
24000000;//E3
1530000; //E4
0.006;   //e1, e1-e4: end strain of the four straight lines
0.022;   //e2
0.037;   //e3
0.084;   //e4
39700000;//Ef, mean initial modulus
13910000;//Gf, flexible modulus
1.31;   //RHOf, fiber density, g/cm^3
0;      //ethmin, lower limit of rotational strain
7.2;    //ethmax, upper limit of rotational strain
5.59;   //load, applied tension under torsion to avoid
buckling
0.1;    //eymax, upper limit of yarn axial strain
```

Output from the tensile model:

```
    strain(%)       tension(N)
      0.030000        0.000445
      1.030000        0.068444
      2.030000        0.382163
      3.030000        1.129584
      4.030000        2.261751
      5.030000        3.564647
```

```
6.030000        4.869215
7.030000        6.119183
8.030000        7.300577
9.030000        8.414025
```

Output from the torsional model:

```
rotation(ram/cm)   torque(mgf.cm)
0.000000               0
0.600000         28.020579
1.200000         55.781614
1.800000         83.636460
2.400000        111.662727
3.000000        140.096569
3.600000        170.294103
4.200000        212.945290
4.800000        256.356081
5.400000        300.420732
6.000000        346.721780
6.600000        395.985521
7.200000        448.875236
```

3.3 Experiments

Experimental evaluation of the theory was conducted on a series of wool fibers and woolen spun carpet yarns. Radii of fiber and yarn were measured with a projection microscope. The yarn twist level was tested using a twist tester. In order to get an average load-strain curve of fiber under tension, 50 fiber specimens were tested on an Instron Tensile Tester. The crosshead speed was 20mm/min and the sampling rate was five pts/sec.

The yarns were boil-set before testing to ensure almost zero residual torque. Average fiber length was 6.2 cm. In order to guarantee the maximum number of fiber ends were clamped by the test heads and taking equipment limitation into account, the gauge lengths of the yarn were selected to be 5 cm for the tensile test and 3 cm for the torsional test. Yarn tensile and torsional tests were conducted using an Instron Tensile Tester and a KES-YN1 tester (Kawabata Evaluation System for Yarns) respectively. In order to eliminate the time effect of fibrous material in tensile behavior the crosshead speed in the yarn tensile test was set to be the same as for the fiber tensile test.

As stated by Carnaby *et al*. (Carnaby and Grosberg, 1976), initial fiber packing density varies along yarn radius. This directly affects fiber movement during deformation and the final strain distributions of fibers. The method described by Choi (Choi, 1998) was employed to estimate the initial fiber packing density. Ten yarn cross-sections were selected randomly along the length of the yarn. Then ten yarn density distributions were obtained and the mean value was used as the final packing density.

3.4 Results and discussion

The experimental data and theoretical calculations are presented and compared in this section for both tensile and torsional behavior of singles yarn. All experimental results on yarn were mean values of 20 repeated tests. ϕ_{jam} was $1 g/cm^3$. The physical parameters of yarn and fiber are listed in Table 3.1:

Table 3.1 Characteristics of yarn and fiber

<table>
<tr><th colspan="3">Yarn</th><th colspan="3">Fiber</th></tr>
<tr><td rowspan="2">Linear density
(tex)</td><td>Mean</td><td>SD</td><td rowspan="2">Fiber radius, r_f
(mm)</td><td>Mean</td><td>SD</td></tr>
<tr><td>245.91</td><td>35.9</td><td>0.01878</td><td>0.0049</td></tr>
<tr><td rowspan="2">Twist level
(tpm/Z)</td><td>Mean</td><td>SD</td><td rowspan="2">Fiber density, ρ_f
(kg/m^3)</td><td rowspan="2" colspan="2">1.31×10^3</td></tr>
<tr><td>191.24</td><td>32.3</td></tr>
<tr><td rowspan="2">Yarn radius, r_y
(mm)</td><td>Mean</td><td>SD</td><td rowspan="2"></td><td rowspan="2" colspan="2"></td></tr>
<tr><td>0.601</td><td>0.077</td></tr>
</table>

The mean load-strain curve of fiber is shown in Figure 3.6. Four piecewise linear straight lines, as shown in Figure 3.7, were fitted to the mean curve profile in order to simplify the calculation.

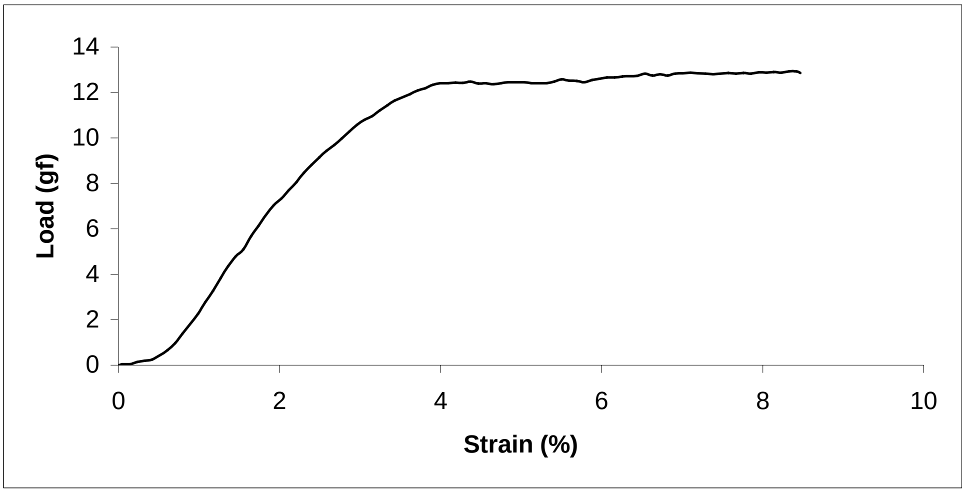

Figure 3.6 Load-strain curve of wool fiber

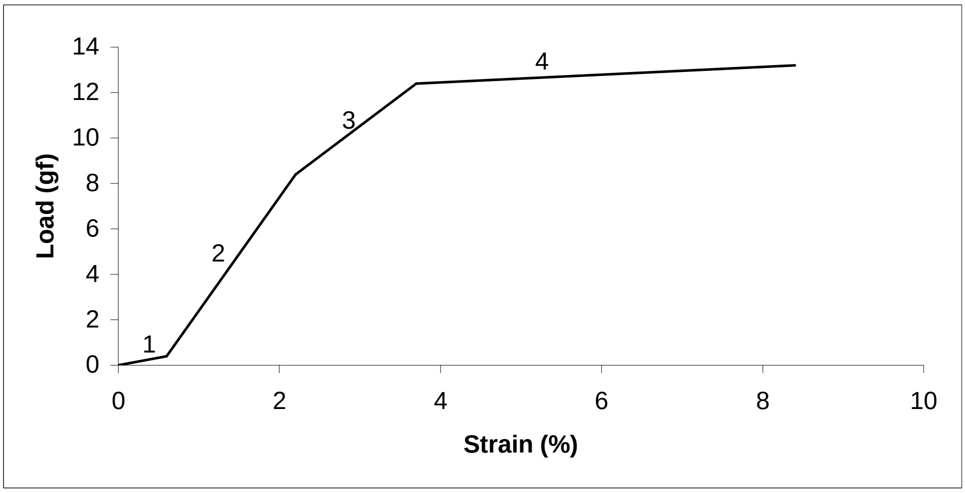

Figure 3.7 Simplified load-strain curve of wool fiber

The moduli of the four strain intervals are shown in Table 3.2. With reference to material mechanics theory, we can derive fiber bending and torsional rigidity from the corresponding tensile modulus at different stages with the assumption that the Poisson's ratio of the fiber is equal to 0.5.

Table 3.2 Moduli of the four stages in tensile test of fiber

ξ (%)	$E(gf\cdot cm^{-2})$	
$0 \le \xi < 0.6$	E_1	4.50×10^6
$0.6 \le \xi < 2.2$	E_2	4.51×10^7
$2.2 \le \xi < 3.7$	E_3	2.40×10^7
$\xi \ge 3.7$	E_4	1.53×10^6

A cubic function was adopted to fit the mean yarn packing density:

$$\phi(r_0) = 2.278r_0^3 - 4.069r_0^2 + 1.372r_0 + 0.4436 \tag{3.28}$$

Figure 3.8 gives a comparison of the tensile response deriving from theoretical calculation with experimental data, with a strain of up to nine percent.

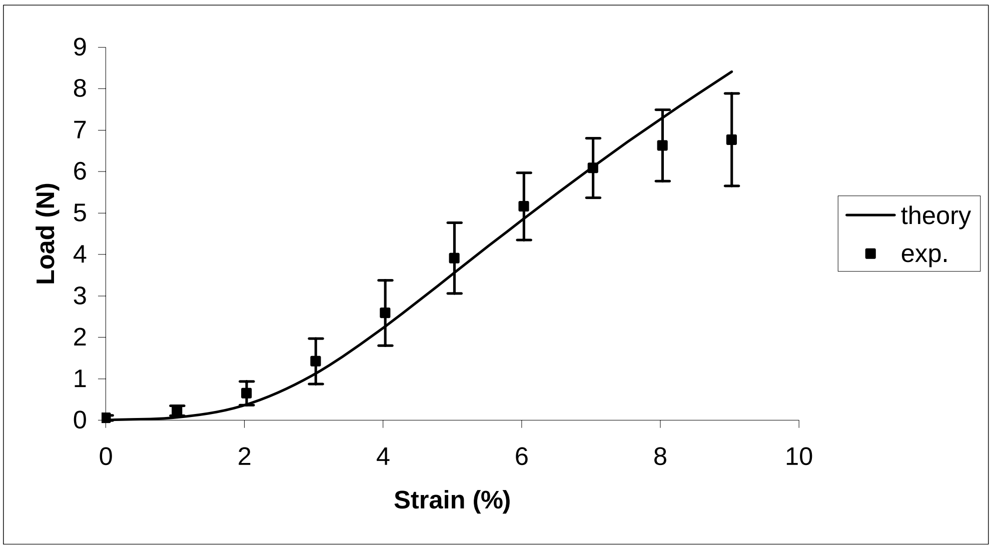

Figure 3.8 Load-strain curve of singles yarn

Figure 3.8 suggests that there is considerable agreement between the prediction and the experimental data with a strain up to around eight percent. At the beginning of the deformation, both theoretical and experimental load data increase steadily with strain up to about two percent. The comparatively small modulus of yarn may be due to the initial crimp of fiber and yarn. Then an almost linear rise from two percent strain to seven percent strain follows for both theoretical and experimental cases. After around seven percent strain the experimental data shows a very slow upward trend with a small slope and comes to a comparatively stable stage, whereas the theoretical prediction continues to increase dramatically. This leads to a significant difference between the experimental data and theoretical prediction from seven percent strain to nine percent strain. This may be due to the fact that some fibers are subject to slippage when subjected to a high degree of yarn extension. Although the test gauge length is short, not all the fiber ends are clamped. The slippage reduces the strength of the yarn.

Three kinds of energy of fibers are calculated in the energy method to get the tension applied on the yarn. They are tensile energy, bending energy and torsional energy. Figure 3.9 shows relative contributions to the calculated yarn tension due to fiber tension T_{ten}, fiber bending T_{ben} , fiber torsion T_{tor} and the total T_{tot}.

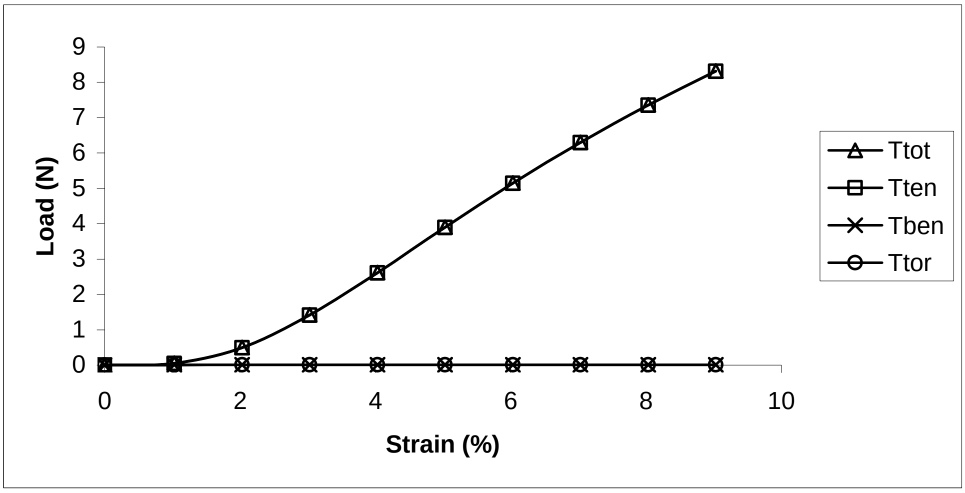

Figure 3.9 Comparison of contributions to the total yarn tension

From Figure 3.9 we can see that the calculated yarn tension due to fiber tension dominates the other two. When compared with fiber tension, contributions to yarn tension due to fiber bending and fiber torsion are negligible. Hence, we can conclude that in the tensile model of singles yarn, use of yarn tension due to fiber tension as the total yarn tension can give a quite accurate approximation.

Figure 3.10 presents a comparison of theoretical calculation of torsional response of a singles yarn with experimental results.

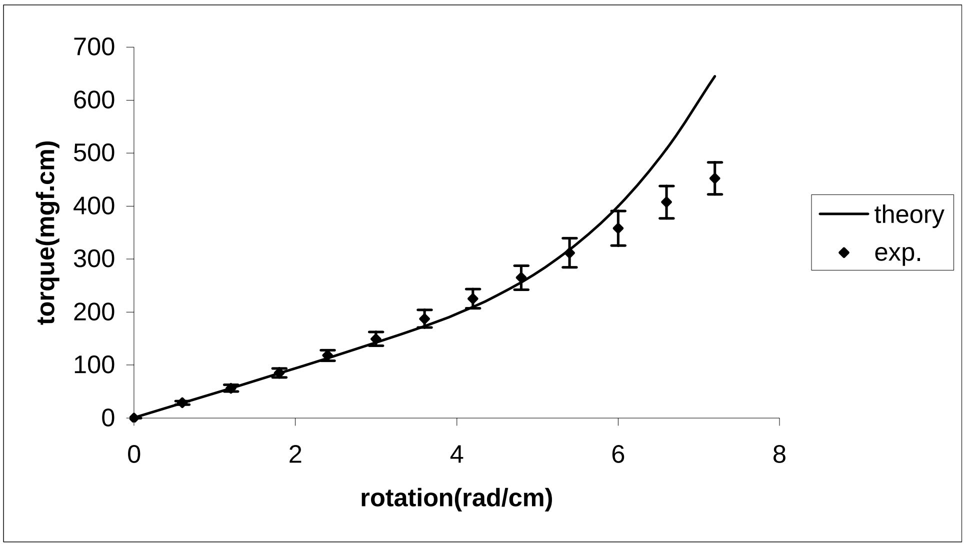

Figure 3.10 Torque-rotation curve of singles yarn (Pre-tension=5gf)

Figure 3.10 shows that the prediction agrees well with the experimental data, and yarn torque is an approximately linear function of yarn rotation at small twist. However, the model output differs significantly from the experimental data after around rotation 6rad/cm. To examine possible reasons of this discrepancy, fiber tensile distribution of the jammed region in the strained yarn was calculated and the results are shown in Figure 3.11.

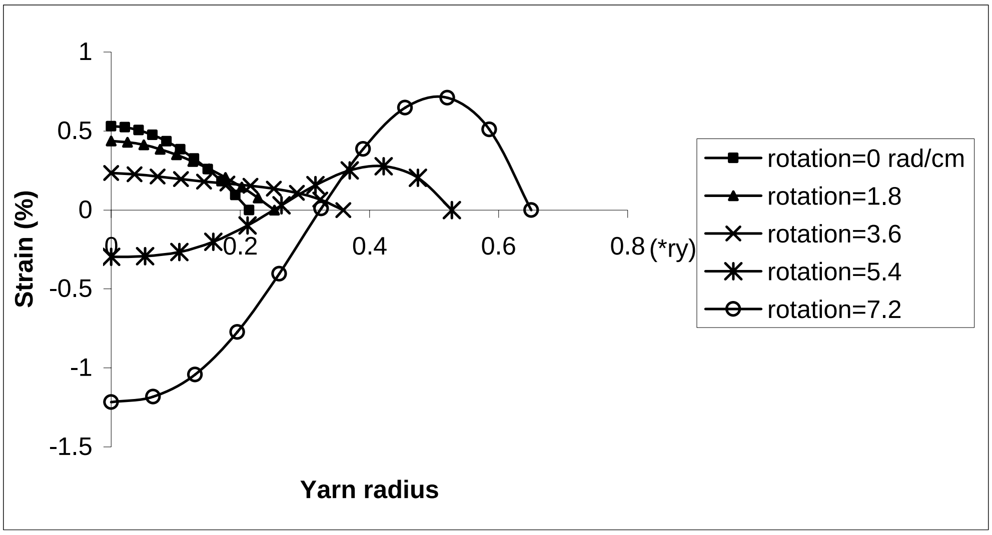

Figure 3.11 Fiber tensile strain distribution in the yarn

Figure 3.11 indicates that when twist is small, all fibers within the jammed region undergo tension. Actually this occurs when the yarn is under tension as well (Jiang *et al.*, 2002). However, when the yarn is further twisted the fibers near the yarn axis begin to undergo compression. The larger the twist of the yarn, the larger is the region under compression. However, fiber cannot sustain significant compression unless there is sufficient lateral pressure. Therefore, under large twist, some fibers in the central area of the yarn appear to buckle to release the compressional energy. This may be one of the reasons why the model prediction is higher than the experimental result at high twist level. If buckling of fibers is considered, and the buckled fibers are allowed to release their compressional energy while still maintaining their helical profiles, the computational results are presented and compared with experimental data in Figure 3.12.

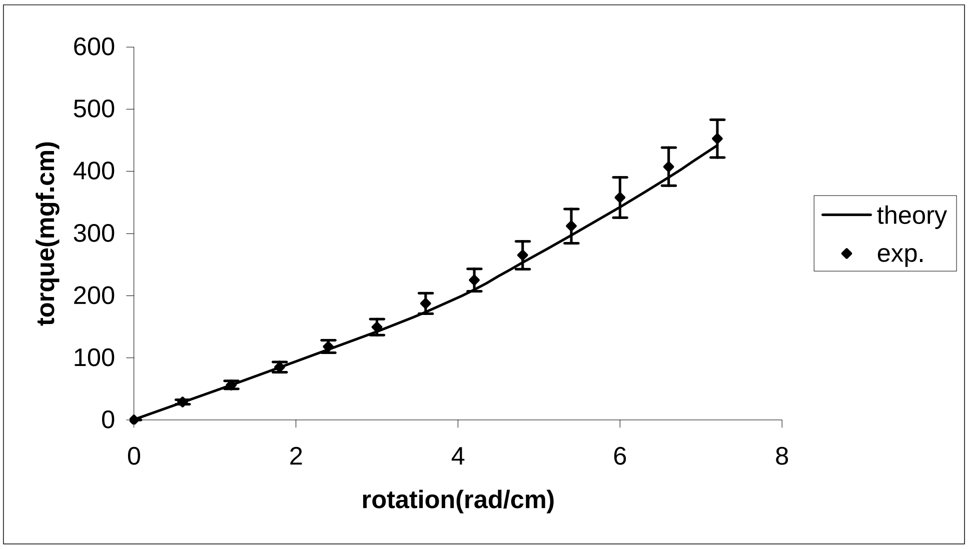

Figure 3.12 Torque-rotation curve of singles yarn (Pre-tension=5gf) (buckling of fibers is considered in the theory)

It may be seen from Figure 3.12 that the calculation agrees well with experimental results even at large rotation.

Identical to the tensile model, total yarn torque is also composed of components due to fiber tension, fiber bending and fiber torsion. A comparison of contributions to the calculated yarn torque attributed to each of them is shown in Figure 3.13.

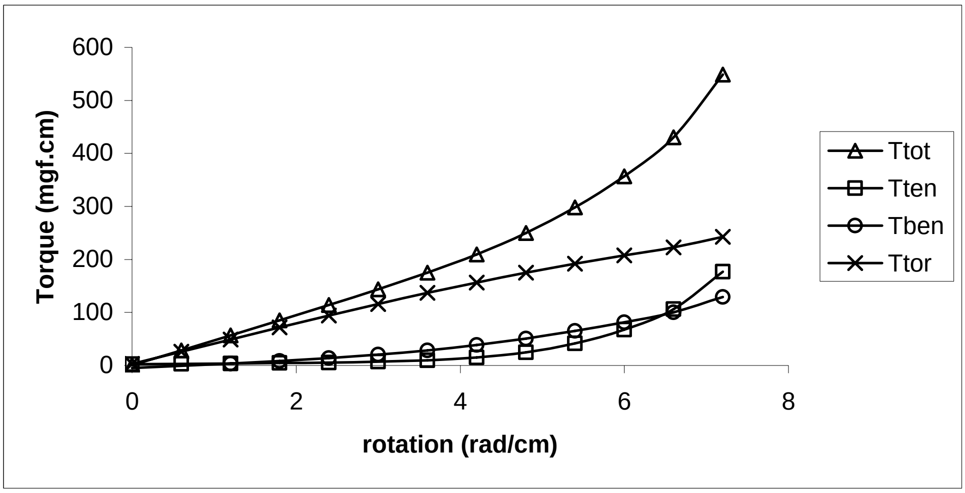

Figure 3.13 Comparison of contributions to total yarn torque (Pre-tension =5gf)

Figure 3.13 illustrates that for a comparatively small given pre-tension fiber torsion contributes the most to the total yarn torque, and fiber bending plays an important role as well. This observation is different from that of Tondon *et al.* (Tandon *et al.*, 1995b) who stated that the contributions to yarn torque due to fiber bending and torsion are negligible. With the increase of yarn twist, the contributions to yarn torque due to fiber bending and fiber tension become more important. Neglect of any contribution of the three components will lead to inaccurate results.

For different pre-tension levels, Figure 3.14 to Figure 3.17 present comparisons of the theoretical predictions of yarn torque with the experimental data, with and without consideration of the buckling of fibers.

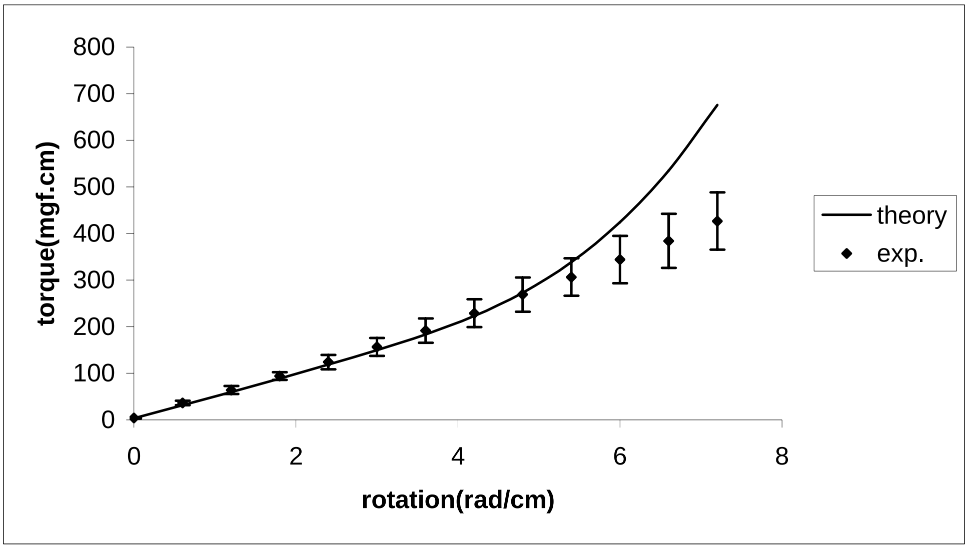

Figure 3.14 Torque-rotation curve of singles yarn (Pre-tension =10gf)

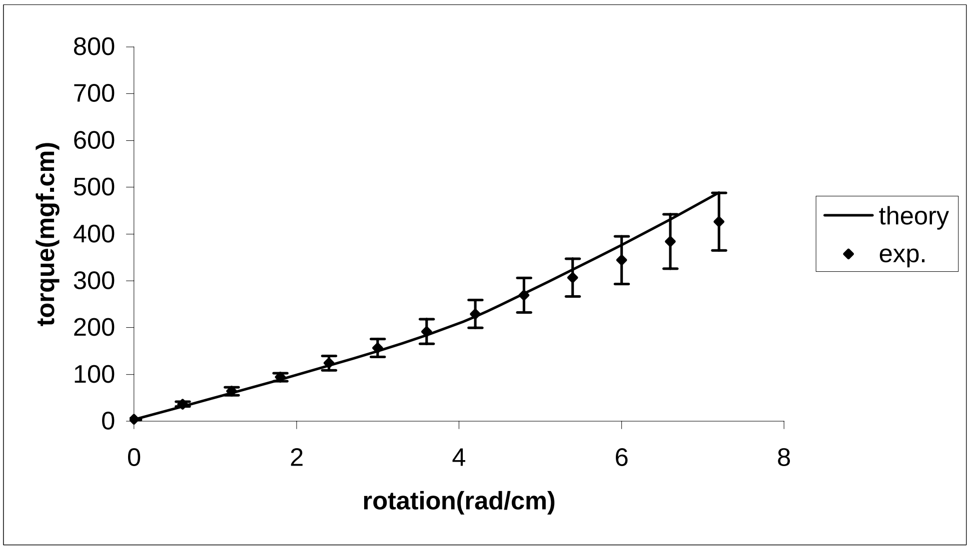

Figure 3.15 Torque-rotation curve of singles yarn (Pre-tension=10gf) (buckling of fibers is considered in the theory)

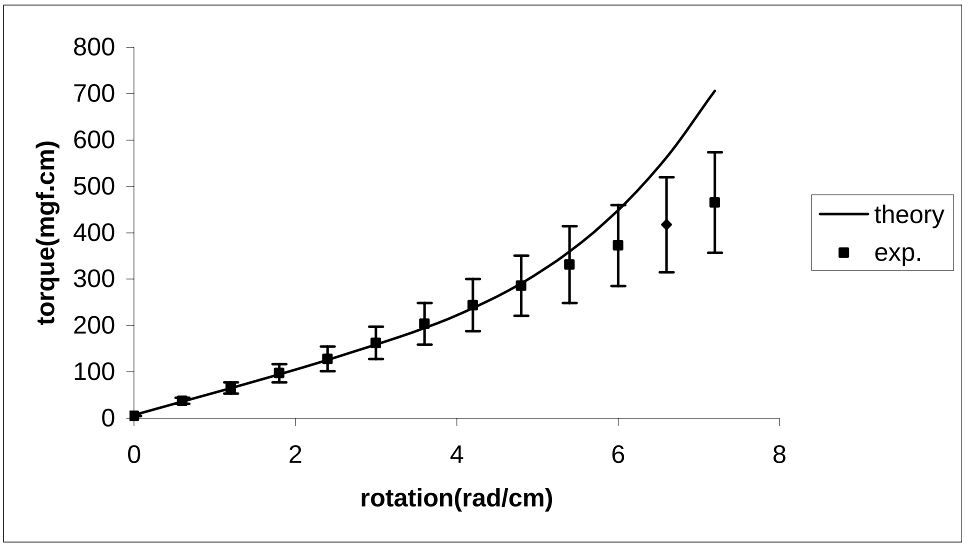

Figure 3.16 Torque-rotation curve of singles yarn (Pre-tension =15gf)

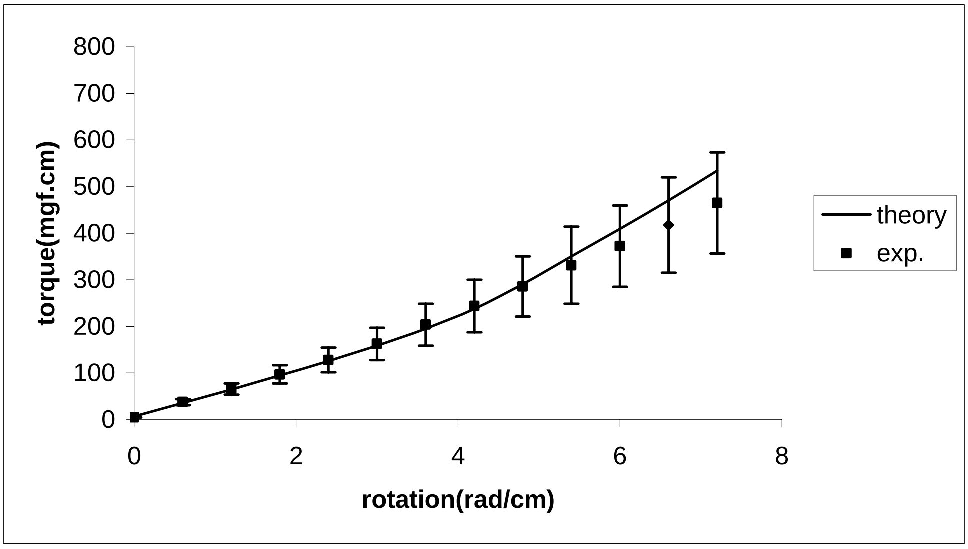

Figure 3.17 Torque-rotation curve of singles yarn (Pre-tension=15gf) (buckling of fibers is considered in the theory)

For both cases the predictions from the model without consideration of fiber buckling show good agreement with experimental results at small twist, whereas they are higher than the experimental values under large twist which can be explained in the same way as the case of 5gf pre-tension. However, if buckling of fibers is incorporated into the model, the prediction agrees well with the experimental data at all rotation levels up to around 8 rad/cm.

3.5 Conclusions

The tensile and torsional behaviors of singles yarn were theoretically modeled using an energy method. Generally both tensile and torsional predictions at small strain were found to agree very well with experimental data obtained from bulky wool yarns whose initial fiber packing density was non-uniform. The whole stress-strain curve of constituent fiber was used in the calculation of energy of fiber. The nonlinearities of tensile, bending and torsional behaviors of fiber material were all considered, for the first time, in the analysis of yarn mechanics. These considerations led to accurate predictive outputs of the model. In the tensile model, contribution to yarn tension of fiber tension was proved to be much greater than even the sum of the contributions of fiber bending and fiber torsion. In contrast, all the three contributions were significant in the torsional model when the degree of pre-tension was comparatively small. This finding is different from that of Tandon *et al*. (Tandon *et al.*, 1995b) who concluded that both contributions to yarn torque of fiber bending and torsion were negligible.

Chapter 4. Capillary rise between cylinders

4.1 Introduction

Capillary rise in fibrous structures is a frequently observed phenomenon in wetting and wicking in textiles. In textile structures, fibers are more or less parallel to each other inside a fiber bundle; also, most synthetic textile fibers are very close to cylinders in shape. Therefore, a study of wicking behavior between cylinders is fundamental, and may provide a better understanding of the capillary penetration of liquid into more complicated structures such as fiber bundles, twisted yarns.

This chapter discusses the theoretical and experimental work on wicking between two cylinders of different sizes. Two special cases, i.e., wicking between two identical cylinders as well as wicking between a cylinder and a plate, were firstly discussed. Wicking height of the liquid at equilibrium in the gap was derived from an interfacial analysis. On the basis of the results, a more general case, which was wicking between two cylinders of unequal sizes, was analyzed. A series of experiments was carried out to validate the theoretical analysis. The predictions agreed very well with the experimental data.

4.2 Model development

4.2.1 Notation

The following notations are used in this chapter.

R	circumferential radius of the solid-vapor contact line in the horizontal cross-section just below the meniscus
R_L	circumferential radius of the solid-vapor contact line in the horizontal cross-section at a height of L above the bulk surface
r, r_1, r_2	radii of the solid cylinders
r_h	hydraulic radius
r_c	radius of circular capillary
$2d$	distance of separation between the two cylinders
$\overset{\frown}{AB}$, $\overset{\frown}{CD}$, $\overset{\frown}{AC}$, $\overset{\frown}{BD}$	arc length
α, α_1, α_2	angles between the line connecting the two cross-sectional centers of cylinders and the line connecting the cross sectional center of cylinder and the corresponding contact point
θ	contact angle between the liquid and the solid cylinder
A	cross-sectional area of the liquid column
P	perimeter wetted by the liquid
c	constant

p	capillary pressure
γ, γ_{LV}	liquid-vapor interfacial tension
γ_{SL}, γ_{SV}	solid-liquid and solid-vapor interfacial tensions
A_{SL}, A_{SV}, A_{LV}	solid-liquid, solid-vapor and liquid-vapor interfacial areas
F	driving force
ρ_l	density of the liquid
U	total energy of the system
L	capillary rise of the liquid above the horizontal surface
L_{equ}	capillary rise at equilibrium

4.2.2 Wicking between two identical cylinders

When two identical cylinders are closely placed in a liquid, the liquid will penetrate into the space between the two rods provided the contact angle, measured through the liquid, is smaller than 90^o (Figure 4.1).

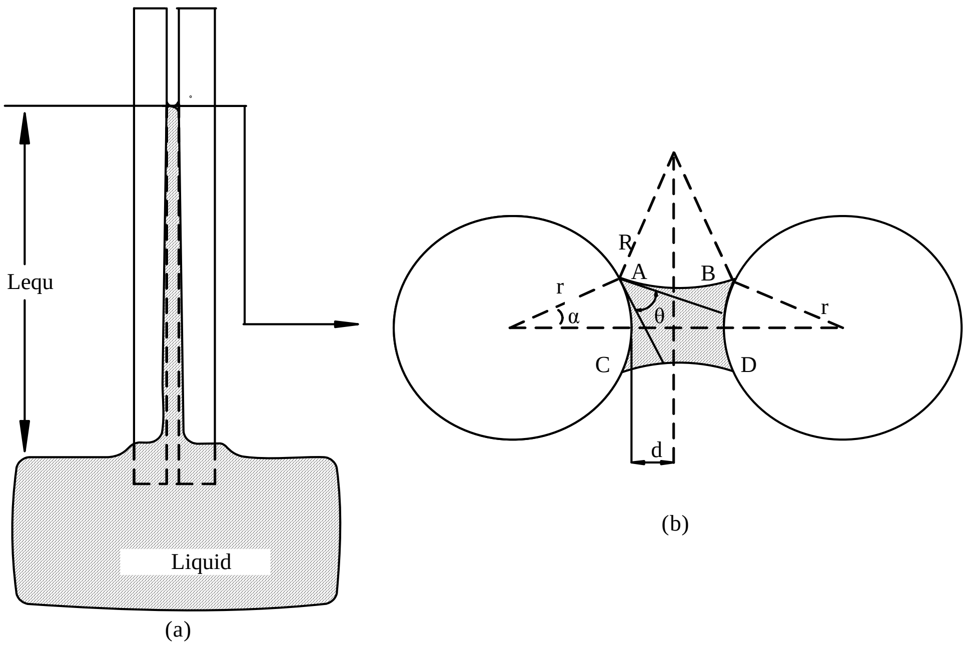

Figure 4.1 (a) Capillary rise of liquid between two vertical cylinders with equal radii (*b*) Horizontal cross-section just below the meniscus

The meniscus is saddle-shaped (Figure 4.2), and will reach an equilibrium height above the horizontal surface with a given distance of separation of the two cylinders.

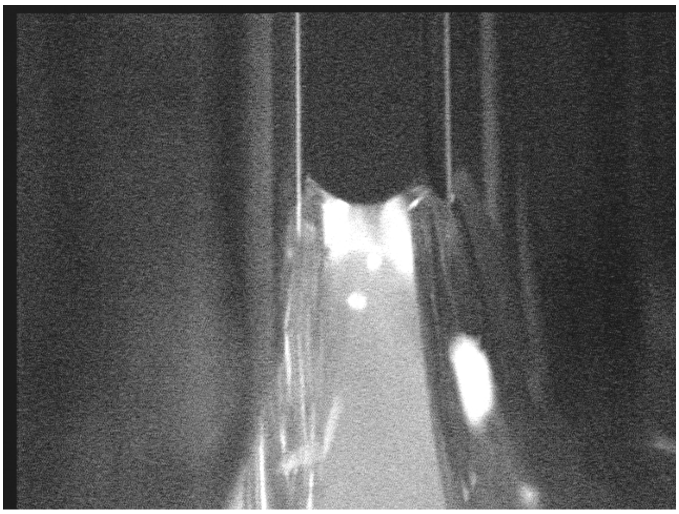

Figure 4.2 The meniscus of the liquid front

To find the cross-sectional shape of the liquid column between the two cylinders we start with analysis of the geometry of the cross-section just below the meniscus (Figure 4.1). We assume that the arcs *AB* and *CD* constitute portions of circumferences with radii *R*, and the contact angle between the cylinder and the liquid is the same all along the contact line. From a simple geometrical analysis, we have:Equation Chapter 4 Section 1

$$R = \frac{r + d - r\cos\alpha}{\cos(\theta + \alpha)} \tag{4.1}$$

The cross-sectional area of the liquid column is:

$$\begin{aligned} A = 2r^2 &\left[2\frac{R}{r}\sin\alpha\cos(\theta+\alpha) - \alpha + \sin\alpha\cos\alpha \right] \\ &- 2R^2\left[\frac{\pi}{2} - (\theta+\alpha) - \sin(\theta+\alpha)\cos(\theta+\alpha) \right] \end{aligned} \tag{4.2}$$

The meniscus has a complicated saddle shape. However, when L_{equ} is very large ($L_{equ} \gg d$) the dimension of the meniscus is negligible. The wicking liquid column thus is from the bulk surface to just below the meniscus. The capillary pressure *p* due to the cylindrical liquid surface in the region just below the meniscus therefore can be given by the Laplace equation (Adamson, 1990) (one principal radius is zero):

$$p = \frac{\gamma\cos\theta}{R} \tag{4.3}$$

On the other hand the capillary pressure at height *L* across the interface must equal the hydrostatic pressure. That means:

$$\rho_l g L = \frac{\gamma \cos\theta}{R_L} \tag{4.4}$$

Equation (4.4) shows that R_L is inversely proportional to L. The capillary pressure across the interface thus varies along the liquid column and reaches the maximum at the liquid front where

$$\rho_l g L_{equ} = \frac{\gamma \cos\theta}{R} \tag{4.5}$$

In order to obtain the wicking height at equilibrium L_{equ}, two approaches are adopted, they are, force approach and free energy approach.

4.2.2.1 Force approach

The weight of the liquid column F_1 is:

$$F_1 = \rho_l g A L_{equ} \tag{4.6}$$

The force due to surface tension F_2 consists of two parts:

(1) An upward force F_{21} resulting from the contact of the liquid and cylinders along AC and BD. This force is given by:

$$F_{21} = \gamma \cos\theta \left(\overset{\frown}{AC} + \overset{\frown}{BD} \right) \tag{4.7}$$

where

$$\overset{\frown}{AC} = \overset{\frown}{BD} = 2r\alpha \tag{4.8}$$

(2) A downward force F_{22} due to the free vertical liquid surface along *AB* and *CD* which tend to pull down the liquid column. This component force can be expressed by:

$$F_{22} = \gamma\left(\overset{\frown}{AB} + \overset{\frown}{CD}\right) \tag{4.9}$$

where

$$\overset{\frown}{AB} = \overset{\frown}{CD} = 2R\left(\frac{\pi}{2} - \theta - \alpha\right) \tag{4.10}$$

When equilibrium is established, we have:

$$F_1 = F_{21} - F_{22} \tag{4.11}$$

This leads to:

$$\gamma\left[\left(\overset{\frown}{AC} + \overset{\frown}{BD}\right)\cos\theta - \left(\overset{\frown}{AB} + \overset{\frown}{CD}\right)\right] = \rho_l gAL_{equ} \tag{4.12}$$

From the system of Equations (4.1), (4.2), (4.5), (4.8), (4.10) and (4.12), we can solve L_{equ} numerically with different *d*.

4.2.2.2 Free energy approach

According to the minimum free energy approach (Butt *et al.*, 2006), at equilibrium the change of free energy *dU* upon an infinitesimal disturbance *dL* of the liquid front from the equilibrium position must satisfy the following equation:

$$\frac{dU}{dL} = 0 \tag{4.13}$$

In the case of the solid-liquid-vapor system described in this chapter, the free energy changes upon the penetration of the liquid with the solid-liquid and liquid-vapor interfacial areas increasing while the solid-vapor interfacial area decreasing. In addition, the total energy U also changes with the rise of the liquid in the gravitational field. Therefore,

$$dU = \gamma_{SL} dA_{SL} + \gamma_{SV} dA_{SV} + \gamma dA_{LV} + \rho_l gALdL \tag{4.14}$$

It should be noted that any increase of A_{SL} is achieved at the expense of A_{SV}, thus

$$dA_{SL} = -dA_{SV} \tag{4.15}$$

Meanwhile, using the Young equation (Adamson, 1990) for the contact angle,

$$\cos\theta = \frac{\gamma_{SV} - \gamma_{SL}}{\gamma} \tag{4.16}$$

By simple geometrical analysis, we can derive:

$$dA_{SL} = \left(\overset{\frown}{AC} + \overset{\frown}{BD}\right) dL \qquad dA_{LV} = \left(\overset{\frown}{AB} + \overset{\frown}{CD}\right) dL \tag{4.17}$$

Substituting Equations (4.15), (4.16) and (4.17) into Equation (4.14), we have:

$$dU = -\gamma\cos\theta\left(\overset{\frown}{AC} + \overset{\frown}{BD}\right) dL + \gamma\left(\overset{\frown}{AB} + \overset{\frown}{CD}\right) dL + \rho_l gALdL \tag{4.18}$$

Therefore,

$$F = -\frac{dU}{dL} = \gamma\cos\theta\left(\overset{\frown}{AC} + \overset{\frown}{BD}\right) - \gamma\left(\overset{\frown}{AB} + \overset{\frown}{CD}\right) - \rho_l gAL \tag{4.19}$$

At equilibrium,

$$\gamma\left[\left(\overset{\frown}{AC}+\overset{\frown}{BD}\right)\cos\theta-\left(\overset{\frown}{AB}+\overset{\frown}{CD}\right)\right]=\rho_l gAL_{equ} \tag{4.20}$$

Equation (4.20) is just the same as Equation (4.12). Using the two different approaches, we obtain the same solution. This suggests that the two approaches are equivalent in nature in the analysis of the problem in question.

4.2.3 Wicking between a cylinder and a plate

In an extreme case where radius r_2 tends to infinity and the corresponding covering angle α_2 to zero, one cylinder will degenerate to a plate (Figure 4.3)

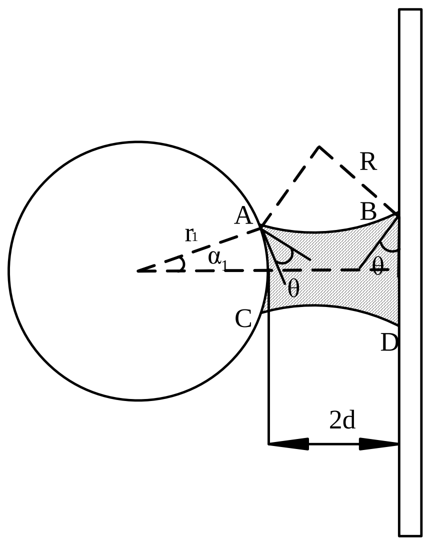

Figure 4.3 Horizontal cross-section just below the meniscus for wicking of liquid between a cylinder and a plate

By geometrical analysis, we can derive:

$$R = \frac{r_1 + 2d - r_1 \cos\alpha_1}{\cos(\theta + \alpha_1) + \cos\theta} \tag{4.21}$$

$$\begin{aligned} A = {} & r_1^2 \sin\alpha_1 \cos\alpha_1 + r_1 \sin\alpha_1 \cdot R\cos(\theta+\alpha_1) + R^2 \sin(\theta+\alpha_1)\cos(\theta+\alpha_1) \\ & + BD \cdot R\cos\theta + R^2 \sin\theta\cos\theta - \left[\alpha_1 r_1^2 + R^2(\pi - 2\theta - \alpha_1)\right] \end{aligned} \tag{4.22}$$

$$\begin{aligned} & \overset{\frown}{AB} = \overset{\frown}{CD} = R(\pi - 2\theta - \alpha_1) \qquad \overset{\frown}{AC} = 2r_1\alpha_1 \\ & \overset{\frown}{BD} = 2\left[R\sin(\theta+\alpha_1) - R\sin\theta + r_1 \sin\alpha_1\right] \end{aligned} \tag{4.23}$$

The wicking height at equilibrium can be obtained by solving the system of Equations (4.5), (4.12), (4.21), (4.22) and (4.23).

4.2.4 Wicking between two cylinders with different radii

In a general case where the radii of cylinders are different (Figure 4.4) we can obtain the solution of L_{equ} as a function of d in the same fashion as above.

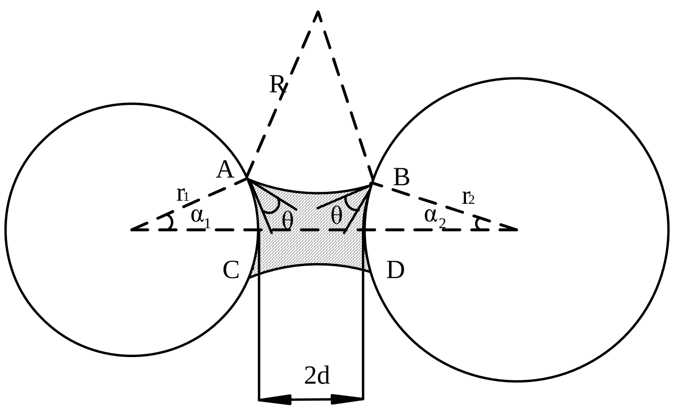

Figure 4.4 Horizontal cross-section of the solid-liquid system when the radii of the two cylinders are different

Here we also assume that the arcs *AB* and *CD* have a cylindrical shape of radius *R*. With this assumption Equations (4.5) and (4.12) still apply while the others for calculating the geometrical parameters do not. Furthermore the value of α_1 is different from that of α_2 which makes it necessary to find one more relationship in order to get a closed solution. If we reconsider the case discussed in Section 4.2.3, when the radius r_2 tends to infinity the angle α_2 tends to zero. Also, if the system of Equations (4.5), (4.12), (4.21), (4.22) and (4.23) is numerically solved with different *d*, and the solution of length *BD* is linearly fitted with respect to that of *AC*, perfect fit is found and the slope is nearly 1 (Figure 4.5).

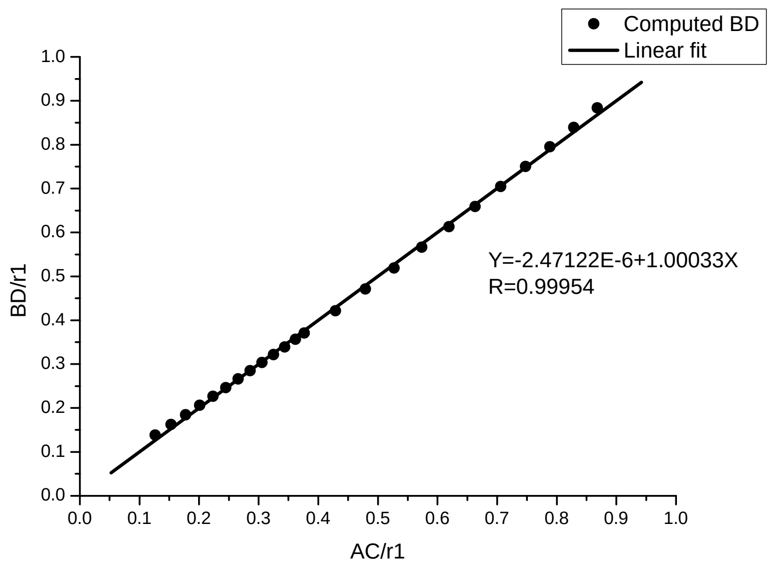

Figure 4.5 Linear fit of computed BD with respect to AC, normalized by r_1

This indicates that the arc lengths of *AC* and *BD* are equal. Since $\widehat{AC} = 2r_1\alpha_1$, $\widehat{BD} = 2r_2\alpha_2$ (Figure 4.4), we thus get:

$$\frac{r_1}{r_2} = \frac{\alpha_2}{\alpha_1} \tag{4.24}$$

Equation (4.24) is valid when $L_{equ} \gg d$ is satisfied. Once the relationship of Equation (4.24) has been obtained, the wicking height at equilibrium L_{equ} between two cylinders of different sizes can be solved numerically in the same fashion as in Section 4.2.2 and 4.2.3. The other geometrical parameters are given by:

$$R = \frac{r_1 + r_2 + 2d - r_1\cos\alpha_1 - r_2\cos\alpha_2}{\cos(\theta+\alpha_1) + \cos(\theta+\alpha_2)} \tag{4.25}$$

$$\widehat{AB} = \widehat{CD} = R\left(\pi - 2\theta - \alpha_1 - \alpha_2\right) \quad \widehat{AC} = 2r_1\alpha_1 \quad \widehat{BD} = 2r_2\alpha_2 \tag{4.26}$$

$$\begin{aligned} A = {} & r_1^2 \sin\alpha_1 \cos\alpha_1 + 2r_1 \sin\alpha_1 \cdot R\cos(\theta+\alpha_1) \\ & + R^2 \sin(\theta+\alpha_1)\cos(\theta+\alpha_1) + r_2^2 \sin\alpha_2 \cos\alpha_2 \\ & + 2r_2 \sin\alpha_2 \cdot R\cos(\theta+\alpha_2) + R^2 \sin(\theta+\alpha_2)\cos(\theta+\alpha_2) \\ & - \left[\alpha_1 r_1^2 + \alpha_2 r_2^2 + R^2\left(\pi - 2\theta - \alpha_1 - \alpha_2\right)\right] \end{aligned} \tag{4.27}$$

4.3 Experiments

To evaluate the theoretical analysis, we conducted a series of experiments on a piece of experimental apparatus shown in Figure 4.6. Both identical cylinders and cylinders of different radii were considered in the experiments.

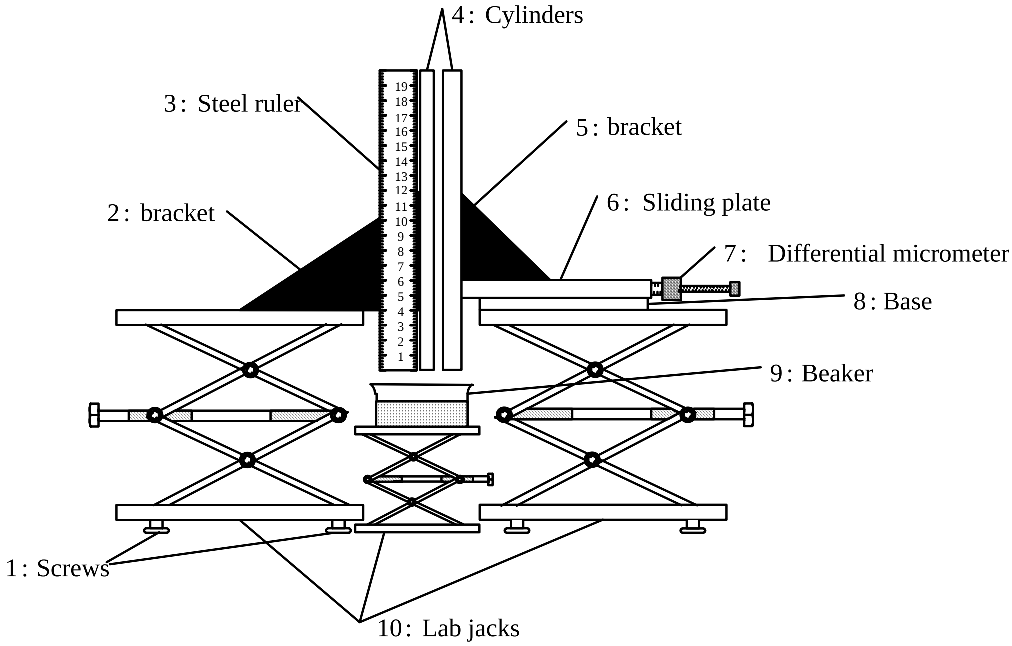

Figure 4.6 Experimental apparatus

With this apparatus, the capillary rise of liquid through the gap between two closely spaced vertical cylinders with different distances of separation can be measured. The apparatus is mainly made up of three lab jacks. The small lab jack is used to hoist the beaker 9 containing the wicking liquid while the other two to support the cylinders 4 which are glued onto the front surfaces of the 90^{o} angle brackets 2 and 5 respectively. Bracket 2 is mounted onto the top side of the left lab jack and bracket 5 onto sliding plate 6 which can slide along the base 8 fixed on the top of the right lab jack. The movement of the sliding plate 6, thereby the movement of the right cylinder to the other, is precisely controlled by a differential micrometer 7. The micrometer 7 offers a sub-micron that achieves long range and fine adjustability, and the graduation of the fine travel is 0.5μm. The distance of separation of the two cylinders can be read from the micrometer 7.

A CCD camera is horizontally positioned in front of the apparatus to observe the liquid front as well as the readout of the wicking height from the steel ruler 3 glued onto the side face of bracket 2.

Glass rods were chosen as the cylinders and distilled water as the wicking liquid. Firstly, the glass rods were glued onto the brackets with the axes of the cylinders perpendicular to the horizontal surfaces of the brackets. The amount of the glue was so small that it would not influence the wicking behavior of liquid through the gap. Then the rods were immersed for twenty-four hours into the mixture of acetone, ethanol and water. Afterwards they were washed with distilled water, and finally blown dry with nitrogen. The beaker was treated with the same cleaning procedure before use. After mounting the brackets, the four screws 1 were adjusted to ensure the horizontality of top plates of lab jacks indicated by a spirit level with the bubble positioned on the top sides of lab jacks. Then the lab jacks were moved and adjusted to position the ends of the glass rods at the same vertical level and the axes of the two rods at same level in the direction perpendicular to the paper. Afterwards the sliding plate 6 was driven through micrometer 7 to move close the rods until they touched. The readout from the micrometer 7 was set to be the zero position of distance between the two rods. The two rods were then set apart until there was no obvious wicking. Subsequently the beaker 9 was hoisted until the ends of glass rods were slightly immersed into the distilled water. Again, the rod was moved close until there was obvious capillary rise observed from the monitor connected to the CCD camera.

The distance of separation and the wicking height were recorded. The procedure of moving and recording was repeated until sufficient data were obtained.

The distilled water was prepared by boiling the water and re-condensing the steam into a clean container. The surface tension of the distilled water was measured using a KRUSS digital tensionmeter. The capillary rise method was employed to determine the contact angle between glass and distilled water. A glass capillary tube with inner diameter 0.75mm was used. After being cleaned using the same procedure as for the glass rods, the glass tube was dipped into the distilled water and the capillary rise was measured. With given surface tension of distilled water, diameter of the glass tube and measured capillary rise, the contact angle was calculated.

Errors in the experimental results may arise from several aspects:

1. Error due to manufacture. Such as error from the micrometer, or a deviation of the glass rods from a pure cylinder.
2. Error introduced through the operations and adjustments.
3. Chemical contamination affecting the wicking behavior of liquid, despite the fact that the glass rods had been washed using acetone and distilled water.
4. Finally, when the two glass rods became very close, the liquid column turned out to be sensitive to the change of separation. Therefore, the error due to distance measurement was magnified.

In order to minimize the error due to 2 and 4, each experiment was repeated 10 times. All the experimental results are mean values of data from 10 experiments. Furthermore, we measured the radius of the rod at 10 different positions along the length and used the mean value as the final value to average the deviation of the glass rods from a pure cylinder.

4.4 Results and discussion

The theoretical prediction and experimental dada are presented and compared in this section. Theoretically speaking, there are no two entirely identical glass rods. However, without losing the generality two rods with radii of 6.2752mm and 6.4738mm were considered as identical and the average value of 6.3745mm was used in the theoretical calculation. For wicking between two cylinders with different radii, the radii r_1 were 6.2752mm and r_2 4.1015mm. The characteristics of cylinders used in the experiments are listed in Table 4.1.

Table 4.1 Characteristics of the two rods

	Mean value	Standard deviation along rod surface
Radius of rod 1, r_1	6.2752	0.04297
Radius of rod 2, r_2	4.1015	0.03979

All the rods have a length of 200mm. The density of deionized water ρ_l is 1000kg/m^3, and surface tension γ is 72 mN/m at 25^{o}C. The gravitational acceleration is 9.81 m/s^2. The calculated contact angle between the distilled water and glass was very small and therefore assumed to be zero. All cylinders are assumed to have the same surface properties and the same contact angle with water.

Figure 4.7 shows a comparison of the normalized wicking heights at equilibrium L_{equ}/r, derived from theory presented in this chapter and experiments, as a function of the normalized half distance of separation of the two rods d/r.

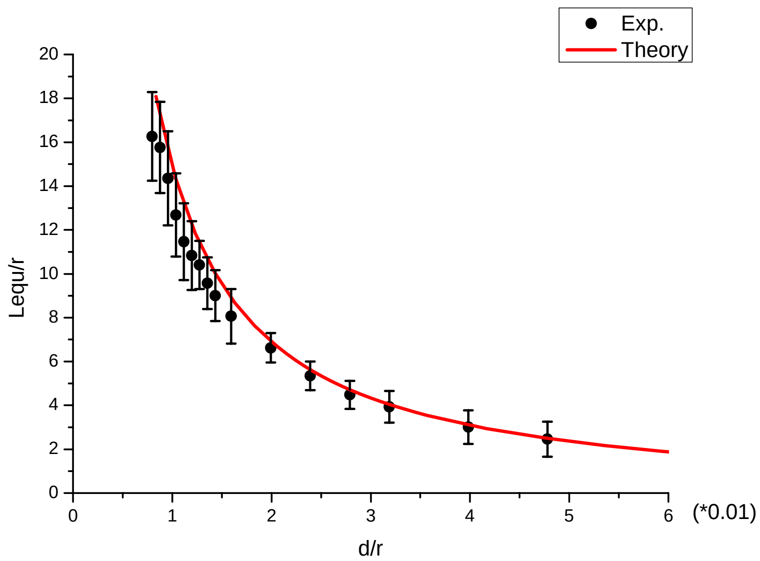

Figure 4.7 Comparison of L_{equ} as a function of d, normalized with respect to r (two identical rods)

Figure 4.7 suggests that there is considerable agreement between the theoretical prediction and experimental data within experimental error, except for small d. The deviation of the theoretical result from experimental data for small d may be attributed to the error due to reason number 1 and 4 discussed in Section 4.3. In accordance with the theoretical prediction, the wicking height will tend to infinity when d tends to zero. This was partially proved to a certain extent by placing a piece of blotting paper at the top of the cylinders. When the two cylinders touched, the paper became wet. This indicates that the wicking height is very large (L_{equ}/r is larger than 47.8=300/6.2752). As may be observed from Figure 4.7, L_{equ} decreases gradually with increase of d. This suggests that there may be an inverse proportional relationship between them. When L_{equ} is plotted with respect to $1/d$, the result is as presented in Figure 4.8.

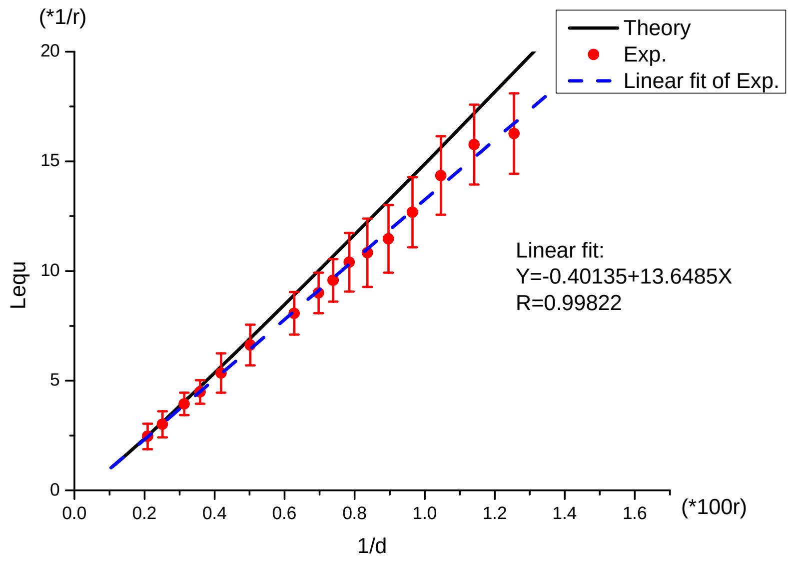

Figure 4.8 Comparison of L_{equ} as a function of $1/d$, normalized with respect to r (two identical rods)

By linearly fitting the experimental L_{equ}/r_1 with respect to $1/d$, a good fit result is found and the fitting straight line almost passes the origin. This indicates that L_{equ} is nearly inversely proportional to $1/d$.

Traditionally a hydraulic radius is always employed to treat noncircular capillaries as well as porous structures as round capillary tubes (Scheidegger, 1974). A hydraulic radius r_h is defined by:

$$r_h = \frac{A}{P} \tag{4.28}$$

where A is the cross-sectional area of the liquid and P the perimeter wetted by the liquid. For a circular tube with a radius r_c the hydraulic radius is $r_c/2$. If a hydraulic radius is adopted to model the wicking between two cylinders, the capillary rise at equilibrium should be proportional to inverse hydraulic radius:

$$L_{equ} \sim \frac{1}{r_h} \tag{4.29}$$

In order to investigate the dependency of L_{equ} to $1/r_h$, the experimental data of L_{equ} was fitted with respect to $1/r_h$ by a linear as well as a nonlinear scheme. The result is shown in Figure 4.9.

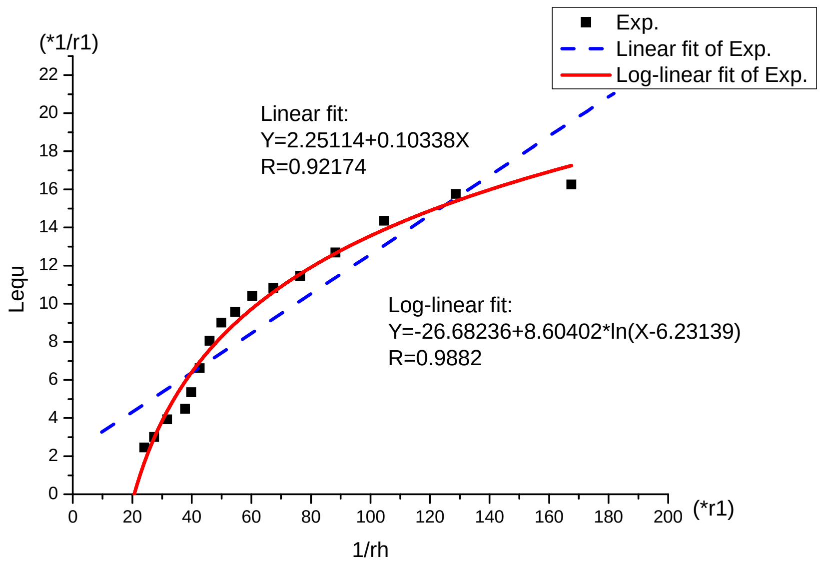

Figure 4.9 Fit of experimental L_{equ} with respect to $1/r_h$, normalized by r_1

From Figure 4.9, we can see that the result of linear fit is very poor while the nonlinear (three-parameter logarithmic) scheme gives a more accurate fit. This suggests that a log-linear relationship seems to be more appropriate to describe the capillary rise between cylinders in terms of inverse hydraulic radius.

Figure 4.10 to Figure 4.12 present results for two rods with different radii.

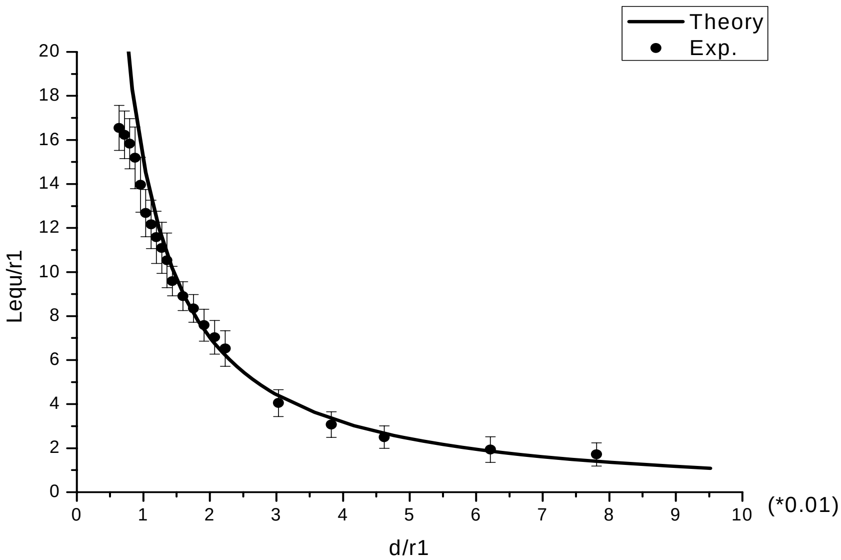

Figure 4.10 Comparison of L_{equ} as a function of d, normalized with respect to r (two different rods)

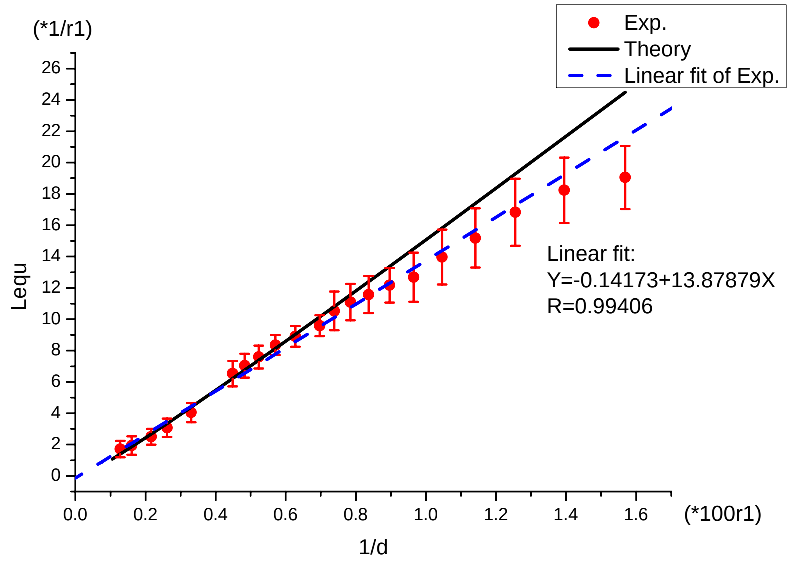

Figure 4.11 Comparison of L_{equ} as a function of $1/d$, normalized with respect to r

(two different rods)

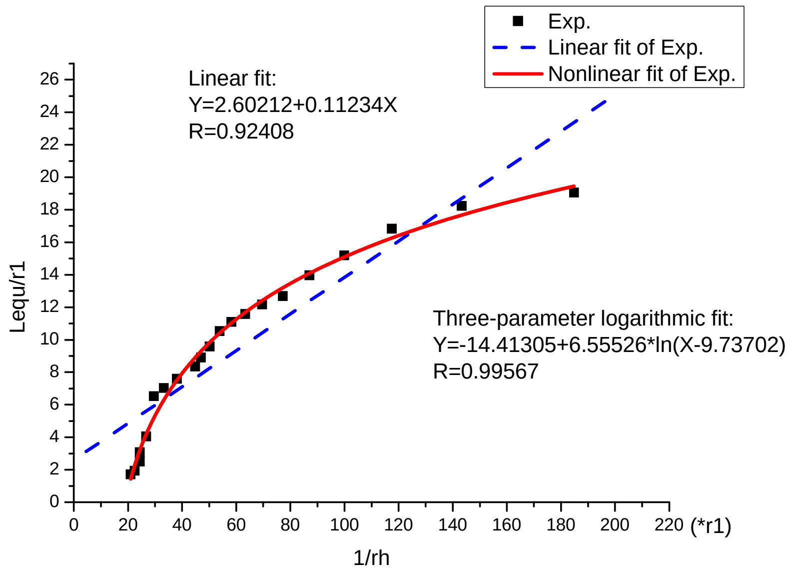

Figure 4.12 Fit of experimental L_{equ} with respect to $1/\ r_h$, normalized by r_1

Similar to the case of two identical rods, a nearly linear relationship is also observed between L_{equ} and $1/d$. A nonlinear fit using a three-parameter logarithmic scheme gives quite an accurate fit. As previously discussed, the variation of the local cylinder radius along its surface is a source of experimental error. In order to quantify this effect the sensitivity of L_{equ} with respect to r_1 and r_2 was calculated using the central difference method:

$$\frac{\partial L_{equ}}{\partial r_i} \approx \frac{L_{equ}\left(d, r_i + \Delta r_i\right) - L_{equ}\left(d, r_i - \Delta r_i\right)}{2\Delta r_i} \qquad i = 1, 2 \qquad (4.30)$$

where Δr_i is a small increment (e.g. 0.01% of r_i). The result is shown in Figure 4.13.

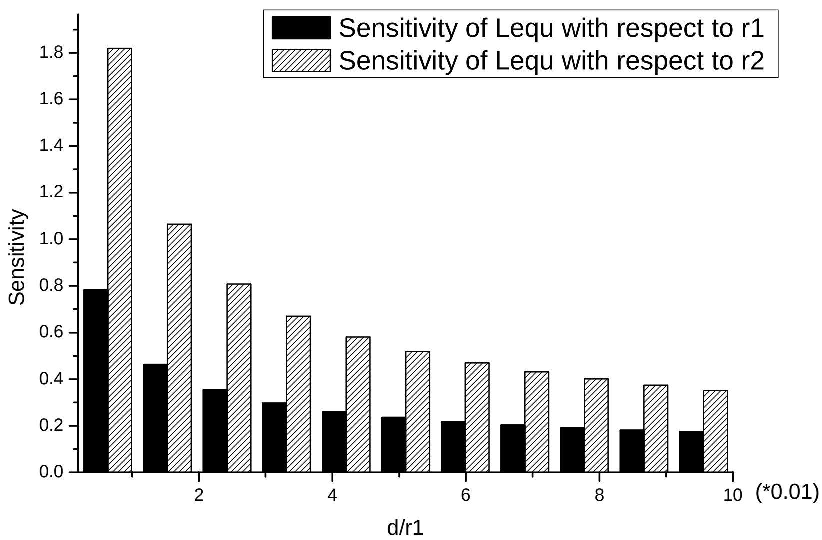

Figure 4.13 Sensitivities of capillary rise at equilibrium L_{equ} with respect to the radii of the rods

Figure 4.13 implies that for both radii L_{equ} is more sensitive to the variation of rod radius at smaller d/r_1 than larger d/r_1. While at a specific d/r_1 the influence of variation of r_2 on L_{equ} is more significant than that of r_1.

4.5 Conclusions

The wicking of a liquid in the gap between two vertically positioned parallel cylinders was discussed in this chapter. On the basis of an interfacial analysis, the wicking height of liquid at equilibrium was obtained as a function of the distance of separation of the two cylinders. The relation between the wicking height at equilibrium and the distance of separation was found to be nearly inversely proportional. Experimental verification showed that our theory can predict the wicking behavior of the liquid with reasonable accuracy. Due to the ease of manipulation, glass rods with quite large diameters were used in our experiments. In the case of textile materials, fibers may be very thin, and the principal radius of the meniscus may be of the same order for magnitude as the fibers. This problem has been discussed by Bouaidat and Zhao *et al*. (Bouaidat *et al.*, 2005; Zhao *et al.*, 2001). However, as long as the assumption $L_{equ} \gg d$ is satisfied the dimension of the meniscus is still negligible. Therefore, the theory presented in this chapter applies to the case of textile fibers as well since the terms that enter the theoretical calculation are normalized dimensionless quantities. We have also illustrated that a three-parameter logarithmic model seems to be more appropriate to describe the wicking between cylinders in terms of the inverse hydraulic radius. With minor modifications, the theory can be easily extended to model the wicking behavior of a liquid in a regularly packed fiber bundle with a small amount of fibers. However, textile structures, such as textile yarns, always consist of a large number of fibers. When the number of constituent fibers becomes very large, the analysis of the wicking mechanism may turn out to be very complicated due to the complex structure of liquid-gas and liquid-solid interfaces. Therefore, for wicking through a more complicated structure, like twisted yarns, more investigation is needed.

Chapter 5. Wicking in twisted yarns

5.1 Introduction

In this chapter, capillary flow through twisted yarns is discussed. Firstly, the wicking mechanism in a fiber bundle was analyzed. A theoretical model was developed based on a macroscopic force balance analysis of the liquid. Secondly, capillary flow of the liquid in a twisted yarn was investigated. A twist coefficient was introduced to consider the influence of the twist of the yarn on the wicking mechanism. A series of experiments on polyester yarns was conducted to validate the model. As a first stage, packing of fibers in the yarn was assumed to be uniform.

5.2 Model development

5.2.1 Notation

The following notations are used in this chapter.

F_c	capillary force
F_{cu}, F_{cd}	upward capillary force, downward capillary force
F_g, F_v, F_i	forces due to gravity, viscous drag and inertia
ρ_l	density of liquid
ρ_f	density of fiber
A	area available for liquid flow in the yarn cross section
L	axial wicking height of the liquid

k	frictional coefficient (for the initial yarn without further twist)
λ	twist coefficient
β	factor
P	perimeter wetted by the liquid
P_l	cross-sectional perimeter of the liquid column
θ_a	advancing contact angle between the liquid and the fiber
γ	surface tension of the liquid
A_y	cross-sectional area of the yarn
r_y	radius of the yarn
ϕ	packing density of fibers in the yarn
r_{fi}	radius of individual fiber
$\overline{r_f}$	average radius of fiber
n	number of fibers
H	pitch length of the helix of the fiber path
T	twist level
r	radius of the fiber helical path
L_f	fiber length
α	helix angle
g	gravitational acceleration
t	time
M, N	parameters in expression describing the wicking mechanism
U_{equ}	total potential energy of the liquid

5.2.2 Wicking in a fiber bundle

Let us first consider the wicking of a liquid in a vertical positioned fiber bundle with slight twist. Supposing the fiber cross section is circular, the fiber bundle can therefore be treated as an assembly of parallel cylinders. The schematic illustration of the cross-section of the fiber bundle is shown in Figure 5.1.

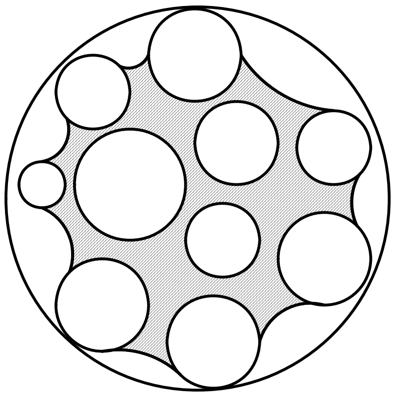

Figure 5.1 Cross section of the liquid-solid-gas system

When the wicking height L is large enough ($L \gg r_y$), the dimension of the meniscus of the liquid front is negligible and the following forces determine the movement of the liquid:

capillary force: F_c

gravity: $F_g = \rho_l gAL$

viscous drag: $F_v = kL\frac{dL}{dt}$

inertia: $F_i = \frac{d}{dt}\left[\rho_l AL\frac{dL}{dt}\right]$

Capillary force F_c consists of a upward force F_{cu} arising from the interaction between the liquid and the fibers, and a downward force F_{cd} due to the concave liquid-gas interface (Princen, 1968; Princen, 1969, 1970). Therefore, similar to Equation (4.19) we have: Equation Chapter 5 Section 1

$$F_c = F_{cu} - F_{cd} = P\gamma\cos\theta - P_l\gamma \tag{5.1}$$

The inertia term arises from Newton's second law of motion. However, except for the early stage of wicking, the inertia term is negligible when the acceleration of the liquid flow is slow (Reed and Wilson, 1993). The balance of forces hence is:

$$F_c - \rho_l gAL - kL\frac{dL}{dt} = 0 \tag{5.2}$$

Rearranging Equation (5.2), we have:

$$\frac{dL}{dt} = \frac{1}{k}\left(\frac{F_c}{L} - \rho_l gA\right) \tag{5.3}$$

Let

$$M = \frac{F_c}{\rho_l gA}, \quad N = \frac{k}{\rho_l gA} \tag{5.4}$$

In Equation (5.4), M is the driving capillary force term, and N is the wicking resistance term. By integrating and applying the initial condition $t = 0,\ L = 0$, we can obtain the solution:

$$t = N\left(M \ln \frac{M}{M - L} - L \right) \tag{5.5}$$

When the equilibrium is established, the capillary force should be balanced by the gravity of the liquid penetrating into the yarn. That means:

$$L_{equ} = \frac{F_c}{\rho_l g A} = M \tag{5.6}$$

Therefore, Equation (5.5) becomes:

$$t = N\left(L_{equ} \ln \frac{L_{equ}}{L_{equ} - L} - L \right) \tag{5.7}$$

In the calculation of capillary force F_c, the perimeter wetted by the liquid P is given by:

$$P = 2\pi \sum_{i=1}^{n} r_{fi} \tag{5.8}$$

In textile research, packing density is always used which is defined by:

$$\phi = \frac{\text{Mass of yarn}}{\text{Volume of yarn}} \tag{5.9}$$

When variation of the radii of the fibers is insignificant, P can therefore be obtained by:

$$P = \frac{A_y H \cdot \phi}{\rho_f \pi \overline{r_f}^2 H} \cdot 2\pi \overline{r_f} = \frac{2A_y \phi}{\rho_f \overline{r_f}} \tag{5.10}$$

P_l is composed of many parts formed between adjacent fibers in the yarn surface (Figure 5.1). In an individual curve, assuming it constitutes part of a circumference, the arc length can be obtained by the theory developed in Chapter 4. When the number of the constituent fibers is large, the calculation of all the arc lengths is extremely complicated and time-consuming. It is observed from Figure 5.1 that P_l should be less than the perimeter of the yarn cross-section. Therefore, it is reasonable to assume that:

$$P_l = \beta \cdot 2\pi r_y \quad \text{where } 0<\beta \leq 1 \tag{5.11}$$

If the cross-section covered by the liquid is treated as an equivalent circumference, then the cross-sectional area of the liquid column A can be calculated by:

$$\begin{aligned} A &= \beta^2 \pi {r_y}^2 - A_f \\ A_f &= \frac{A_y H \cdot \phi}{\rho_f \pi \overline{r_f}^2 H} \cdot \pi \overline{r_f}^2 = \frac{A_y \phi}{\rho_f} \end{aligned} \tag{5.12}$$

Then the capillary rise at equilibrium L_{equ} is given by:

$$L_{equ} = \frac{F_c}{\rho_l g A} = \frac{P\gamma \cos\theta - P_l \gamma}{\rho_l g A} = \frac{\gamma}{\rho_l g} \frac{P\cos\theta - 2\pi r_y \beta}{\pi {r_y}^2 \beta^2 - A_f} \tag{5.13}$$

Recalling Equation (4.19) and upon integration, and then we can obtain the total potential energy of the liquid at equilibrium U_{equ}:

$$U_{equ} = -P\gamma \cos\theta L_{equ} + P_l \gamma L_{equ} + \frac{\rho_l g A}{2} L_{equ}{}^2 \tag{5.14}$$

In Equation (5.14), the first two terms are internal free energy. The last term is the potential energy of the external force. According to the minimum total potential energy principle (Richards, 1977), the liquid shall deform or displace to a position that minimizes the total potential energy. Therefore, among those possible values of β, the true β should satisfy:

$$\frac{\partial U_{equ}}{\partial \beta} = 0 \tag{5.15}$$

Substitute Equations (5.11), (5.12) and (5.13) into Equation (5.15) and solve the resultant equation, and then we obtain the solution:

$$\beta = \frac{2A_f}{P\cos\theta r_y} \tag{5.16}$$

It has been verified that $\partial^2 U_{equ} \big/ \partial\beta^2 > 0$. Therefore $2A_f \big/ P\cos\theta r_y$ is the root. The schematic diagram of the flow of the modeling is shown in Figure 5.2.

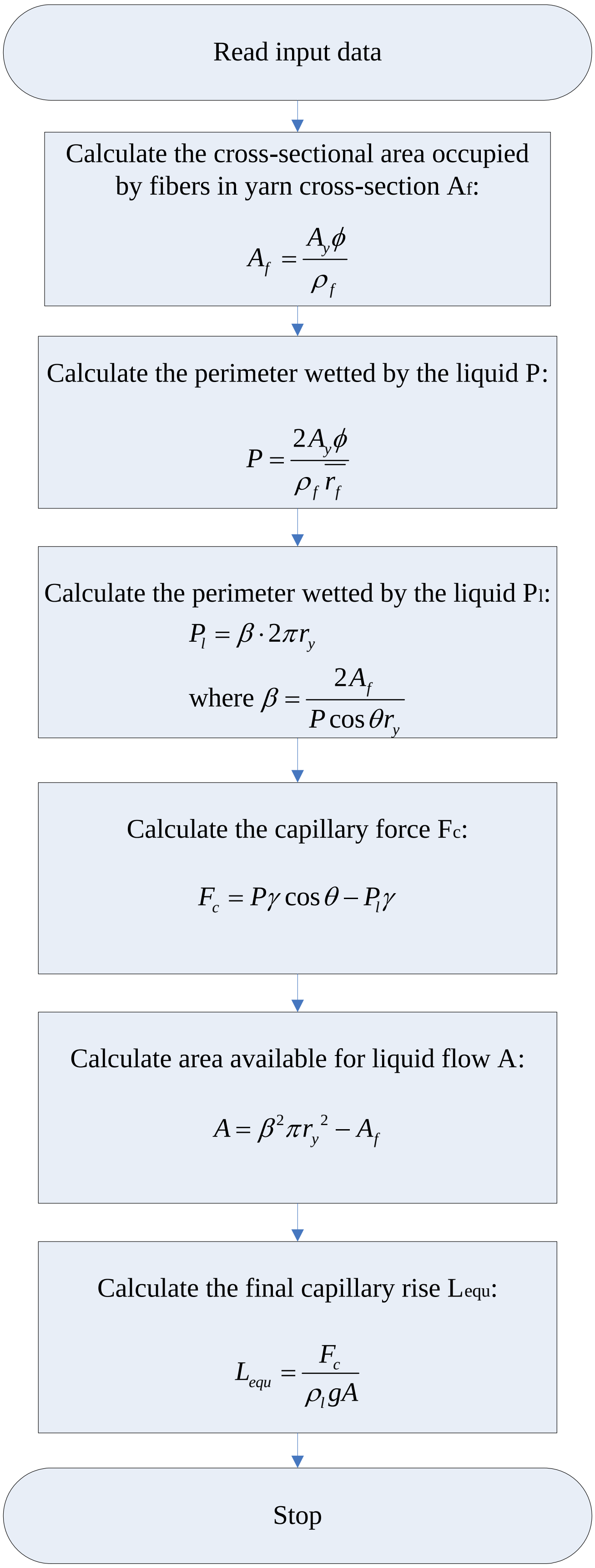

Figure 5.2 Flow chart of calculation of L_{equ}

5.2.3 Wicking in a twisted yarn

If a twist is applied to the fibre bundle, individual fibers will not be parallel to each other any more and will form different inclinations to the horizontal from yarn center to yarn surface. An idealized yarn model presented in Chapter 3 is adopted in which the yarn is assumed to be circular in cross section, and composed of a series of concentric cylinders of differing radii. Each fiber follows a uniform helical path around one of the concentric cylinders, so that its distance from the yarn axis remains constant. A typical constitute fiber is shown in Figure 5.3.

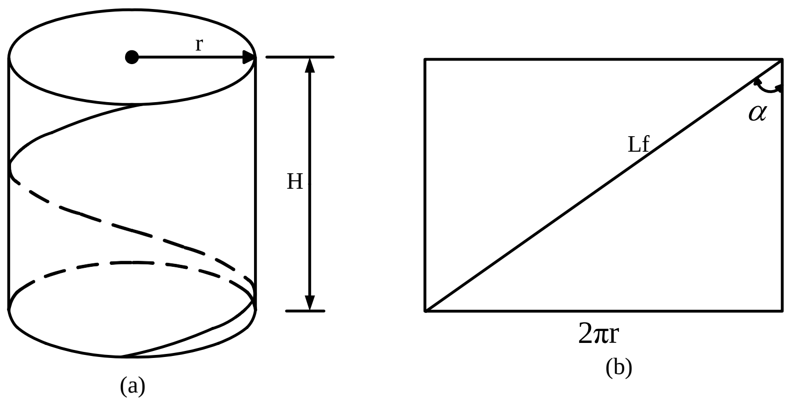

Figure 5.3 (a) Idealized fiber path (b) "open-out" diagram of the cylinder

When a twist is inserted into the yarn, fibers in the outer layers tend to move inward and reduce their helical radii. In order to examine the influence of twist on the wicking mechanism while excluding the effect of transverse movement of fibers, it is assumed that packing of fibers in the fiber bundle is uniform, and the fiber bundle is circularly close-packed (this will be discussed in Section 5.3). This prevents fibers from moving inward when a twist is introduced into the yarn, and consequently transverse deformations of fibers occur. Therefore, cross section of constituent fiber may no longer be circular in shape any more. This may change the structures of pores between fibers, and subsequently influence the wicking behavior of the liquid in the yarn. However, when the twist level applied on the yarn is not too high this effect should not be very significant. Thus diameters of the twisted yarn and the constituent fibers are assumed to be the same as the case of fiber bundle in the model. Since fibers within the yarn are not parallel to each other any more, inclinations of fibers to the vertical line (α in Figure 5.3) should be taken into account. Consider an element of area of cross section of the yarn between radii r and $r+dr$. The number of composed fibers inside this area can be obtained by:

$$dn = \frac{\phi \cdot 2\pi r dr \cdot H}{\rho_f \cdot \pi \overline{r_f}^2 \cdot L_f} = \frac{2H\phi r dr}{\rho_f \overline{r_f}^2 \sqrt{H^2 + 4\pi^2 r^2}} \tag{5.17}$$

Therefore, the upward capillary force contributed by this element area is given by:

$$dF_{cu} = 2\pi \overline{r_f} \cdot dn \cdot \gamma \cos\left(\theta + \alpha\right) = \frac{4\pi\phi H\gamma}{\rho_f \overline{r_f}} \frac{r\cos\left(\theta + \alpha\right)}{\sqrt{H^2 + 4\pi^2 r^2}} dr \tag{5.18}$$

where

$$\alpha = \arccos\left(\frac{H}{\sqrt{4\pi^2 r^2 + H}}\right) \tag{5.19}$$

By integrating Equation (5.18), we have:

$$F_{cu} = \frac{4\pi\phi H\gamma}{\rho_f \overline{r_f}} \int_0^{r_y} \frac{r\cos\left(\theta+\alpha\right)}{\sqrt{H^2+4\pi^2 r^2}} dr \tag{5.20}$$

The downward capillary force F_{cd} can be obtained in the same fashion as in the case of wicking in a fiber bundle. In order to take the twist of the yarn into account, a twist coefficient λ is introduced into the viscous drag term. Therefore, the viscous drag term becomes:

$$F_v = \lambda k L \frac{dL}{dt} \tag{5.21}$$

In the same fashion as in Equation (5.7), the solution of wicking time can be derived in terms of wicking height with

$$N = \frac{\lambda k}{\rho_l g A} \tag{5.22}$$

5.3 Experiments

In order to validate the theoretical model, a series of experiments was conducted on polyester yarn with distilled water as the wicking liquid. The fiber bundle was assumed to be circularly close-packed to establish a roughly uniform packing of fibers, and to simplify the analysis of influence of twist on the wicking behavior of the yarn. The radii of the fibers were assumed identical. The experimental apparatus is shown in Figure 5.4:

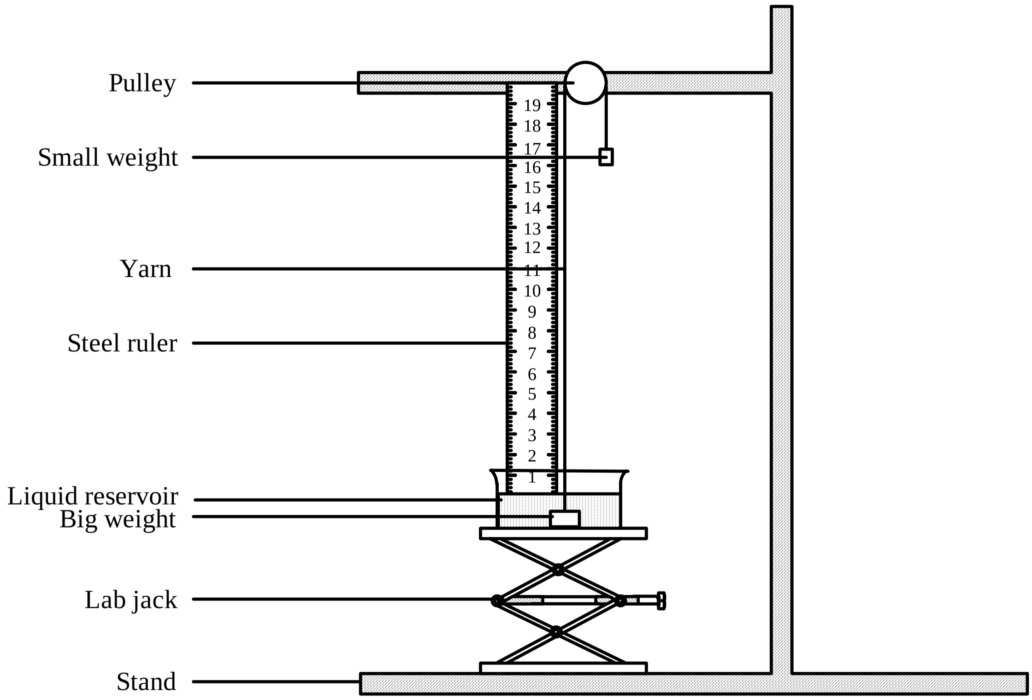

Figure 5.4 Experimental apparatus

In the apparatus, the lab jack was used to hoist the liquid reservoir containing the wicking liquid, and the steel ruler to measure the wicking height. In order to apply different tensions on the yarn, a pulley was employed with one big weight (e.g., 50g) attached to one end of the yarn, and an appropriate small weight to the other end.

The yarn wicking experiments were conducted in a standard atmosphere of 20 ± 2^{o}C and $65 \pm 2\%$ relative humidity, and the yarn packages were conditioned for 24 hours before testing. The height of the liquid rise in the yarn was observed by means of a traveling microscope. The image was captured by a CCD camera and displayed on a monitor. To enhance the observation of the liquid front advancement, indicating ink was added to the distilled water and the effect of the ink on the viscosity and surface tension of the distilled water was neglected. A stopwatch was used to record the time.

Firstly, the steel ruler and the clean beaker were adjusted to an appropriate position. Then the yarn was positioned with two weights attached to the two ends of the yarn. Attention was paid to prevent the twisted yarn from detwisting. Afterwards, the distilled water was poured into the beaker slowly until the yarn was slightly immersed in the water. At the same time the stopwatch was started. The capillary rise at different times was observed and measured by taking snapshots periodically with the CCD camera. The time and the corresponding capillary rise were continuously recorded until equilibrium was established.

As stated earlier, circularly close-packed yarns were tested in the experiments. A loosely packed polyester fiber bundle (37 fibers) with a slight twist was produced in the laboratory first. In order to prepare a circularly close-packed fiber bundle (Figure 5.5), a slight twist was first introduced into the original fiber bundle to allow the fibers to move inward freely and to rearrange their positions to establish a roughly circular close-packing.

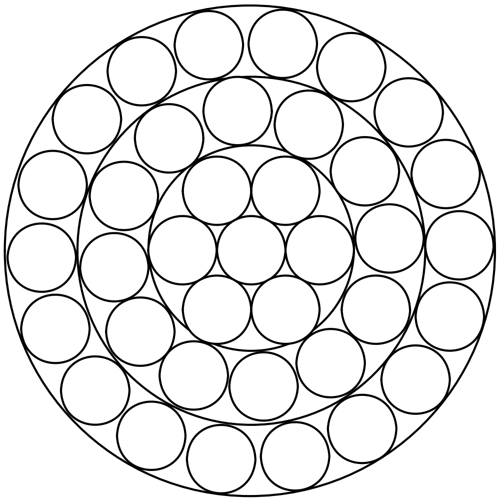

Figure 5.5 Circularly close-packed yarn with four layers

Then the wicking height at equilibrium of the liquid along the fiber bundle was tested subject to different tensions. When the tension increased gradually, the fibers of outer surface of the loose fiber bundle moved inward and the yarn became more compact. The wicking height at equilibrium therefore increased with increasing tension. When the wicking height at equilibrium did not vary significantly, as a rough approximation, the fiber bundle was assumed to be circularly close-packed and the corresponding tension was considered as the critical tension. The fiber bundle prepared by this procedure was treated as a circularly close-packed fiber bundle without twist. As twist was applied to the bundle, the twisted yarn became more compact. Thus the same tension obtained in the fiber bundle was sufficient to ensure a circular close-packing of fibers in the yarn, and therefore it was used in the subsequent tests of twisted yarns. Due to the applied tension, the shift of positions and self-assembling of fibers could be neglected. Various levels of static Z twists ranging from 100 to 500 turns per meter (tpm) were inserted into the fiber bundle using a laboratory twist tester. Due to the yarn heterogeneity, 30 measurements were needed to give a statistical representation of the yarn (Perwuelz *et al.*, 2000). Therefore, for each yarn with a specific twist level, 30 specimens were tested and the final result was the average value of the 30 measurements. Since the test time was short, evaporation of the liquid was negligible. Diffusion of the liquid into the fibers was also neglected.

A KRUSS digital tensionmeter was used to measure the surface tension of the liquid. The advancing contact angle between the fiber and the liquid was determined by the single fiber pulling-out test based on the Wihelmy principle (Batch *et al.*, 1996; Hsieh, 1995) using a dynamic contact angle analyzer.

5.4 Results and discussion

The experimental data is presented and discussed in this section. The radius of the fiber r_f was 8.4 μm and the density of the polyester fiber ρ_f was 1.38 g/cm^3. The yarn was composed of 37 fibers. All yarns had a length of 400mm. The properties of the liquid are listed in Table 5.1:

Table 5.1 Properties of the liquid

Liquid	ρ_l (kg/m^3)	γ (mN/m)	θ_a (^{o})
Distilled water	1000	72	75.75

In the fiber bundle test, the capillary rise of the liquid at equilibrium with different tensions is shown in Figure 5.6.

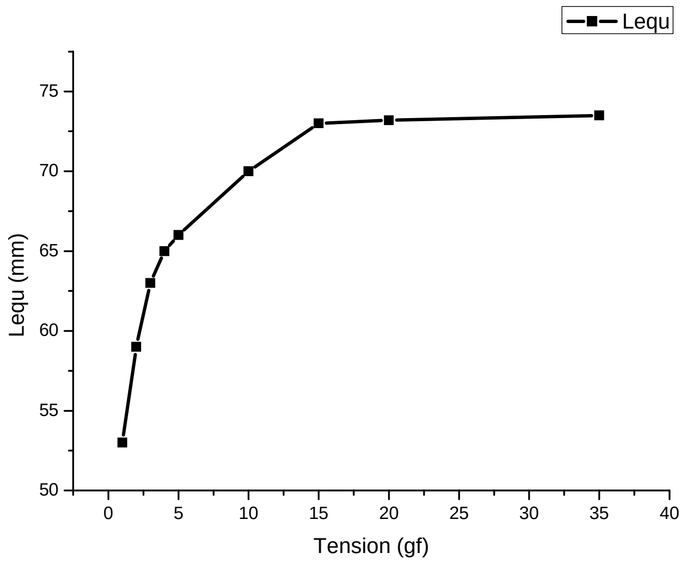

Figure 5.6 Wicking height at equilibrium in the fiber bundle (T=0 tpm)

Figure 5.6 shows that when the tension is larger than 15gf, L_{equ} does not change remarkably. Hence the tension of 15gf is considered as the critical tension, and the fiber bundle with 15gf applied tension is assumed to be circularly close-packed. This tension is then used in the subsequent tests of twisted yarns.

The experimental data and the fit of the experimental result achieved using Equation (5.7) are presented in Figure 5.7.

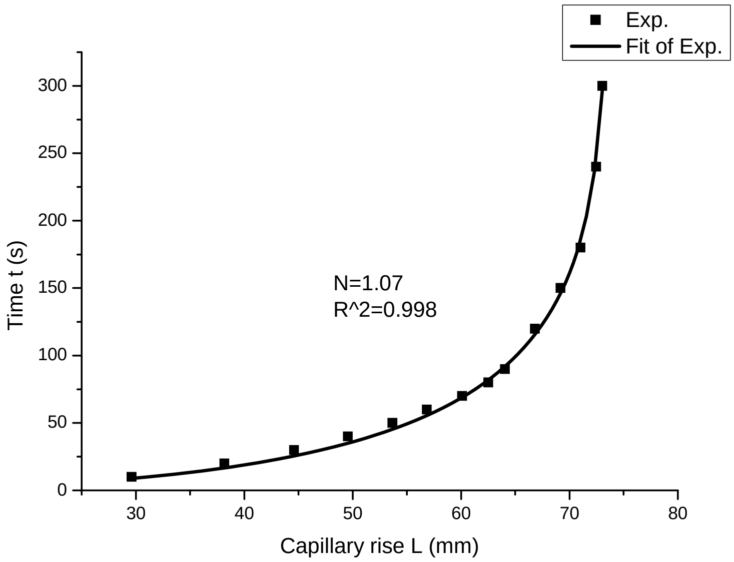

Figure 5.7 Wicking time as a function of capillary rise (T=0 tpm)

Figure 5.7 indicates that the fit result is good. Not surprisingly, the penetrating velocity of the liquid in the early stage is much higher than in the subsequent stage. With the pass of time, the advancement of the liquid becomes slower and slower until equilibrium is established. Figure 5.7 indicates that after around 200s there is no obvious change in the capillary rise, and thus the equilibrium is reached.

Figure 5.8 to Figure 5.12 show the results for twisted yarns with different twist levels. In these figures, good fit results are also found.

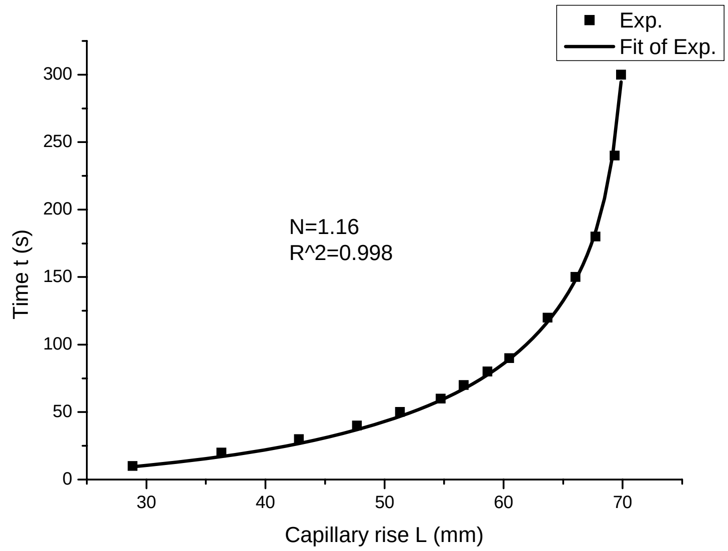

Figure 5.8 Wicking time as a function of capillary rise (T=100 tpm)

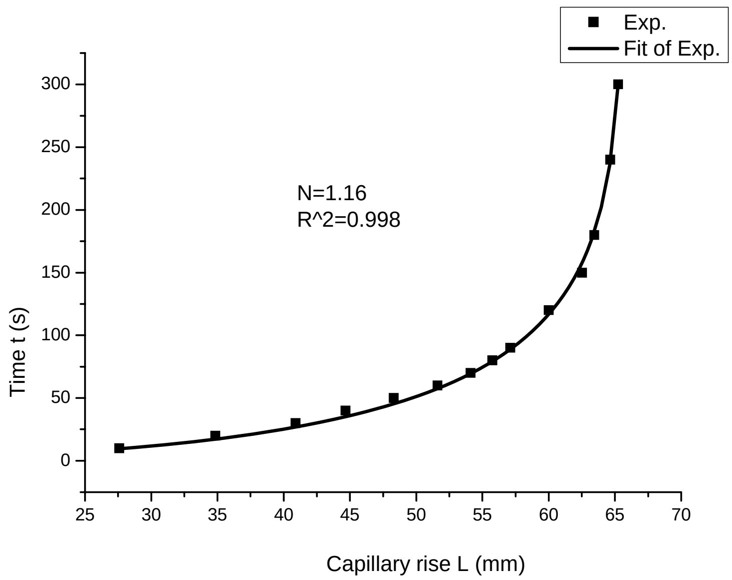

Figure 5.9 Wicking time as a function of capillary rise (T=200 tpm)

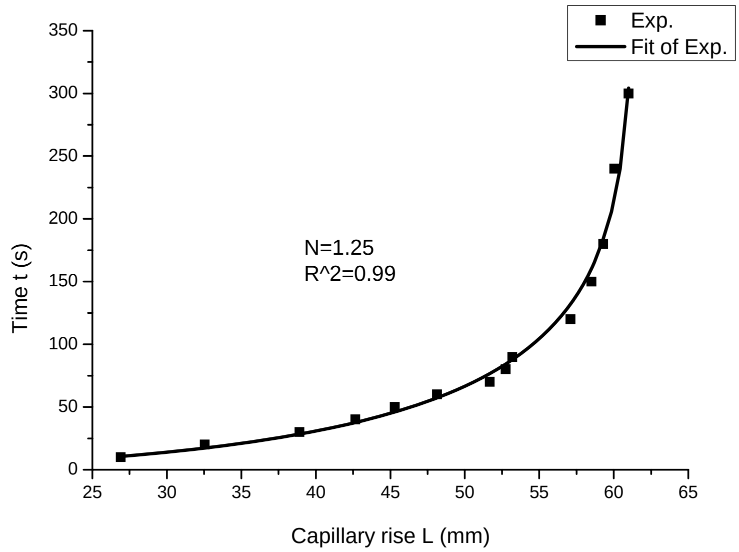

Figure 5.10 Wicking time as a function of capillary rise (T=300 tpm)

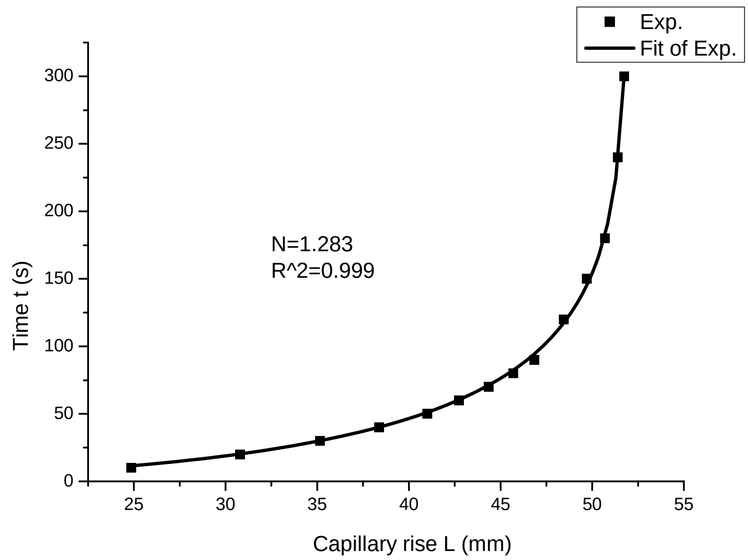

Figure 5.11 Wicking time as a function of capillary rise (T=400 tpm)

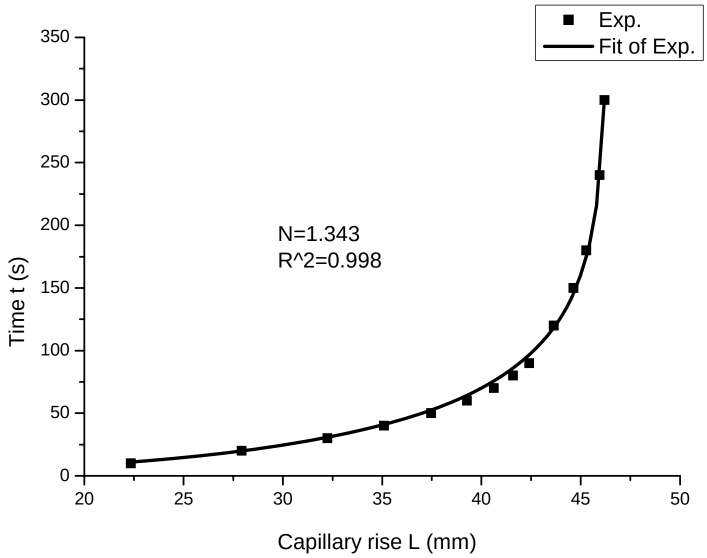

Figure 5.12 Wicking time as a function of capillary rise (T=500 tpm)

As shown in Equation (5.6), M is equivalent to L_{equ}. Figure 5.13 presents a comparison of L_{equ} derived from the calculation in this chapter and experimental results.

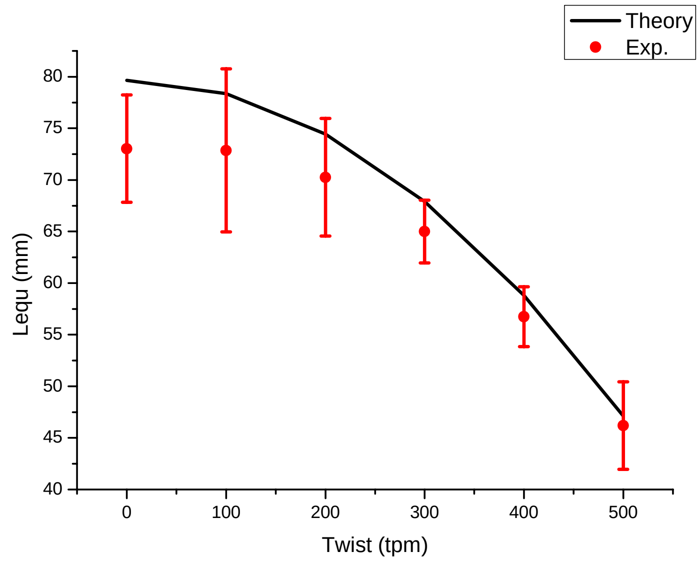

Figure 5.13 Comparison of L_{equ} derived from experimental data and theoretical prediction

Table 5.2 Relative error for different twist levels

Twist (tpm)	0	100	200	300	400	500
Error (%)	9.07	7.54	5.95	4.47	3.61	1.98

Figure 5.13 indicates that the theoretical results deviate significantly from the experimental data. This discrepancy may be attributed to the deviation of packing of the fibers from an idealized circular close-packing. When the number of constituent fibers is large, it is very difficult to accomplish a circular close-packing. Although a tension was applied to the yarn in the experiment and

the yarn may have been closely packed, the packing of fibers may have been far from the idealized circular close-packing. This may partly explain why the experimental data is smaller than the theoretical results at all twist levels. However, when more twist is inserted into the yarn, as fibers move inward and rearrange their positions, the fibers in the yarn may become more compact and close to a circular close-packing. Therefore the discrepancy between the experimental data and the theoretical results should decrease with the increase of twist level. This conclusion is in accordance with what is shown in Table 5.2.

In order to investigate the influence of twist on the wicking behavior of the yarn, the fitted values of N (the wicking resistance term) were plotted as a function of twist level and the result was fitted by means of a linear scheme (Figure 5.14).

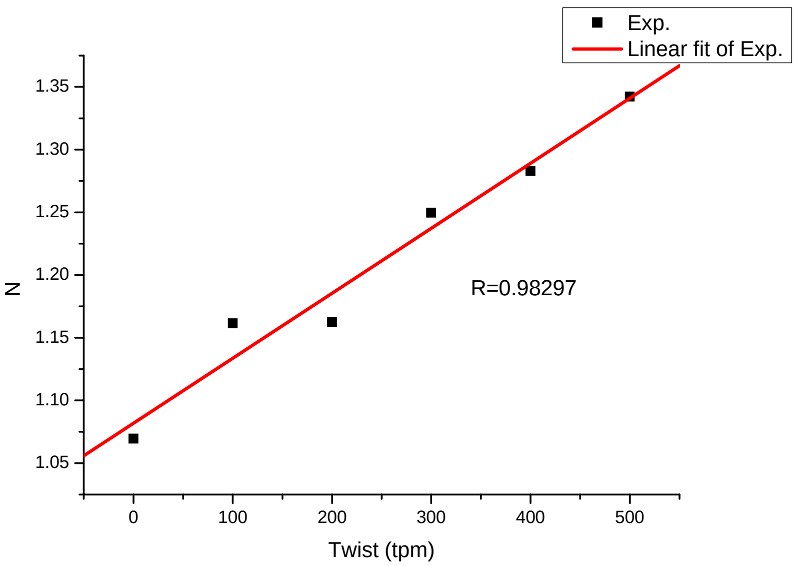

Figure 5.14 Linear fit of experimental value of N

A good linear fit is depicted in Figure 5.14. This suggests that λ grows linearly with the increase of the twist level since $k/\rho_l gA$ is constant in Equation (5.22). It is also concluded that the twist influences the viscous drag by introducing a constant λ, so-called twist coefficient, and λ linearly increases with the increase of twist.

5.5 Conclusion

The wicking behavior of a liquid in a fiber bundle as well as a twisted yarn was discussed. Using a macroscopic force balance method, the wicking time was obtained as a function of the capillary rise. In order to analyze the effect of twist on the wicking of the liquid, a twist coefficient was introduced into the viscous drag term. Experimental apparatus was designed, and a series of experiments was conducted using this apparatus. Data analysis showed that the wicking flow can be accurately described by the equation developed in this chapter. Considering the experimental error, the prediction of the capillary rise at equilibrium agreed well with the experimental data with a reasonable accuracy. By curve fitting of the experimental results, the twist coefficient was found to be constant for a specific twist, while it increases linearly with twist. As previously stated, packing of fibers in the yarn is assumed to be circularly close-packed, and packing fraction is assumed to be uniform in the model. However, packing of fibers in twisted yarn is always non-uniform, and packing density may vary from yarn center to yarn surface. This always occurs in staple fiber yarn. In this case variation of packing density of fibers along the radial direction should be considered.

Chapter 6. Coupled mechanical and liquid transfer behavior of textile yarns

6.1 Introduction

This chapter investigated vertical wicking through textile yarns subject to tension and torque. Packing of fibers in the yarn was non-uniform. A mathematical model to simulate the wicking process was developed based on a capillary penetration mechanism. Using a macroscopic force balance approach, the wicking time was derived as a function of the capillary rise of the liquid. Swelling of fibers and change of mechanical properties of fibers after absorption were considered in the model. The wicking mechanism was coupled with the mechanical properties of the yarn in a way that movement of constituent fibers of the yarn under deformation changed the pore structure of the yarn, and thus influenced the liquid transport behavior in the yarn; on the other hand, adsorption caused the fibers to swell and change their mechanical characteristics. In order to validate our model, a series of experiments was conducted on woolen yarns. Ethyl alcohol and water were used as non-swelling and swelling liquid. The influence of twist level of the yarn on the capillary flow was also investigated.

6.2 Model development

6.2.1 Notation

The following notations are used in this chapter. Subscripts 0 and 1 denote initial state and deformed state. "'" stands for saturated state.

F_c capillary force

F_{cu}, F_{cd} upward capillary force, downward capillary force

F_{cuj}, F_{cuu} upward capillary forces due to jammed region and unstrained region

F_g, F_v, F_i forces due to gravity, viscous drag and inertia

ρ_l density of liquid

ρ_f density of fiber

A area available for liquid flow in the yarn cross section

A_y cross-sectional area of the yarn

A_{fj}, A_{fu} total areas of fibers in jammed region and unstrained region

L axial wicking height of the liquid

k frictional coefficient (for the initial yarn without further twist)

λ twist coefficient

β factor

P_j perimeter wetted by the liquid in the jammed region

P_l	cross-sectional perimeter of the liquid column
θ_a	advancing contact angle between the liquid and the fiber
γ	surface tension of the liquid
r_y	radius of the yarn
ϕ_{jam}	fiber packing density in a jammed region
$\phi(r)$	packing density of fibers in the yarn
r_{fi}	radius of individual fiber
$\overline{r_f}$	average radius of fiber
n	number of fibers
H	pitch length of the helix of the fiber path
T	twist level
r	radius of the fiber helical path
L_f	fiber length
α	helix angle
g	gravitational acceleration
t	time
$\xi_y,\ \xi_\theta$	yarn tensile and torsional strain

r_A initial radial position of fibers that will be the outer boundary of a jammed region

r_{Ajam} radius of the outer boundary of the jammed region after deformation

T_{ten} applied tension on the yarn

U_{tot} total energy of yarn

M, N parameters in expression describing the wicking mechanism

6.2.2 Without considering swelling of fibers

When a yarn is dipped in a liquid, the liquid will penetrate into the yarn due to the drag of capillary force arising from the liquid-solid interfaces. As an elementary model, permeation of liquid into fibers and swelling of fibers are not considered in this section. Mechanical properties of fibers are assumed to remain constant during the wicking process. Supposing radii of constituent fibers are circular, the schematic illustration of the cross-section of the solid-liquid-gas system is shown in Figure 5.1. If wicking height L is sufficiently large ($L \gg r_y$), dimension of the meniscus of liquid front is negligible. Similar to the analysis in Chapter 5, the following forces determine the movement of the liquid:

capillary force: F_c

gravity: $F_g = \rho_l gAL$

viscous drag: $F_v = \lambda kL \dfrac{dL}{dt}$

inertia: $F_i = \frac{d}{dt}\left[\rho_l AL\frac{dL}{dt}\right]$

Capillary force F_c consists of an upward force F_{cu} arising from interaction between the liquid and the fibers, and a downward force F_{cd} due to the concave liquid-gas interface (Liu *et al.*, 2007a; Princen, 1968; Princen, 1969, 1970). Therefore,Equation Chapter 6 Section 1

$$F_c = F_{cu} - F_{cd} \tag{6.1}$$

The inertia term arises from Newton's second law of motion. However, except for the early stage of wicking, the inertia term is negligible when acceleration of the liquid is slow. The balance of forces hence is:

$$F_c - \rho_l gAL - kL\frac{dL}{dt} = 0 \tag{6.2}$$

Rearranging Equation (6.2), we have:

$$\frac{dL}{dt} = \frac{1}{k}\left(\frac{F_c}{L} - \rho_l gA\right) \tag{6.3}$$

Let

$$M = \frac{F_c}{\rho_l gA}, \quad N = \frac{\lambda k}{\rho_l gA} \tag{6.4}$$

where λ is a twist coefficient. For the initial yarn without any further twist, λ is 1. By integrating and applying the initial condition $t = 0,\ L = 0$, we can obtain the solution:

$$t = N\left(M \ln \frac{M}{M-L} - L\right) \tag{6.5}$$

When equilibrium is established, the capillary force should be balanced by the gravity of the liquid penetrating into the yarn. That means:

$$L_{equ} = \frac{F_c}{\rho_l g A} = M \tag{6.6}$$

Therefore, Equation (6.5) becomes:

$$t = N\left(L_{equ} \ln \frac{L_{equ}}{L_{equ}-L} - L\right) \tag{6.7}$$

In this chapter the model of yarn structure developed in Chapter 3 was employed. Fiber migration in the transverse direction was neglected. A typical constitute fiber is shown in Figure 5.3. When a loose staple-fiber yarn is subject to tension and torque, a jammed region will appear in the central area of the yarn, and those fibers which are located in the outer layer are unstrained (Liu *et al.*, 2007b) (Figure 3.1). According to the theory discussed in Chapter 3, the helical radius of one typical fiber r_1 in the strained state can be obtained by:

$$r_1 = \begin{cases} \sqrt{\dfrac{2}{\phi_{jam}\left(1+\xi_y\right)} \displaystyle\int_0^{r_0} r_0 \phi_0\left(r_0\right) dr_0} & r_0 \le r_A \\ \sqrt{\dfrac{4\pi^2 r_0^2 + H_0^2\left(1-\left(1+\xi_y\right)^2\right)}{4\pi^2\left(1+\xi_\theta\right)^2}} & r_0 > r_A \end{cases} \tag{6.8}$$

An energy method (Treloar and Riding, 1963) was employed to determine yarn tensile strain ξ_y in which

$$T_{ten} = \frac{\partial U_{tot}}{\partial \xi_y} / H_0 \tag{6.9}$$

Calculation of total energy of yarn is discussed in detail in Chapter 3. Given T_{ten} and ξ_θ, an iteration method was adopted to obtain ξ_y using Equation (6.9). r_A, r_{Ajam} can be obtained by solving the system of Equations (6.10) and (6.11):

$$\int_0^{r_A} r_0 \phi(r_0) dr_0 = \frac{\left(4\pi^2 r_A{}^2 + H_0{}^2 - H_0{}^2\left(1+\xi_y\right)^2\right)\left(1+\xi_y\right)\phi_{jam}}{8\pi^2\left(1+\xi_\theta\right)^2} \tag{6.10}$$

$$\left(2\pi r_A\right)^2 + H_0{}^2 = \left(2\pi r_{Ajam}\right)^2\left(1+\xi_\theta\right)^2 + H_0{}^2\left(1+\xi_y\right)^2 \tag{6.11}$$

Due to different pore structures, capillary forces arising from interactions between fiber-liquid interfaces are different in the jammed region and the unstrained region, and therefore they should be considered separately. This means:

$$F_{cu} = F_{cuj} + F_{cuu} \tag{6.12}$$

Consider an element area of cross section of the jammed region between radii *r* and *r*+*dr*. Supposing that the radii of fibers are circular, the total perimeter of fibers in the jammed region wetted by the liquid can be obtained by:

$$P_j = 2\pi \sum_{i=1}^{n} r_{fi} \tag{6.13}$$

If a packing density function is introduced, and variation of radii of fibers and change of radii of fibers during deformation is insignificant, then the number of fibers inside the element area can be given by:

$$dn = \frac{H_0\left(1+\xi_y\right)\cdot 2\pi r_1 dr_1 \cdot \phi_{jam}}{\rho_f \cdot \pi \overline{r_f}^2 \cdot L_{f1}} \tag{6.14}$$

Therefore,

$$\begin{aligned} dF_{cuj} &= 2\pi\overline{r_f}\cdot\gamma\cos\left(\alpha+\theta_a\right)\cdot dn \\ &= 2\pi\overline{r_f}\cdot\gamma\cos\left(\alpha+\theta_a\right)\cdot\frac{H_0\left(1+\xi_y\right)\cdot 2\pi r_1 dr_1\cdot\phi_{jam}}{\rho_f\cdot\pi\overline{r_f}^2\cdot L_{f1}} \\ &= \frac{4\pi\phi_{jam}\gamma H_0\left(1+\xi_y\right)}{\rho_f\overline{r_f}}\cdot\frac{r_1\cos\left(\alpha+\theta_a\right)}{\sqrt{4\pi^2 r_1^2\left(1+\xi_\theta\right)^2+H_0{}^2\left(1+\xi_y\right)^2}}dr_1 \end{aligned} \tag{6.15}$$

where

$$\alpha = \arccos\left(\frac{H_0\left(1+\xi_y\right)}{\sqrt{4\pi^2 r_1^2\left(1+\xi_\theta\right)^2+H_0{}^2\left(1+\xi_y\right)^2}}\right) \tag{6.16}$$

Integrating Equation (6.15), we have:

$$F_{cuj} = \frac{4\pi\phi_{jam}\gamma H_0\left(1+\xi_y\right)}{\rho_f\overline{r_f}}\int_0^{r_{Ajam}}\frac{r_1\cos\left(\alpha+\theta_a\right)}{\sqrt{4\pi^2 r_1^2\left(1+\xi_\theta\right)^2+H_0{}^2\left(1+\xi_y\right)^2}}dr_1 \tag{6.17}$$

In a similar fashion, we can obtain:

$$\begin{aligned}dF_{cuu} &= 2\pi\overline{r_f}\cdot\gamma\cos\left(\alpha+\theta_a\right)\cdot dn\\ &=2\pi\overline{r_f}\cdot\gamma\cos\left(\alpha+\theta_a\right)\cdot\frac{H_0\left(1+\xi_y\right)\cdot 2\pi r_1 dr_1\cdot\phi_1\left(r_1\right)}{\rho_f\cdot\pi\overline{r_f}^2\cdot L_{f1}}\\ &=\frac{4\pi\gamma H_0\left(1+\xi_y\right)}{\rho_f\overline{r_f}}\cdot\frac{r_1\cos\left(\alpha+\theta_a\right)\phi_1\left(r_1\right)}{\sqrt{4\pi^2 r_1^2\left(1+\xi_\theta\right)^2+H_0{}^2\left(1+\xi_y\right)^2}}dr_1\end{aligned} \tag{6.18}$$

Thus,

$$F_{cuu}=\frac{4\pi\gamma H_0\left(1+\xi_y\right)}{\rho_f\overline{r_f}}\int_{r_{Ajam}}^{r_{y1}}\frac{r_1\cos\left(\alpha+\theta_a\right)\phi_1\left(r_1\right)}{\sqrt{4\pi^2 r_1^2\left(1+\xi_\theta\right)^2+H_0{}^2\left(1+\xi_y\right)^2}}dr_1 \tag{6.19}$$

In the unstrained region where $r_1 > r_{Ajam}$, supposing the fiber helices in the yarn can not pass one another in the radial direction during deformation, then the mass of fibers inside a specific area remains constant before and after deformation, thus we have:

$$\int_{r_A}^{r_0} 2\pi r H_0\phi_0\left(r\right)dr=\int_{r_{Ajam}}^{r_1} 2\pi r H_0\left(1+\xi_y\right)\phi_1\left(r\right)dr \tag{6.20}$$

By cancelling the same term, we obtain:

$$\int_{r_A}^{r_0} r\phi_0\left(r\right)dr=\int_{r_{Ajam}}^{r_1} r\left(1+\xi_y\right)\phi_1\left(r\right)dr \tag{6.21}$$

Taking the derivative at both sides with respect to r_0 we get:

$$r_0\phi_0\left(r_0\right)dr_0=r_1\phi_1\left(r_1\right)\left(1+\xi_y\right)dr_1=r_1\phi_1\left(r_1\right)\left(1+\xi_y\right)\frac{\dfrac{8\pi^2 r_0}{4\pi^2\left(1+\xi_\theta\right)^2}}{2r_1}dr_0 \tag{6.22}$$

Therefore,

$$\phi_1\left(r_1\right)=\frac{\left(1+\xi_\theta\right)^2}{1+\xi_y}\phi_0\left(r_0\right) \tag{6.23}$$

Substituting Equations (6.8) and (6.23) into Equation (6.19), we have:

$$F_{cuu}=\frac{4\pi\gamma H_0}{\rho_f \overline{r_f}}\int_{r_A}^{r_{y0}}\frac{r_0\phi_0\left(r_0\right)\cos\left(\alpha+\theta_a\right)}{\sqrt{4\pi^2 r_0^{\,2}+H_0^{\,2}}}dr_0 \tag{6.24}$$

Similarly, the total area of fibers A_f also consists of two parts, A_{fj} and A_{fu}. According to Equation (5.12), the area available for liquid flow is therefore obtained by:

$$A=A_y-A_f=\beta\pi r_{y1}^{\,2}-A_{fj}-A_{fu} \tag{6.25}$$

In the jammed region where $r_1 \le r_{Ajam}$,

$$\begin{aligned} dA_{fj} &= dn\cdot\pi\overline{r_f}^{\,2} \\ &= \frac{H_0\left(1+\xi_y\right)\cdot 2\pi r_1 dr_1\cdot\phi_{jam}}{\rho_f\cdot\pi\overline{r_f}^{\,2}\cdot L_{f1}}\cdot\pi\overline{r_f}^{\,2} \\ &= \frac{2\pi\phi_{jam}H_0\left(1+\xi_y\right)}{\rho_f}\frac{r_1}{\sqrt{4\pi^2 r_1^2\left(1+\xi_\theta\right)^2+H_0^{\,2}\left(1+\xi_y\right)^2}}dr_1 \end{aligned} \tag{6.26}$$

Hence,

$$A_{fj}=\frac{2\pi\phi_{jam}H_0\left(1+\xi_y\right)}{\rho_f}\int_0^{r_{Ajam}}\frac{r_1}{\sqrt{4\pi^2 r_1^2\left(1+\xi_\theta\right)^2+H_0^{\,2}\left(1+\xi_y\right)^2}}dr_1 \tag{6.27}$$

In the unstrained region where $r_1 > r_{Ajam}$,

$$
\begin{aligned}
dA_{fu} &= dn \cdot \pi \overline{r_f}^2 \\
&= \frac{H_0\left(1+\xi_y\right) \cdot 2\pi r_1 dr_1 \cdot \phi_1\left(r_1\right)}{\rho_f \cdot \pi \overline{r_f}^2 \cdot L_{f1}} \cdot \pi \overline{r_f}^2 \\
&= \frac{2\pi H_0\left(1+\xi_y\right)}{\rho_f} \frac{r_1 \phi_1\left(r_1\right)}{\sqrt{4\pi^2 r_1^2\left(1+\xi_\theta\right)^2 + H_0^2\left(1+\xi_y\right)^2}} dr_1
\end{aligned}
\tag{6.28}
$$

Therefore A_{fu} is obtained by integrating Equation (6.28):

$$
A_{fu} = \frac{2\pi H_0\left(1+\xi_y\right)}{\rho_f} \int_{r_{Ajam}}^{r_{y1}} \frac{r_1 \phi_1\left(r_1\right)}{\sqrt{4\pi^2 r_1^2\left(1+\xi_\theta\right)^2 + H_0^2\left(1+\xi_y\right)^2}} dr_1 \tag{6.29}
$$

Substituting Equations (6.8) and (6.23) into Equation (6.29), we obtain:

$$
A_{fu} = \frac{2\pi H_0}{\rho_f} \int_{r_A}^{r_{y0}} \frac{r_0 \phi_0\left(r_0\right)}{\sqrt{4\pi^2 r_0^2 + H_0^2}} dr_0 \tag{6.30}
$$

The downward capillary force is given by:

$$
F_{cd} = P_l \gamma \tag{6.31}
$$

P_l can be obtained in the same fashion as in Chapter 5, and β is given by:

$$
\beta = \frac{2A_f \gamma}{F_{cu} r_{y1}} \tag{6.32}
$$

6.2.3 Considering swelling of fibers

When a yarn is dipped in a swelling liquid, the liquid will not only penetrate into the yarn, but also permeate into the fibers. Absorption of the liquid will cause the fibers to swell and change the mechanical properties of the fibers. On the other hand, swelling of fibers will change the pore structures between fibers and the pathway of the liquid flow, thus affecting the whole wicking process. Since the mechanical properties and swelling of fibers vary with time, information on fibers at all time levels should be obtained if the whole wicking process is to be modeled. This seems to by unrealistic. Thus it may be more realistic to consider two extreme cases: dry state and saturated state. In the first case, wool fibers are assumed not to take up any liquid. Hence the wicking can be modeled by means of the theory discussed in Section 6.2.2. In the second case, wool fibers are supposed to become saturated instantly, and change of mechanical properties and swelling of fibers take place immediately once the yarn contacts the liquid. The wicking process is determined by the saturated structures of fibers. These two extreme cases are expected to provide an insight into the dynamic interactions between the fibers and the liquid, and the real wicking is anticipated to lie between these two extreme cases.

In the saturated case, it was found that the longitudinal swelling of fiber was very small (Earland, 1963), therefore only transverse swelling is considered. In the saturated state, the mechanical properties of fiber ($E_1^{'}$, $E_2^{'}$, $E_3^{'}$, $E_4^{'}$), fiber density $\rho_f^{'}$ and fiber radius $r_f^{'}$ can be obtained experimentally. Due to the different structures of jammed and unstrained areas (Figure 3.1), packing density of fibers in these two regions should be calculated separately. Suppose ratio of transverse swelling of fiber is a, then:

$$\overline{r_f}' = (1+a)\overline{r_f} \quad (6.33)$$

Since fibers in the jammed region cannot move transversely, then swelling of fibers will cause expansion of the whole jammed region. Therefore:

$$r'_{Ajam} = (1+a) r_{Ajam} \quad (6.34)$$

The packing density of the jammed region in the saturated state ϕ'_{jam} is given by:

$$\phi'_{jam} = \frac{\dfrac{\phi_{jam} \cdot \pi r_{Ajam}^2 \cdot H_1}{\rho_f \cdot \pi \overline{r_f}^2 \cdot H_1}}{\pi r'^2_{Ajam} \cdot H_1} = \frac{\rho'_f}{\rho_f} \phi_{jam} \quad (6.35)$$

In the unstrained region fibers are comparatively loose and spaces between fibers are large. Therefore, it is reasonable to assume that the swelling of fiber will only fill the pores between fibers while not contacting any other surrounding fibers during swelling. With this assumption, the transverse positions of fibers and boundary of the unstrained region remain the same after swelling. Then packing density of the unstrained region can be obtained by:

$$\phi'_1 = \frac{\rho'_f}{\rho_f} \phi_1 \quad (6.36)$$

Substitute Equations (6.33), (6.34), (6.35)and (6.36) into Equations (6.17), (6.24), (6.27) and (6.30), we get:

$$F_{cuj} = \frac{4\pi \phi_{jam} \gamma H_0 \left(1+\xi'_y\right)}{(1+a)\rho_f \overline{r_f}} \int_0^{(1+a)r_{Ajam}} \frac{r_1 \cos(\alpha + \theta_a)}{\sqrt{4\pi^2 r_1^2 \left(1+\xi_\theta\right)^2 + H_0^2 \left(1+\xi_y\right)^2}} dr_1 \quad (6.37)$$

$$F_{cuu} = \frac{4\pi \gamma H_0}{(1+a)\rho_f} \int_{r_A}^{r_{y0}} \frac{r_0 \phi_0 (r_0) \cos(\alpha + \theta_a)}{\sqrt{4\pi^2 r_0^2 + H_0^2}} dr_0 \quad (6.38)$$

$$A_{fj} = \frac{2\pi\phi_{jam}H_0\left(1+\xi_y^{'}\right)}{\rho_f}\int_0^{(1+a)r_{Ajam}} \frac{r_1}{\sqrt{4\pi^2 r_1^2\left(1+\xi_\theta\right)^2 + H_0^2\left(1+\xi_y\right)^2}}dr_1 \quad (6.39)$$

$$A_{fu} = \frac{2\pi H_0}{\rho_f}\int_{r_A}^{r_{y0}} \frac{r_0\phi_0\left(r_0\right)}{\sqrt{4\pi^2 r_0^2 + H_0^2}}dr_0 \quad (6.40)$$

Once capillary force F_c and area available for liquid flow A are obtained, capillary rise at equilibrium L_{equ} can be calculated using Equation (6.6). The flow of the model development is shown in Figure 6.1.

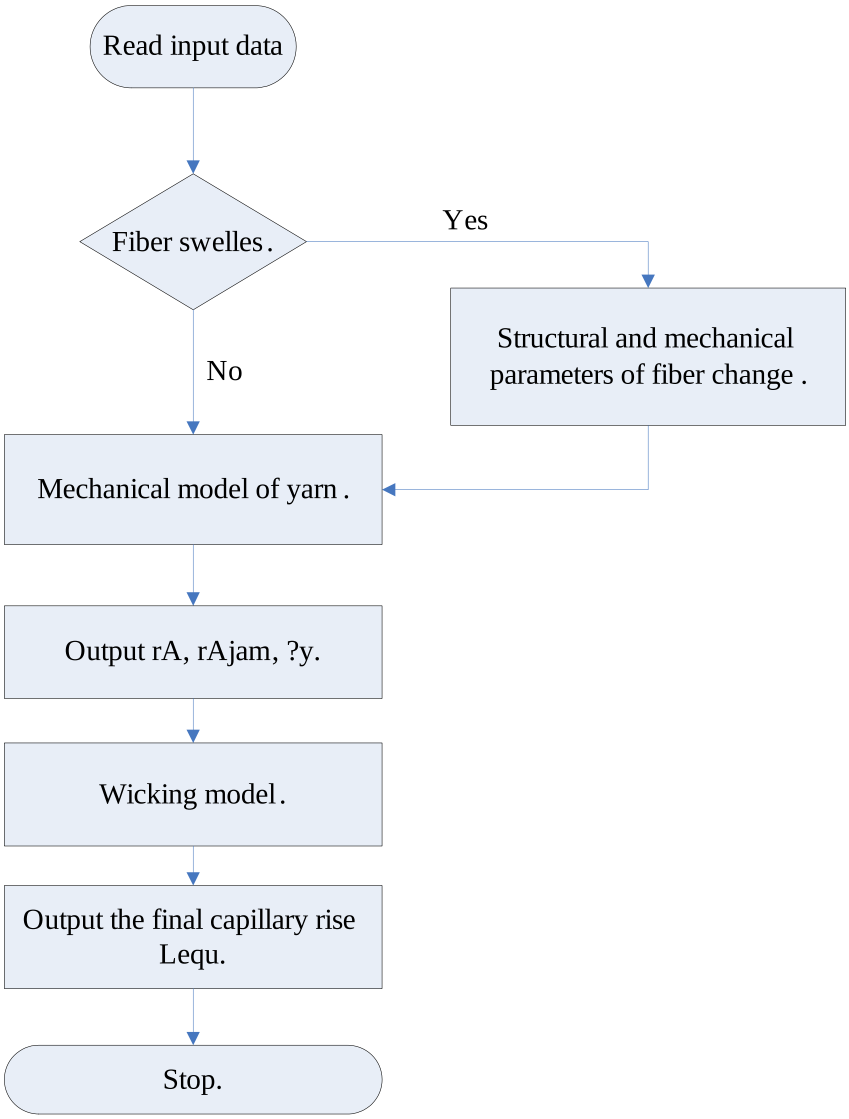

Figure 6.1 Flow chart of the development of the coupled model

6.3 Experiments

In order to validate our theoretical model, a series of experiments was conducted on woolen spun carpet yarns. Two kinds of liquid were used as wicking liquid: ethyl alcohol and water.

Ethyl alcohol was used due to its good wettability. It was found that it took several minutes for capillary rise of ethyl alcohol to reach equilibrium during a vertical wicking test. However, it was established in separate experiments that diffusion of ethyl alcohol into wool fiber was very slow, and it took hours to establish equilibrium. Therefore, ethyl alcohol was considered as a non-swelling liquid, and absorption of ethyl alcohol was negligible during the series of tests. Change of the mechanical properties from dry to wet and swelling of fiber were also neglected.

The considerable affinity of wool fibers for water is a well-known property. However, it was found that wicking of pure water in a wool yarn was very poor. This may be attributed to the nature of the surface of wool fiber and large contact angle between wool fiber and water, whereas the absorption of water proceeds mainly internally. In order to enhance the wicking of water in wool yarns, a small amount of detergent was added to the water. It was found that the wicking was significantly improved, and swelling of fibers occurred simultaneously with wicking. Radial swelling of wool fiber from dry to saturated was measured with a microscope. In order to obtain a saturated fiber, the fiber was immersed into the water mixture for 24 hours allowing the fiber to be fully saturated. Then the fiber was taken out and measured immediately. Fifty fiber specimens were measured and the mean value was used as the final swelling ratio. In order to get the whole load-strain curve of saturated wool fiber, the fiber was firstly immersed to the water mixture to establish a saturated state. Then the fiber was taken out and immediately tested on an Instron Tensile Tester. Fifty fiber specimens were tested to obtain a mean. Four piecewise linear straight lines were fitted to the mean curve profile in order to simplify the calculation.

The experimental apparatus used to test yarn vertical wicking is shown in Figure 5.4. The experiments were conducted in a standard atmosphere of $20 \pm 2^{o}C$ and $65 \pm 2\%$ relative humidity, and the yarn packages were conditioned for 24 hours before testing. The height of the liquid rise in the yarn was observed by means of a traveling microscope. The image was captured by a CCD camera and displayed on a monitor. To enhance the observation of the liquid front advancement, a small amount of basic dye (Ciba Geigy Maxilon Red GRL Pearls) was added to the liquid and the effect of the dye on the viscosity and surface tension of the liquid was neglected. During the experiments, the specimens of yarn were enclosed in a bore glass tube to reduce evaporation. A stopwatch was used to record the time. A laboratory twist tester was employed to introduce various twist levels into the yarn.

The experimental procedure was similar to what had been described in Chapter 5. Due to the yarn heterogeneity, 30 measurements were needed to supply a statistical representation of the yarn (Perwuelz *et al.*, 2000). Therefore, for each yarn with a specific twist level, 30 specimens were tested and the final result was the average value of the 30 measurements.

A KRUSS digital tensionmeter was used to measure the surface tension of the liquid. The advancing contact angle between the fiber and the liquid was determined by the single fiber pulling-out test based on the Wihelmy principle (Batch *et al.*, 1996; Hsieh, 1995) using a dynamic contact angle analyzer.

6.4 Results and discussion

The experimental data and theoretical result are presented and discussed in this section. ϕ_{jam} was 1g/cm^3. The physical parameters of initial yarn and fiber are listed in Table 3.1. The mean load-strain curve of dry fiber is shown in Figure 3.6. Four piecewise linear straight lines as shown in Figure 3.7 are fitted to the mean curve profile in order to simplify the calculation. The moduli of the four strain intervals are shown in Table 3.2. With reference to material mechanics theory, we can derive fiber bending and torsional rigidity from the tensile modulus at different stages with the assumption that the Poisson's ratio of the fiber is equal to 0.5. A cubic function was adopted to fit the experimental data (Equation (3.28)).

6.4.1 Ethyl alcohol

The characteristics of the liquid are shown in Table 6.1.

Table 6.1 Properties of the liquid

Liquid	ρ_l (kg/m^3)	γ (mN/m)	θ_a (^{o})
Ethyl alcohol	789	22.3	53

The experimental data and the fit of the experimental result by Equation (6.7) for the initial yarn are presented in Figure 6.2.

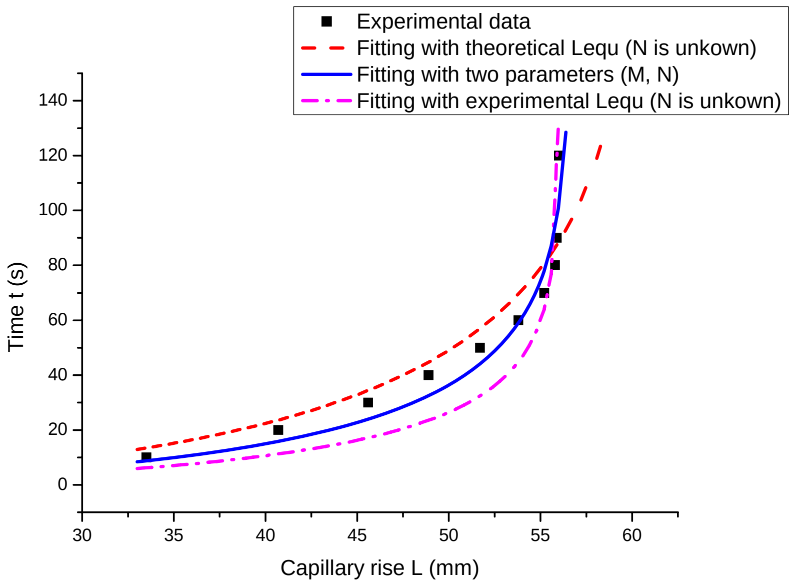

Figure 6.2 Wicking time as a function of capillary rise (T=191 tpm, T_{ten} =10gf)

Figure 6.2 indicates that there is a slight discrepancy between the experimental data and the fitting result with either theoretical L_{equ} or experimental L_{equ}. Although fitting with theoretical L_{equ} deviates slightly with experimental data, this is justifiable since L_{equ} is overestimated using the calculations presented in this Chapter (this will be discussed later). Not surprisingly, the penetrating velocity (gradient of tangent with respect to Y axis) of the liquid in early stage is much higher than in subsequent stages. As time passes, the advancement of the liquid becomes slower and slower until equilibrium is established. Figure 6.2 also suggests that after around 100s there is no obvious change in the capillary rise, and thus equilibrium is reached.

Figure 6.3 to Figure 6.6 show the results for yarns with different additional twist levels. In these figures, similar findings are observed.

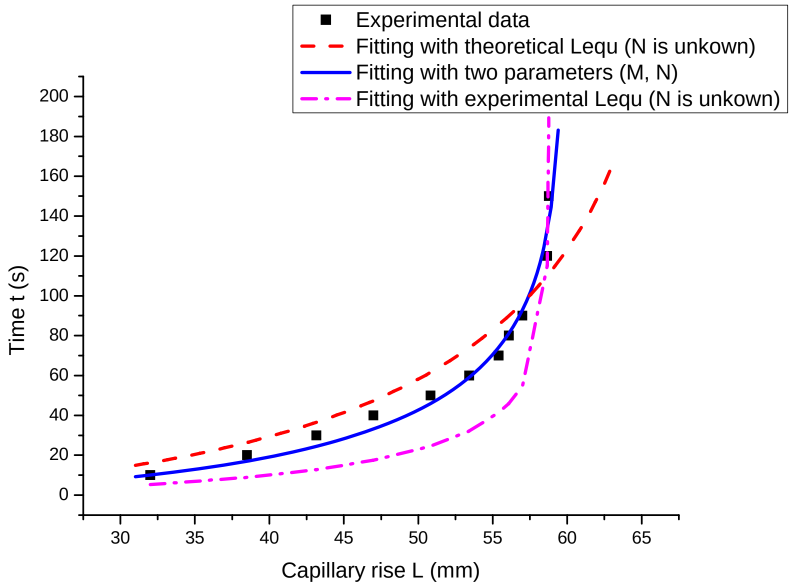

Figure 6.3 Wicking time as a function of capillary rise (T=216 tpm, T_{ten} =10gf)

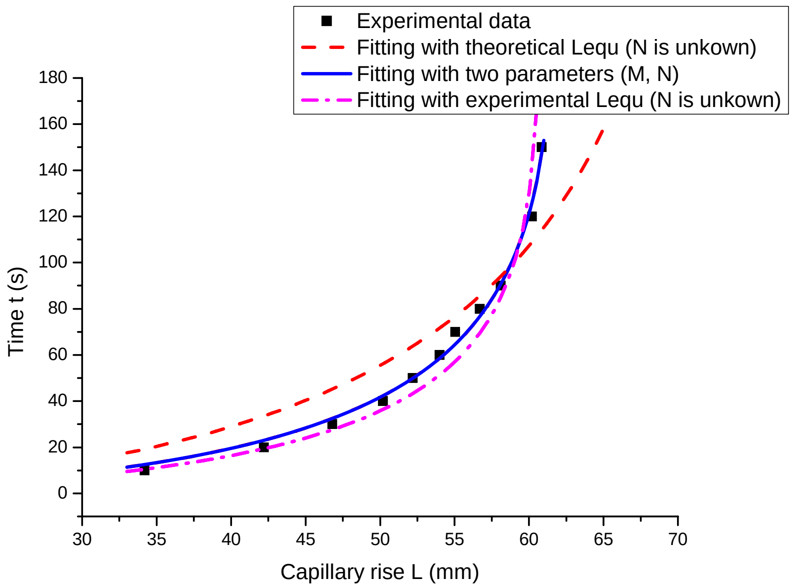

Figure 6.4 Wicking time as a function of capillary rise (T=241 tpm, T_{ten} =10gf)

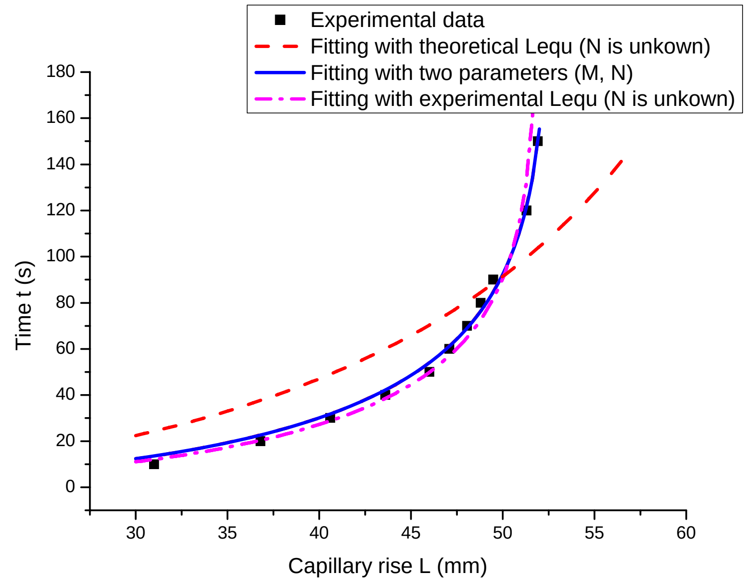

Figure 6.5 Wicking time as a function of capillary rise (T=266 tpm, T_{ten} =10gf)

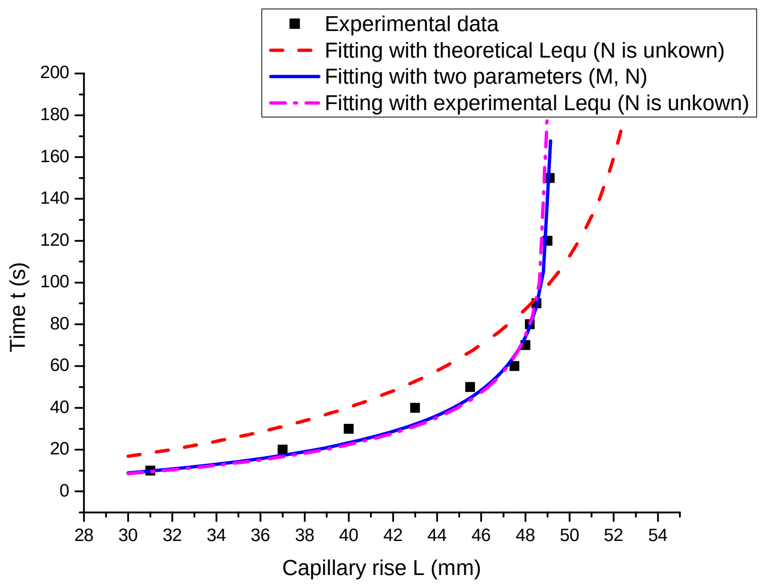

Figure 6.6 Wicking time as a function of capillary rise (T=291 tpm, T_{ten} =10gf)

As shown in Equation (6.6), M is equivalent to L_{equ}. Figure 6.7 presents a comparison of L_{equ} derived from Equation (6.6) and experimental results.

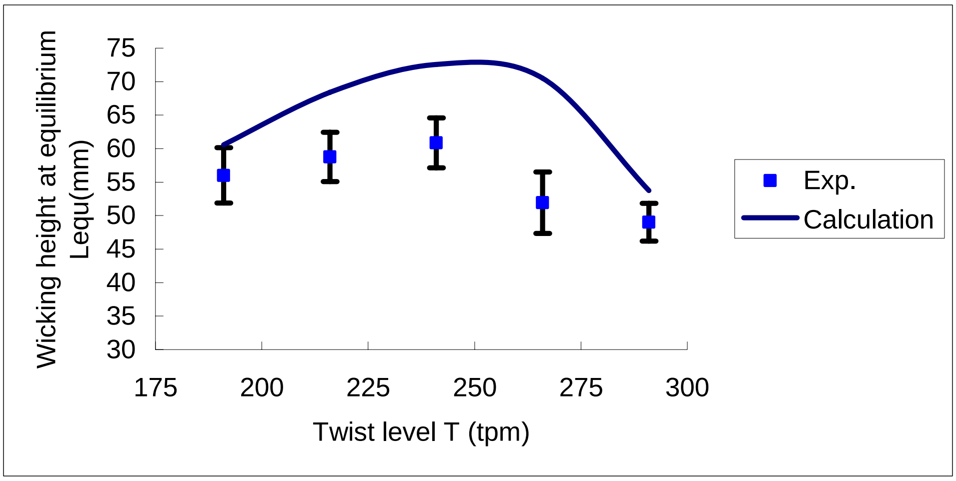

Figure 6.7 Comparison of L_{equ} derived from experimental data and theoretical calculation

Table 6.2 Relative error for different twist levels

Twist (tpm)	191	216	241	266	291
Error (%)	8.12	16.41	19.21	35.85	9.72

Figure 6.7 suggests that the theoretical results deviate significantly from the experimental data, and the relative error is shown in Table 6.2. This discrepancy may be attributed to the deviation of the structure of wool yarn from the idealized

yarn model. To simplify the model, a continuous filament yarn structure was adopted to simulate the wool yarn. However, constituent fibers in wool yarns are discontinuous, and they may migrate inward or outward in the radial direction. The irregularity of fiber path and discontinuity at fiber ends may lead to discontinuity of capillaries between fibers. This apparently reduces the wicking of the liquid in the yarn. Hairiness and evenness of yarn also have impact on the wicking. These factors partly explain why the experimental data is lower than the theoretical result at all twist levels.

From Figure 6.7 it can also be observed that L_{equ} increases with the increase of twist levers at comparatively low twist levers and reaches the maximum at a certain twist level. After that L_{equ} decreases with the advancement of twist level. At lower twist level, the yarn is loosely packed. When additional twist is inserted into the yarn, constituent fibers tend to move inward and the yarn becomes more compact. This appears to reduce the effective radii of interfiber capillaries, and hence enhance the wicking. The wicking reaches the maximum when the yarn is nearly closely packed. After that with the introduction of additional twist into the yarn effective radii of interfiber capillaries do not change a lot, while increase of inclination of fiber may lead to lower upward capillary force (Equations (6.17) and (6.19)). Furthermore, increase of tortuosity may cause longer flow path of the liquid. This may also contribute the reduction of wicking.

As shown in Figure 6.7, the twist level at which the wicking reaches the maximum in experimental data (around 240 tpm) deviates slightly from that of the theoretical prediction (around 250 tpm). This may be partly due to the error introduced in the estimation of packing density of fibers.

In order to investigate the influence of twist on the wicking behavior of the yarn, the values of λ at different twists are calculated by Equation (6.4) where N is obtained by fitting the experimental data using the two-parameter scheme. The result is listed in Table 6.3 and plotted as a function of twist level in Figure 6.8, and the result was fitted by a linear scheme. Calculated value of k is 6.599×10^{-3}.

Table 6.3 Values of λ

Twist (tpm)	191	216	241	266	291
λ	1.000	0.846	0.625	0.503	0.394

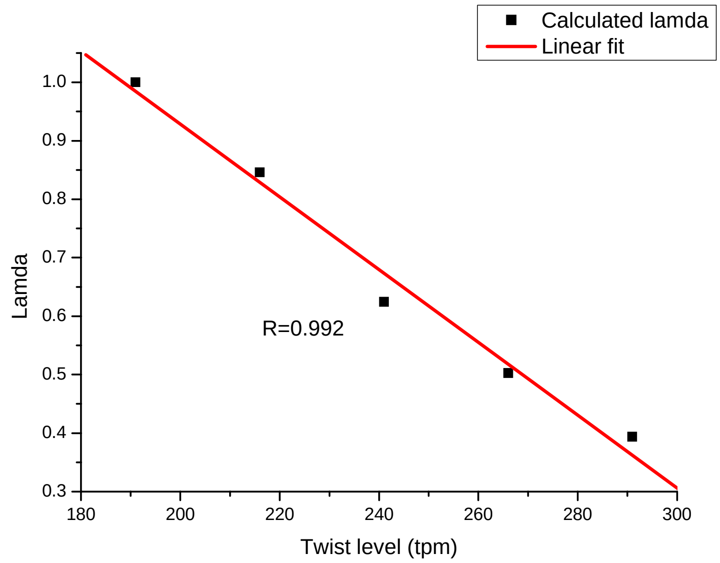

Figure 6.8 Linear fit of calculated values of λ

It may be observed from Figure 6.8 that the result of linear fit is good. It was shown in Chapter 5 that λ grows linearly with the increase of twist (Figure 5.14), whereas in Figure 6.8 λ decreases linearly with the increase of twist. If we rewrite Equation (6.4), and then we have:

$$\lambda = \frac{N\rho_l gA}{k} \tag{6.41}$$

In Chapter 5, the yarn is circularly close-packed and packing of fibers is assumed to be uniform. Therefore, $\rho_l gA/k$ is constant and the only influencing factor on λ is the wicking resistance term *N*. When an additional twist is inserted into the yarn, with the increase of the tortuosity of the yarn *N* tends to increase. This results in an increase of λ during twisting. As discussed this Chapter, however, packing of fibers in the yarn is not only loose but also non-uniform. When the yarn is subject to external forces, the fibers in the outer layer tend to move inward and change their transverse positions. This reduces the area available for the liquid flow A. Figure 6.8 also implies that the effect of the reduction of A greatly exceeds that of the increase of N, and the combination of the movement of fibers and change of the tortuosity of the yarn probably lead to such a linear relationship as shown in Figure 6.8.

6.4.2 Water

Water was mixed with a small quantity of detergent. The density of the mixture was 1053 kg/m^3. Surface tension of the mixture was 73.3mN/m. The advancing contact angle between the wool fiber and the mixture was 47^o. The radial swelling ratio of wool fiber from dry to saturated state was 15.2%. The density of saturated fiber was 1330 kg/m^3. The mean and simplified load-strain curves of the saturated wool fiber are shown in Figure 6.9 and Figure 6.10 respectively.

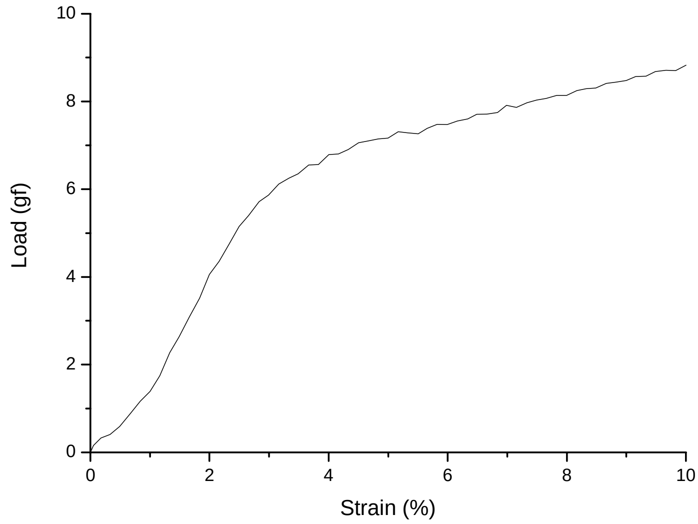

Figure 6.9 Load-strain curve of saturated wool fiber

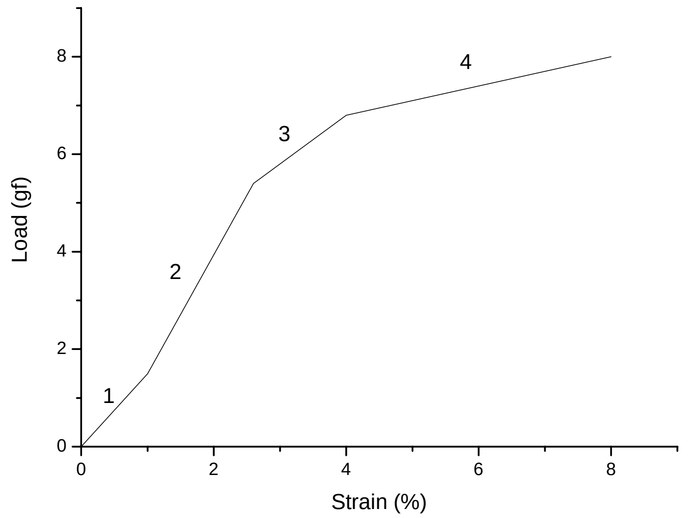

Figure 6.10 Simplified load-strain curve of saturated wool fiber

In order to investigate the impact of water on the tensile properties of wool fiber, the tensile behavior of wet wool fiber was compared with that of dry fiber in

Figure 6.11. It is shown that the modulus of fiber is greatly reduced from dry to wet. Actually this happens to yarn as well (Figure 6.12)

.

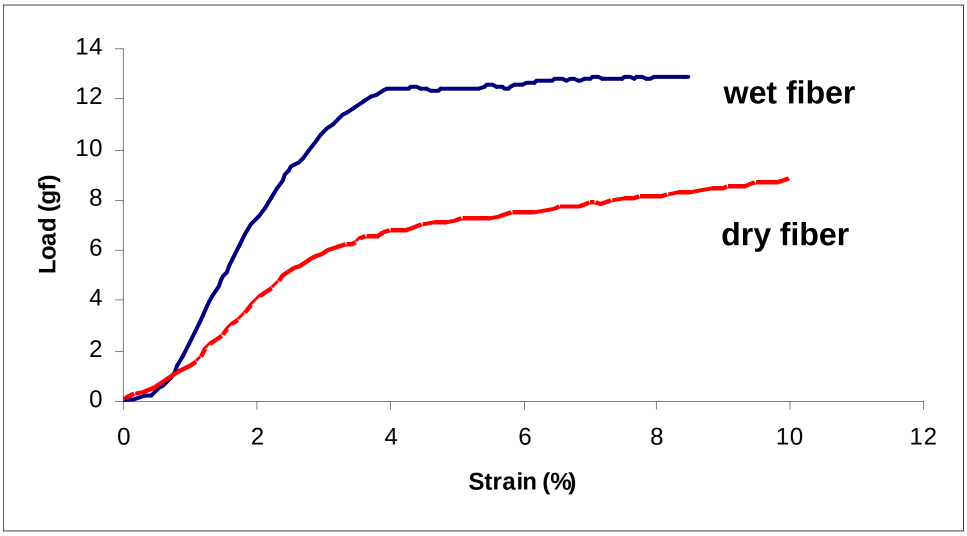

Figure 6.11 Tensile behaviors of wet and dry fibers

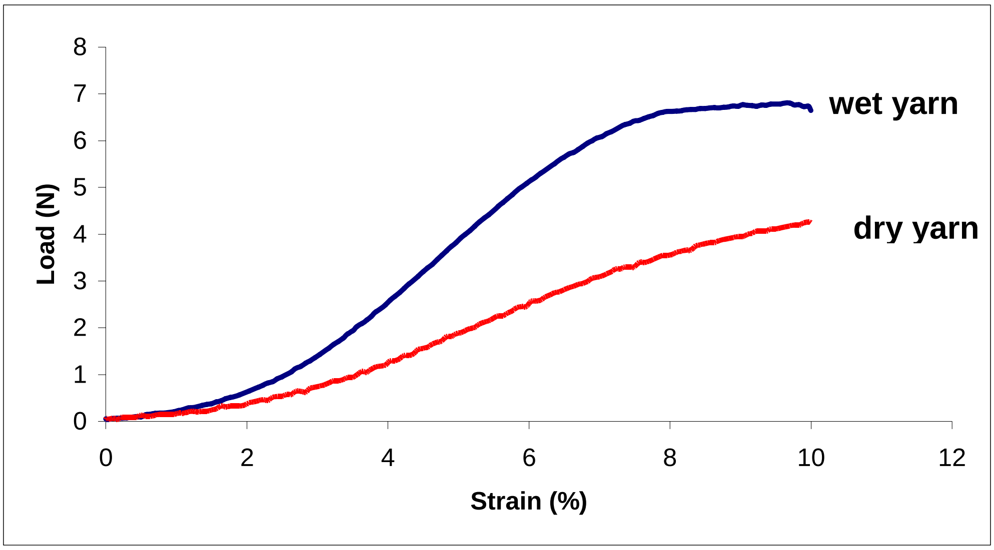

Figure 6.12 Tensile behaviors of wet and dry yarns

The moduli of the four strain intervals in simplified tensile behavior of fiber are shown in Table 6.4 Referring to material mechanics theory we can derive fiber bending and torsional rigidity from its tensile modulus at different stages with the assumption that the Poisson's ratio of the fiber is equal to 0.5.

Table 6.4 Moduli of the four stages in tensile test of fiber

ξ (%)	$E(gf{\cdot}cm^{-2})$	
$0 \le \xi < 1$	E_1	1.02×10^7
$1 \le \xi < 2.6$	E_2	1.66×10^7
$2.6 \le \xi < 4$	E_3	6.8210^7
$\xi \ge 4$	E_4	2.05×10^6

The experimental data of the wicking test and theoretical calculations for the initial yarn are presented in Figure 6.13.

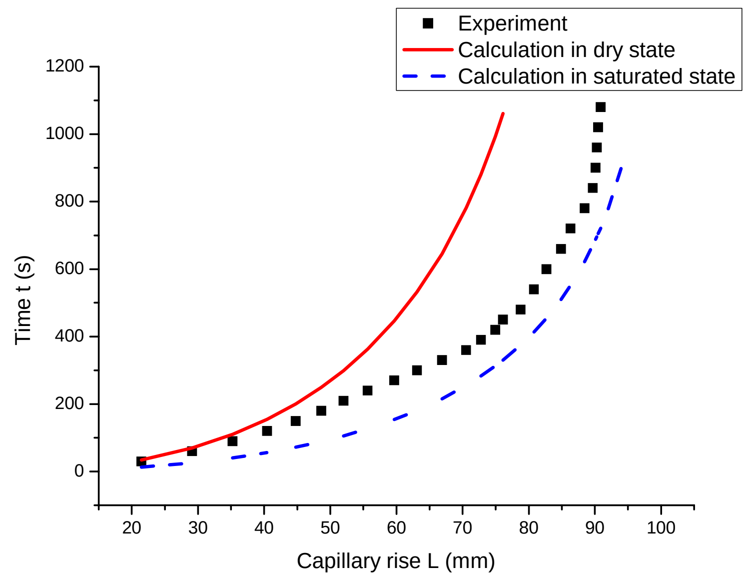

Figure 6.13 Wicking time as a function of capillary rise (T=191 tpm, T_{ten} =10gf)

In Figure 6.13, the solid line and dash line represent calculations without and with considering swelling of fibers respectively, using Equation (6.7). L_{equ} is computed by Equation (6.6) and N is obtained by Equation (6.4). λ is given in Table 6.3. Figure 6.13 shows that the experimental results fall between the theoretical calculations of the two cases. At the beginning of the wicking, as swelling of fibers is insignificant, the experimental data agrees well with the calculation in the dry state. As the swelling of fibers becomes appreciable, the experimental results deviate significantly from the calculation in the dry state, and tend to be close to the calculation in the saturated state. This may be due to the fact that swelling of fibers reduces capillaries between fibers, and thus enhances the wicking.

Figure 6.14 to Figure 6.17 present the results of yarn with different twists. All figures show the same trend as Figure 6.13.

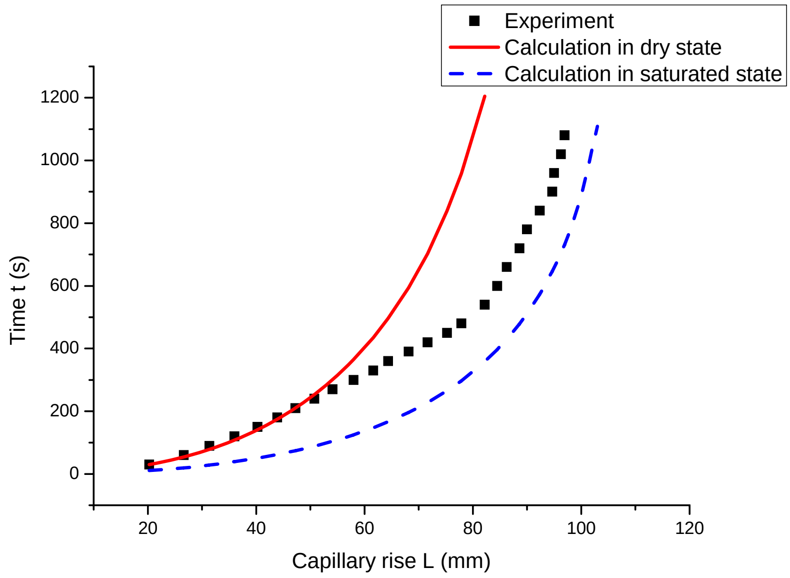

Figure 6.14 Wicking time as a function of capillary rise (T=216 tpm, T_{ten} =10gf)

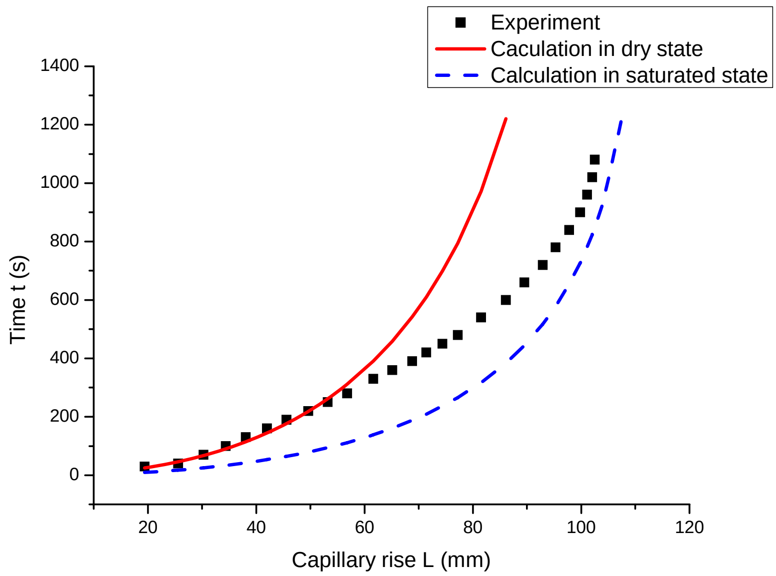

Figure 6.15 Wicking time as a function of capillary rise (T=241 tpm, T_{ten} =10gf)

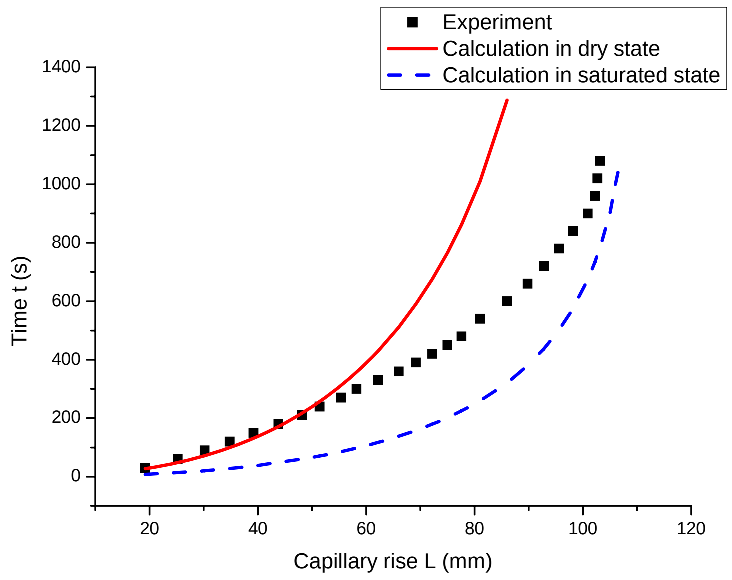

Figure 6.16 Wicking time as a function of capillary rise (T=266 tpm, T_{ten} =10gf)

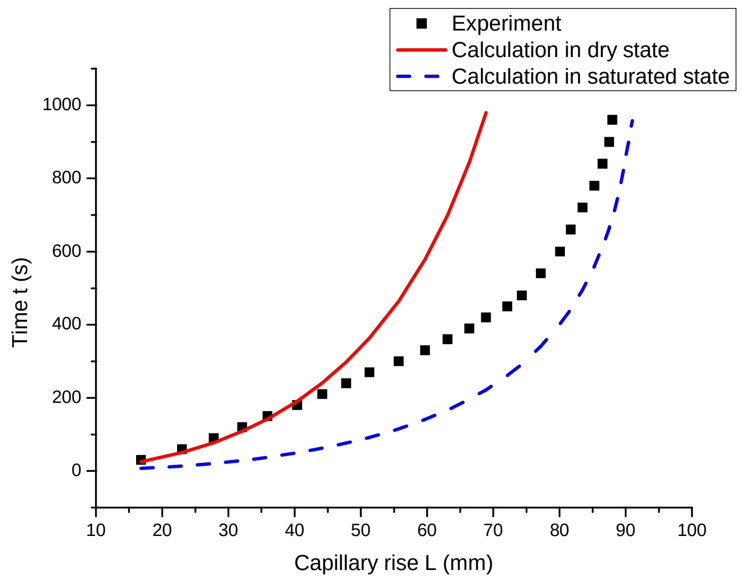

Figure 6.17 Wicking time as a function of capillary rise (T=291 tpm, T_{ten} =10gf)

In order to examine the influence of twist on the wicking, the final capillary rise was calculated in saturated state and compared with experimental data in Figure 6.18, and the error was shown in Table 6.5.

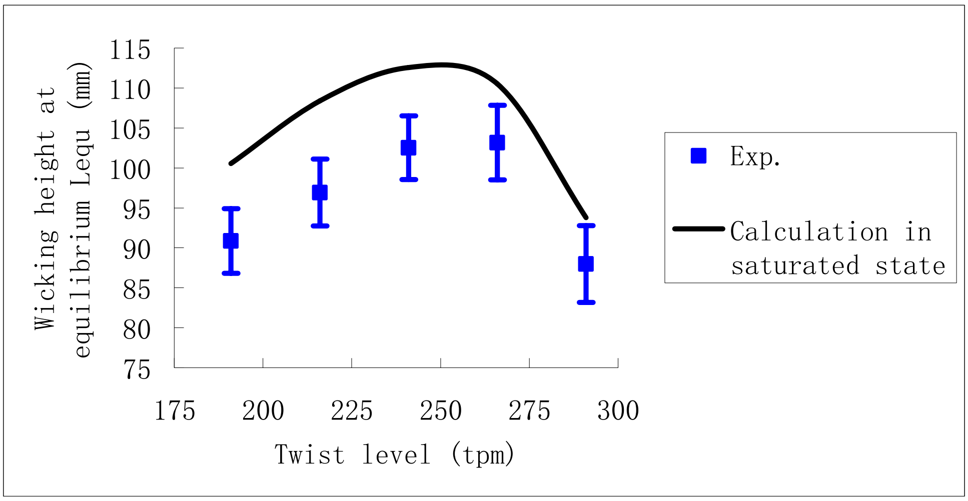

Figure 6.18 Comparison of L_{equ} derived from experimental data and theoretical calculation

Table 6.5 Relative error for different twist levels

Twist (tpm)	191	216	241	266	291
Error (%)	10.66	11.86	9.79	7.15	6.59

Figure 6.18 shows the same trend as Figure 6.7, and the deviation between experiment and calculation can also be explained similarly.

6.5 Conclusion

The investigation of the wicking behavior of a liquid (swelling or non-swelling) in a staple-fiber yarn was discussed in this chapter. Using a macroscopic force balance method, wicking time was obtained as a function of capillary rise. In order to analyze the influence of fiber movement during deformation of yarn and swelling of fibers on the wicking mechanism, a coupled model was developed. For the swelling liquid, two extreme cases, dry state and saturated state, were investigated. Experimental apparatus was designed, and a series of experiments was conducted on it. Data analysis showed that for non-swelling liquid the wicking flow can be accurately described by the model developed in this chapter. Considering the experimental error and heterogeneity of the yarn, the prediction of the capillary rise at equilibrium agreed reasonably well with the experimental data. Using a curve fitting technique it was found that there was an approximate linear relationship between twist level and the viscous drag. For the swelling liquid, the wicking process was shown to fall between the calculations of the two extreme cases. However, spun yarn is much more complex than an idealized continuous filament yarn model. Furthermore, when a high twist is introduced into the yarn, fibers near the yarn center may buckle due to twist retraction. This may damage the pore structures between fibers and affect the wicking behavior of the liquid. Therefore wicking in textile yarns is very complicated, and the mechanism has not been fully understood. Nevertheless, this research attempts to gain an insight into this area and to construct a framework for further study.

Modeling of wicking in structures that are more complicated will form the subject of subsequent research.

Chapter 7. Conclusions and suggestions for future work

7.1 Introduction

This project was undertaken in order to study the coupled mechanical and liquid transfer behavior of textile materials. As yarn was the most important intermediate stage in textile production, this research focused mainly on yarn structures and liquid flow through those structures. Since the mechanical properties of yarn and liquid flow behavior through yarn were fundamental to examine the coupled mechanism, the mechanical behavior of yarn and the wicking through yarn were separately modeled first. Then the two models were combined to analyze the coupled mechanism. In this chapter, the conclusions drawn from this study were summarized, and the future work was suggested.

7.2 Conclusions

7.2.1 Literature survey

In order to identify the research gaps and the research objectives, publications on yarn mechanics and liquid flow through fibrous assemblies were critically reviewed in Chapter 2. On basis of the literature survey, the research gaps were identified, and methodology and theories employed in this study were established.

The three commonly used methods to study yarn mechanics, namely, the force method, the finite element method (FEM) and the energy method were investigated respectively. The force method has been developed for many years, and has been proved to be successful to study simple structures like continuous filament yarns. The FEM also has been employed by some researchers. Compared to the force method and the FEM, the energy method has a much simpler form in terms of the calculation of the total energy since energy is a scalar. With this consideration, the energy method was adopted to model the mechanical behaviors of the yarn in this study.

The research literatures on capillary flow through tube, porous media as well as textile assemblies were also reviewed. The survey revealed that the textile assembly was always considered either as a bundle of capillary tubes or as porous media. In the first case, the wicking process could be described by Lucas-Washburn equation. In the second case, the liquid flow could be characterized by the Darcy’s law. However, in the first case, the effective capillary force and the effective contact angle were difficult to quantify, and they were always obtained by fitting the experimental data. In the second case, similarly, the structural features, such as porosity, were also obtained experimentally. As we know, however, textile assemblies like continuous filament yarns have comparatively regular structures. Therefore, a more comprehensive model based on the structural characteristics with less fitting parameters is possible.

7.2.2 Yarn mechanics

A comprehensive mechanical model to predict the tensile as well as torsional behaviors of singles yarn was developed as discussed in Chapter 3. The model was based on three basic theories, namely discrete fiber modeling principle, shortest path hypothesis and energy method. In the model, the yarn was assumed to be made up of a large number of discrete fibers. Each fiber was a discrete component of the yarn structure and the aggregate response of the assembly was obtained simply by adding the separate contributions of individual fibers. It was also assumed that the work done by the external force could totally be transferred and stored as the elastic energy of the yarn. The applied external force was obtained by taking derivative of the total energy with respect to the corresponding strain. The whole load-strain curve of fiber material was considered, and nonlinearities of tensile, bending and torsional behaviors of fiber material were taken into account, for the first time, in the calculation of the total energy. The gauge length of the yarn examined was small, and fiber migration and inter-fiber slippage were neglected.

Experimental validation showed that both tensile and torsional behaviors of singles yarn at low strain could be accurately predicted using the model. Contributions of fiber tension, fiber bending and fiber torsion to applied external force were calculated and compared using the energy method. It was found that in the tensile model the contribution to yarn tension due to fiber tension played the most important role, while in the torsional model all three contributions were significant. This finding was different from previous research (Tandon *et al.*, 1995a; Tandon *et al.*, 1995b) in which the authors stated that the contributions of fiber bending and torsion were negligible. By examining the tensile strain distribution of fibers, a buckling area was identified in torsional model, and buckling of fibers was investigated for the first time. If the fibers in the buckling area were allowed to release their tensile strains while still keep their helical profiles, more accurate results were found at large yarn strain. This model may enrich the knowledge of yarn mechanics and provide a better understanding of the mechanism of yarn fracture and twist stability.

7.2.3 Capillary rise between cylinders

In Chapter 4, the method by which wicking between two cylinders could be theoretically modeled was discussed. Firstly, the capillary rise in the gap between two identical cylinders was examined. Two approaches, a force approach and a minimum free energy approach, were used to derive the final capillary rise in terms of the distance of the separation of the two rods, and the two approaches were found to be equivalent. The final capillary rise was obtained by solving a series of equations. In the force analysis approach, the upward capillary force, the downward capillary force and the gravity of the liquid were considered. The free energy approach was based on an interfacial analysis.

Secondly, wicking between a cylinder and a plate were also examined. On the basis of the two special cases, a more general case which was wicking between two cylinders of different sizes was analyzed. Experimental verification showed that the theory can predict the final capillary rise of the liquid with reasonable accuracy. The relation between the wicking height at equilibrium and the distance of separation was found to be nearly inversely proportional. It was also illustrated that modeling the wicking between cylinders using a capillary tube was inadequate. This model can be easily applied to regularly packed cylinders, which are more or less similar to a fiber bundle.

Due to the ease of manipulation, glass rods with quite large diameters were used in the experiments. In the case of textile materials, fibers may be very thin, and the principal radius of the meniscus may be of the same order for magnitude as the fibers. However, as long as the assumption $L_{equ} \gg d$ is satisfied the dimension of the meniscus is still negligible. Therefore the theory presented in Chapter 4 applies to the case of textile fibers as well since the terms that enter the theoretical calculation are normalized dimensionless quantities. It has also been illustrated that a three-parameter logarithmic model seems to be more appropriate to describe the wicking between cylinders in terms of the inverse hydraulic radius. With minor modifications, the theory can be easily extended to model the wicking behavior of a liquid in a regularly packed fiber bundle with a small amount of fibers.

7.2.4 Liquid transfer through textile yarns

The investigation of the wicking behavior of a liquid in a fiber bundle as well as a twisted yarn was discussed in Chapter 5. Firstly, the wicking in a fiber bundle was analyzed. Using a macroscopic force balance method, the wicking time was obtained as a function of the capillary rise. In the macroscopic force balance analysis, capillary force, gravity of the liquid and viscous drag was considered. The inertia of the liquid was neglected. In the calculation of the perimeter of the liquid column, a minimum potential energy principle was employed.

Secondly, the same approach in the analysis of the wicking in a fiber bundle was used to examine the wicking process in a twisted yarn. The packing of fibers in the yarn was assumed to be uniform. In order to analyze the effect of twist on the wicking of the liquid, a twist coefficient was introduced into the viscous drag term. A simple helical yarn structure was employed. Experimental apparatus was designed, and a series of experiments was conducted using this apparatus. A circularly close-packed yarn was obtained using this apparatus, and the packing of fibers in the yarn was assumed to be uniform. Data analysis showed that the wicking flow can be accurately described using the equation developed in this research. Considering the experimental error, the prediction of the capillary rise at equilibrium agreed well with the experimental data with reasonable accuracy. The twist coefficient was found to be constant for a specific twist and increase linearly with twist level. Although N in Equation (5.5) still needs to be obtained by fitting the experimental data, only one parameter is required in the fitting. As stated in Section 2.3.4 of Chapter 2, when the textile yarn is modeled either as a capillary tube or as porous media, at least two parameters are unknown, and they are always obtained using curve fitting technique.

7.2.5 Coupled mechanical and liquid transfer behavior of textile yarns

A basic coupled model to investigate the coupled mechanism between mechanical and liquid transfer behavior of yarn was presented in Chapter 6. Firstly, a simple case which was the wicking of non-swelling liquid in the yarn was investigated. In contrast to the uniformly packed yarn discussed in Chapter 5, the packing of fibers in the yarn considered in Chapter 6 was not only loose, but also variable along radial direction. When the yarn was subject to external forces, the fibers moved inward and a jammed region occurred. The change of radial positions of fibers greatly altered the shape and size of the pore between fibers. Therefore, the movement of fibers should be considered. The system was coupled in a fashion that the movement of fibers changed the pore structures, hence influencing the wicking process. The mechanical model of yarn discussed in Chapter 3 was employed to analyze the change of radial positions of fibers, and the same macroscopic balance analysis of the liquid as discussed in Chapter 5 was combined into the model to study the wicking process.

Secondly, the wicking of a swelling liquid in the yarn was examined. The mechanical properties of the yarn were coupled with the liquid transfer behavior through the yarn in a way that absorption of the liquid caused the fibers to swell and changed the mechanical properties of the fibers. On the other hand, swelling of fibers changed the pore structures between fibers and the pathway of the liquid flow, thus affecting the entire wicking process. Two extreme cases were considered to study the coupled mechanism. They were dry state and wet state. In the first case, the fibers were assumed not to take up any liquid. In the second case, the fibers were supposed to become saturated instantly, and change of mechanical properties and swelling of fibers took place immediately once the yarn contacted the liquid.

Experimental verification showed that for non-swelling liquid the wicking flow could be accurately described by the model developed in this research. Considering the experimental error and heterogeneity of the yarn, the prediction of the capillary rise at equilibrium agreed reasonably well with the experimental data. For the swelling liquid, the wicking process was shown to fall between the calculations of the two extreme cases.

During active sport, it is likely that liquid sweat occurs on the skin. Therefore, the fabrics for active wear and sportswear are always specially constructed both in terms of the geometry, packing density and structure of the constituent fibers in yarns and in terms of the construction of the fabric in order to achieve the necessary dissipation of liquid sweat at high metabolic rates. An example is the development of ‘Sportwool’ technology. ‘Sportwool’ is a double knit fabric in which wool and polyester are bound back-to-back to form a single fabric. When the liquid sweat forms on the skin, the soft, comfortable inner wool, which is next to the skin, ‘pump’ the liquid sweat to the outer synthetic fiber layer, where it spreads out and evaporates, creating a cooling effect. As wool may take up liquid sweat and swell and the mechanical properties of wool changes significantly after absorption, the wicking through wool layer is coupled with the mechanical behaviors of wool. It has been revealed by many researchers that wicking through yarns take up the main portion of wicking through fabric. Therefore, the coupled model of yarn in this study may provide a understanding of the mechanism of wicking through this fabric. The coupled model implies that there is an optimal twist for the yarn to obtain the best wicking, and actually the optimal twist can be predicted from the model. This may be helpful to yarn production and garment design.

7.3 Suggestions for future work

Despite the achievements of this project, there are still several limitations, and some of them deserve further investigation:

1. The yarn structure used in this study was based on a helical geometry of fiber, and fiber migration and slippage were neglected. This model has been proved to be successful to study continuous filament yarns as well as staple

fiber yarns with short gauge length. However, the structure of staple fiber yarn is much more complicated than an assembly of helices, and fiber migration is one of the main reasons why an assembly of short fibers holds as a yarn. Therefore, fiber migration should be considered in future work. When a yarn is subject to considerable tension, fibers may partly slip. If inter-slippage is considered, a more robust model that can predict tensile behavior of yarn up to failure point is possible.

2. Due to time limit, only tensile and torsional behaviors of singles yarn were examined in this study. The bending behavior of singles yarn was not studied in this research partly due to the fact that it involves much more complicated movement and deformation of fibers. However, bending properties are also important characteristics of yarn. Therefore, it is desirable to study the bending behavior, even more complicated combined deformation modes of singles yarn in the future.

3. In the wicking model proposed in this research the frictional coefficient in viscous drag is obtained by fitting the experimental data. If it can be modeled based on properties of the liquid and structural features of the yarn, a totally predictive model can be obtained, and this will constitute a whole theory and enrich the knowledge of wicking in fibrous structures.

4. Two extreme cases were investigated attempting to examine the coupled mechanism and provide boundaries of the wicking dynamics in this study. It

is valuable to deepen the research by considering the change of swelling and mechanical properties of fiber with adsorption/time. If the influence of adsorption/time on swelling and mechanical properties of fiber can be modeled or fitted with a specific function, it is possible to simulate the entire wicking dynamics.

5. Only polyester yarn and wool yarn were used to validate the model. In order to verify the robusticity of the model, more experiments on other fiber materials need to be tested in the future. Impact of structural features of yarn such as hairiness, evenness, on the wicking mechanism should also be examined.

6. Only singles yarn was studied in this research. In textile production, however, ply yarn is more commonly used due to its good twist stability. Therefore research on mechanical properties as well as behavior of ply yarn, or even more complicated structures like fabric, may form the subject of future research.

Appendix I: Computer program in Matlab language for mechanical model of singles yarn

```
% head.m, defined parameters

% tensile moduli of fiber at four stages, unit: gf.cm-2
E1=4.5E6;
E2=45.1E6;
E3=24.3E6;
E4=1.53E6;
Gfiber=13.91E6; % shear modulus
RF=0.0018; % mean fiber radius, unit: cm
RFSQ=3.5279E-6; % mean squared fiber radius
H0=1/1.91; % pitch, unit: cm
ry=0.06;  % yarn radius, unit: cm
H0=H0/ry;  % normalization
Rfiber=RF/ry;
RHOf=1.31; % fiber density, unit: g.cm3

JAM=1; % density in jammed region

% parameters for fitting function of packing density
phia=2.278;
phib=-4.069;
phic=1.372;
phid=0.4436;
```

```
% main.m, main function

function main

head;

eth0=-7.2*ry*H0/2/pi; % minimum rotational strain
eth1=12*ry*H0/2/pi; % maximum rotational strain
stepth=4*ry*H0/2/pi; % step
force=10.59; % applied pre-tension for torsional model
```

```
tor=fopen('torque.dat','w+');
fprintf(tor,'rotation  torque  ey  rA\n');

ten=fopen('tension.dat','w+');
fprintf(ten,'      strain        tension\n');

tendis=fopen('tendis.dat','w');
fclose(tendis);

% tensile model
for ey=0.0003:0.01:0.1 % increment of tensile strain
%    load=tension(ey); % calculate applied tension by
force method
   load=tensile(ey); % calculate applied tension by energy
method
   fprintf(ten,'%15f   %15f\n',ey*100,load*9.8/1000); %
tension: N
end

fclose(ten);

% torsional model
for eth=0:stepth:eth1 % increment of torsional strain
   [torque,ey,rA]=torsional(eth,force); % torque:
applied torque
   fprintf(tor,'%15f   %15f    %15f
%15f\n',eth*2*pi/ry/H0,torque*1000,ey*100,rA);
end

fclose(tor);




%CalEf.m, calculate fiber tensile strain
%ey,eth: tensile strain and rotational strain of yarn
%rf0: fiber helix radius before deformation
%rstrain0: within rstrain0, fibers buckle
function strainf=CalEf(ey,eth,rh,rf0,rstrain0)

head;

lamday=1+ey;
```

```
lamdath=1+eth;

rf1sq=phia*rf0^5/5+phib*rf0^4/4+phic*rf0^3/3+phid*rf0^
2/2;
rf1sq=rf1sq*2/lamday/JAM+rh*rh;
Lf0=sqrt(H0*H0+(2*pi*rf0)^2);

if rf0<rstrain0||rf0==rstrain0

lamdath=(4*pi*pi*rf0.^2+H0*H0*(1-lamday*lamday))/pi/pi
/rf1sq/4;
   lamdath=sqrt(lamdath);

Lf1=sqrt(H0*H0*lamday*lamday+4*pi*pi*rf1sq*lamdath*lam
dath);
else

Lf1=sqrt(H0*H0*lamday*lamday+4*pi*pi*rf1sq*lamdath*lam
dath);
end


Lf1=sqrt(H0*H0*lamday*lamday+4*pi*pi*rf1sq*lamdath*lam
dath);

lamdaf=Lf1/Lf0;
strainf=lamdaf-1;


% finding a root lies in the interval [lower,upper] by
bisection method
function root=bisection(ey,eth,rh,lower,upper)

head;

small=lower;
big=upper-0.000001;
center=(small+big)/2;

strain=CalEf(ey,eth,rh,center);

while abs(strain)>1e-6
   strainl=CalEf(ey,eth,rh,small);
   strainu=CalEf(ey,eth,rh,big);
```

```
    product1=strainl*strain;
    product2=strainu*strain;

    if (product2)<0
        small=center;
    end

    if (product1)<0
        big=center;
    end

    center=(small+big)/2;
    strain=CalEf(ey,eth,rh,center);
end

root=center;




% CalRh.m, calculate the radius of hollow region

function rh=CalRh(ey,eth)

rh=0.001;
dh=1e-6;
steph=0;

rA=rootrA(ey,eth,rh);
Utotu=CalTot(ey,eth,rh+dh,rA);
Utotm=CalTot(ey,eth,rh,rA);
Utotl=CalTot(ey,eth,rh-dh,rA);

diffh1=(Utotu-Utotl)/dh/2;
diffh2=(Utotu-2*Utotm+Utotl)/dh/dh;

steph=diffh1/diffh2;

while abs(steph)>1e-8
    rh=rh-steph;

    rA=rootrA(ey,eth,rh);
    Utotu=CalTot(ey,eth,rh+dh,rA);
    Utotm=CalTot(ey,eth,rh,rA);
```

```
    Utotl=CalTot(ey,eth,rh-dh,rA);

    diffh1=(Ututu-Utotl)/dh/2;
    diffh2=(Ututu-2*Utotm+Utotl)/dh/dh;

    steph=diffh1/diffh2;
end
```

```
% CalTot.m, calculate the total energy of single yarn

function Utot=CalTot(ey,eth,rh,rA,rstrain0)

head;

% tensile energy
% if the integration interval is [0,rA], there is no
buckling
% if the integration interval is [rstrain0,rA], there is
buckling
% the buckling means the fibers in buckled region don't
have tensile
% energy, but still have bending and torsional energy with
the same shape
% as unbuckled
Uten=quadl(@CalTen,rstrain0,rA,{},{},ey,eth,rh);


% bending and torsional energy of jammed region
Ubt1=quadl(@CalBT,1e-6,rA,{},{},ey,eth,rh,0,1);

% bending  and torsional energy of unstrained region
Ubt2=quadl(@CalBT,rA,1,{},{},ey,eth,rh,1,1);

Utot=Uten+Ubt1+Ubt2;

% calculate the integrand of tensile energy
function y=CalTen(rf0,ey,eth,rh)

head;

lamday=1+ey;
```

```
lamdath=1+eth;

rf1sq=phia*rf0.^5/5+phib*rf0.^4/4+phic*rf0.^3/3+phid*r
f0.^2/2;
rf1sq=rf1sq*2/lamday/JAM+rh*rh;
Lf0=sqrt(H0*H0+(2*pi*rf0).^2);
Lf1=sqrt(H0*H0*lamday*lamday+4*pi*pi*rf1sq*lamdath*lam
dath);
lamdaf=Lf1./Lf0;
ef=lamdaf-1;

phi=phia*rf0.^3+phib*rf0.^2+phic*rf0+phid;


n=length(lamdaf);
for i=1:n
   if (ef(i)<0.008)||(ef(i)==0.008)
      y(i)=E1*ef(i)^2*phi(i)*rf0(i)*lamdaf(i)/2;
      y(i)=y(i)*2*pi*H0*ry^3/RHOf;
   else if (ef(i)>0.008&&ef(i)<0.022)||(ef(i)==0.022)

y(i)=(E1*0.008^2/2+E1*0.008*(ef(i)-0.008)+E2*(ef(i)-0.
008)^2/2)*phi(i)*rf0(i)*lamdaf(i);
         y(i)=y(i)*2*pi*H0*ry^3/RHOf;
      else if
(ef(i)>0.022&&ef(i)<0.037)||(ef(i)==0.037)

y(i)=E1*0.008^2/2+E1*0.008*(ef(i)-0.008)+E2*0.014^2/2+
E2*0.014*(ef(i)-0.022)+E3*(ef(i)-0.037)^2;
            y(i)=y(i)*rf0(i)*phi(i)*lamdaf(i);
            y(i)=y(i)*2*pi*H0*ry^3/RHOf;
         else

y(i)=E1*0.008^2/2+E1*0.008*(ef(i)-0.008)+E2*0.014^2/2+
E2*0.014*(ef(i)-0.022)+E3*0.015^2+E3*0.015*(ef(i)-0.03
7)+E4*(ef(i)-0.037)^2/2;
            y(i)=y(i)*rf0(i)*phi(i)*lamdaf(i);
            y(i)=y(i)*2*pi*H0*ry^3/RHOf;
         end
      end
   end
end
```

```
% calculate the integrand of bending energy and torsional
energy
% flag=0, jammed region
% flag=1, unstrained region
% banner=0, buckling region in jammed region
% banner=1, non-buckling region in jammed region
function y=CalBT(rf0,ey,eth,rh,flag,banner)

head;

lamday=1+ey;
lamdath=1+eth;

if flag==0

rf1sq=phia*rf0.^5/5+phib*rf0.^4/4+phic*rf0.^3/3+phid*r
f0.^2/2;
    rf1sq=rf1sq*2/lamday/JAM+rh*rh;
    rf1=sqrt(rf1sq);
end

if flag==1

rf1sq=(4*pi*pi*rf0.^2+H0*H0*(1-lamday*lamday))/pi/pi/l
amdath/lamdath/4;
    rf1=sqrt(rf1sq);
end

alpha0=atan(2*pi*rf0/H0);

if banner==0

lamdath=(4*pi*pi*rf0.^2+H0*H0*(1-lamday*lamday))/pi/pi
/rf1sq/4;
    lamdath=sqrt(lamdath);
    alpha1=atan(2*pi*rf1*lamdath/H0/lamday);
else
    alpha1=atan(2*pi*rf1*lamdath/H0/lamday);
end

kappa0=sin(alpha0).*sin(alpha0)./rf0;
kappa1=sin(alpha1).*sin(alpha1)./rf1;
tau0=sin(alpha0).*cos(alpha0)./rf0;
tau1=sin(alpha1).*cos(alpha1)./rf1;
```

```
phi=phia*rf0.^3+phib*rf0.^2+phic*rf0+phid;

Uben=0;
Utor=0;

Uben=(kappa1-kappa0).^2.*phi.*rf0;
Uben=Uben*pi*H0*Ef*RFSQ*ry/RHOf/4;

Utor=(tau1-tau0).^2.*phi.*rf0;
Utor=Utor*pi*H0*Gfiber*RFSQ*ry/RHOf/2;

y=Uben+Utor;
```

```
% rootrA.m, calculate jammed radius rA
% phia-phid: parameters defining the packing density
% ey,eth: strain
% H0: pitch
% rh: hollow radius

function y=rootrA(ey, eth, rh);

head;

lamday=1+ey;
lamdath=1+eth;

a0=(H0*H0*lamday*lamday-H0*H0)*lamday*JAM/pi/pi/8/lamd
ath/lamdath+rh*rh*lamday*JAM/2;
a1=0;
a2=(phid-lamday*JAM/lamdath/lamdath)/2;
a3=phic/3;
a4=phib/4;
a5=phia/5;

a=[a5 a4 a3 a2 a1 a0];

r=roots(a);

flag=0;
for i=1:5
```

```
    if imag(r(i))==0&&real(r(i))>0 && real(r(i))<1
        y=r(i);
        flag=1;
    end

    if flag==1
        break;
    end
end

if flag
else y=0;
end




% TenDistri.m, fiber tensile distribution
% rstrain0: radius where fiber tensile strain is zero
% fibers within this radius are under compression, ouside
under tension

function rstrain0=TenDistri(ey,eth,rh,rA)

head;

rf0=0;
strainf=CalEf(ey,eth,rh,rf0);

if strainf<0
    rstrain0=bisection(ey,eth,rh,rh,rA);
else rstrain0=0;
end


% finding a root lies in the interval [lower,upper] by
bisection method
function root=bisection(ey,eth,rh,lower,upper)

head;

small=lower;
big=upper-0.01;
center=(small+big)/2;
```

```
strain=CalEf(ey,eth,rh,center);

while abs(strain)>1e-6
   strainl=CalEf(ey,eth,rh,small);
   strainu=CalEf(ey,eth,rh,big);
   product1=strainl*strain;
   product2=strainu*strain;

   if (product2)<0
      small=center;
   end

   if (product1)<0
      big=center;
   end

   center=(small+big)/2;
   strain=CalEf(ey,eth,rh,center);
end

root=center;



% tensile.m, tensile property

function tension=tensile(ey)

head;

dy=1E-6;

rh=0;
eth=0;

rA=rootrA(ey,eth,rh);
Utotu=CalTot(ey+dy,eth,rh,rA,0);
Utotm=CalTot(ey,eth,rh,rA,0);
Utotl=CalTot(ey-dy,eth,rh,rA,0);


tension=Utotm/ey/H0/ry;
```

```
% tension.m, calculate yarn tension with given yarn strain
function tension=CalTension(ey)

head;

eth=0;
rh=0;
rA=rootrA(ey,eth,rh);
tension=quadl(@CalInten,0,rA,{},{},ey,eth,rh);

% calculate the integrand of tension
function y=CalInten(rf0,ey,eth,rh)
head;

lamday=1+ey;
lamdath=1+eth;

rf1sq=phia*rf0.^5/5+phib*rf0.^4/4+phic*rf0.^3/3+phid*r
f0.^2/2;
rf1sq=rf1sq*2/lamday/JAM+rh*rh;
Lf0=sqrt(H0*H0+(2*pi*rf0).^2);
Lf1=sqrt(H0*H0*lamday*lamday+4*pi*pi*rf1sq*lamdath*lam
dath);
lamdaf=Lf1./Lf0;

phi=phia*rf0.^3+phib*rf0.^2+phic*rf0+phid;

n=length(lamdaf);
 for i=1:n
     if (lamdaf(i)<1.0092)||(lamdaf(i)==1.0092)

y(i)=Efi*(lamdaf(i)-1)^2*phi(i)*rf0(i)*lamdaf(i)/2;
        y(i)=y(i)*2*pi*H0*ry^3/RHOf;
     else if
(lamdaf(i)>1.0092&&lamdaf(i)<1.0337)||(lamdaf(i)==1.00
37)

y(i)=(Efi*0.0092^2/2+Efi*0.0092*(lamdaf(i)-1.0092)+Ef*
(lamdaf(i)-1.0092)^2/2)*phi(i)*rf0(i)*lamdaf(i);
            y(i)=y(i)*2*pi*H0*ry^3/RHOf;
        else
```

```
y(i)=Efi*0.0092^2/2+Efi*0.0092*(lamdaf(i)-1.0092)+Ef*0
.0245^2/2+Ef*0.0245*(lamdaf(i)-1.0337)+Efy*(lamdaf(i)-
1.0337)^2;
           y(i)=y(i)*rf0(i)*phi(i)*lamdaf(i);
           y(i)=y(i)*2*pi*H0*ry^3/RHOf;
        end
     end
 end




% torsional.m, torsional property

function [torque,ey,rA]=torsional(eth,force)

head;

ey=0.01;
rh=0;
dy=1E-6;
dt=1E-6;

stepy=0;

ey=ey-stepy;
rA=rootrA(ey,eth,rh);
rstrain0=TenDistri(ey,eth,rh,rA);
Ututu=CalTot(ey+dy,eth,rh,rA,rstrain0);
Utotm=CalTot(ey,eth,rh,rA,rstrain0);
Utotl=CalTot(ey-dy,eth,rh,rA,rstrain0);

diffy1=(Ututu-Utotl)/dy/2/H0/ry-force;
diffy2=(Ututu-2*Utotm+Utotl)/dy/dy/H0/ry;

stepy=diffy1/diffy2;

while abs(stepy)>1E-8
   ey=ey-stepy;
   rA=rootrA(ey,eth,rh);
   rstrain0=TenDistri(ey,eth,rh,rA);
   Ututu=CalTot(ey+dy,eth,rh,rA,rstrain0);
   Utotm=CalTot(ey,eth,rh,rA,rstrain0);
   Utotl=CalTot(ey-dy,eth,rh,rA,rstrain0);
```

```
    diffy1=(Utotu-Utotl)/dy/2/H0/ry-force;
    diffy2=(Utotu-2*Utotm+Utotl)/dy/dy/H0/ry;

    stepy=diffy1/diffy2;
end

rstrain0=TenDistri(ey,eth,rh,rA);

tendis=fopen('tendis.dat','a+');
fprintf(tendis,'rotation=%f\n',eth*2*pi/ry/H0);
fprintf(tendis,'       rf0           strain\n');

for rf0=0:rA/50:rA
    strain=CalEf(ey,eth,rh,rf0);
    fprintf(tendis,'%15f   %15f\n',rf0,strain*100);
end
fclose(tendis);


Utotu=CalTot(ey,eth+dt,rh,rA,rstrain0);
Utotm=CalTot(ey,eth,rh,rA,rstrain0);
Utotl=CalTot(ey,eth-dt,rh,rA,rstrain0);

torque=(Utotu-Utotl)/dt/pi/4;
```

Appendix II: Computer program in Matlab language for model of wicking in twisted yarn

```
% head.m, defined parameters
banner=3; % banner=1, polyester yarn, 37 fibers, open
packing; banner=2, wool yarn (no swelling)
        % banner=3, wool yarn (swelling)

%%%%%%%%%%%%%%%%%%%%%%%%%%%%%%%%%%%%%%%%%%%%%%%%%%%%%%%%%%%%%%%%%%%%%%%%%%%%%%%%
%%%%%%%%%%%%%%%%%%%%%
% polyester yarn
if banner==1
   rf=8.4e-6; % fiber radius, unit: m
   theta=75.75; % contact angle between water and
polyester, unit: degree
   gammaa=72e-3; % surface tension of water, unit: N/m
   rho=1000; % density of water
   rhof=1380; % density of fiber
   eta=1e-3; % viscosity of water, unit: Pa.s
   g=9.8; % gravitational acceleration
   n=37; % number of fibers
   P=n*2*pi*rf; % perimeter to be wetted by the liquid
   Pl=6*(6+(2*3^0.5))*rf; % cross-sectional perimeter of
the liquid colum
   A=(30*3^0.5-15*pi)*rf^2; % area avaliable for liquid
flow
   ry=(6+2*3^0.5)*rf; % yarn radius
%%%%%%%%%%%%%%%%%%%%%%%%%%%%%%%%%%%%%%%%%%%%%%%%%%%%%%%%%%%%%%%%%%%%%%%%%%%%%%%%
%%%%%%%%%%%%%%%%%%%%%

%%%%%%%%%%%%%%%%%%%%%%%%%%%%%%%%%%%%%%%%%%%%%%%%%%%%%%%%%%%%%%%%%%%%%%%%%%%%%%%%
%%%%%%%%%%%%%%%%%%%%%
% wool yarn (no swelling)
else if banner==2
   E1=4.5E6; % modulus at different stages, unit: gf.cm-2
   E2=45.1E6;
   E3=24.3E6;
   E4=1.53E6;
```

```
    Gfiber=13.91E6; % shear modulus 1.391E7 tensile: 6.1E6
    a=0; % ratio of swelling of fiber diameter after
absorbing water
    rf=1.8e-3*(1+a); % mean fiber radius, cm
    ry=6e-2;   % yarn radius, cm
    rho=0.789; % density of water: 1, 0.789 for ethyl
alcohol
    rhof=1.310/(1+a)^2; % fiber density
    theta=53*pi/180; % contact angle between water and wool,
unit: radian
    gammaa=22.3e-2/9.8; % surface tension of
water:72.8,22.3 for ethyl alcohol , unit: gf/cm
    g=1;%e2; % gravitational acceleration
    tension=10;%*9.8e-3; % applied tension, gf
    T0=1.91; % initial twist, turn per cm
    JAM=1.000; % density of jammed region
    phia=2.278; % parameters describing packing density of
fibers
    phib=-4.069;
    phic=1.372;
    phid=0.4436;
%%%%%%%%%%%%%%%%%%%%%%%%%%%%%%%%%%%%%%%%%%%%%%%%%%%%%%
%%%%%%%%%%%%%%%%%%%%%

%%%%%%%%%%%%%%%%%%%%%%%%%%%%%%%%%%%%%%%%%%%%%%%%%%%%%%
%%%%%%%%%%%%%%%%%%%%%
% wool yarn (swelling)
    else
        E1=10.2E6; % modulus at different stages, unit:
gf.cm-2
        E2=16.6E6;
        E3=6.82E6;
        E4=2.05E6;


        Gfiber=13.91E6; % shear modulus 1.391E7 tensile:
6.1E6
        a=0; % ratio of swelling of fiber diameter after
absorbing water
        rf=1.8e-3*(1+a); % mean fiber radius, cm
        ry=6e-2;   % yarn radius, cm
        rho=1.053; % density of water: 1, 0.789 for ethyl
alcohol
```

```
        rhof=1.33; % fiber density
        theta=47*pi/180; % contact angle between water and
wool, unit: radian
        gammaa=73.3e-2/9.8; % surface tension of
water:72.8,22.3 for ethyl alcohol , unit: gf/cm
        g=1;%e2; % gravitational acceleration
        tension=10;%*9.8e-3; % applied tension, gf
        T0=1.91; % initial twist, turn per cm
        JAM=1.000; % density of jammed region
        phia=2.278; % parameters describing packing density
of fibers
        phib=-4.069;
        phic=1.372;
        phid=0.4436;
    end
end
%%%%%%%%%%%%%%%%%%%%%%%%%%%%%%%%%%%%%%%%%%%%%%%%%%%%%%%%%%%%%%%%%%%%%%%%%%%%%%%


% mian function

function main

head;

result=fopen('result.dat','w');

if banner==1 % polyester yarn, SI unit system is used
    fprintf(result,'twist(tpm)           Lequ(mm)\n');
    for T=0:100:500 % twist level
        Lequ=CalLequ(T); % calculate Lequ
        fprintf(result,'%4d
%10.6f\n',T,Lequ*1000);
    end
else % wool yarn, gf, cm unit system is used
    fprintf(result,'twist(tpm)           Lequ(mm)\n');
    for T=1.91:0.5:3.91 % twist level
        Lequ=CalLequW(T,tension,a); % capillary rise at
equilibrium
        fprintf(result,'%4d
%10.6f\n',T*100,Lequ*10);
```

```
    end
end

fclose(result);




% CalLequ.m, calculate capillary rise at equilibrium Lequ
for polyester
% yarn
% T: twist level, tpm
function Lequ=CalLequ(T)

head;

beta=2*Af/P/cos(theta)/ry;
if T==0 % fiber bundle, no twist
    P=n*2*pi*rf; % perimeter to be wetted by the liquid
    Pl=beta*2*pi*ry; % cross-sectional perimeter of the
liquid colum
    A=beta^2*pi*ry^2-n*pi*rf^2; % area avaliable for
liquid flow
    Fcu=P*gammaa*cos(theta); % upward capillary force
    Fcd=Pl*gammaa; % downward capillary force
    Fc=Fcu-Fcd; % capillary force
    Lequ=Fc/rho/g/A; % capillary rise at equiliabrium
else % twist yarn
    Pl=beta*2*pi*ry; % cross-sectional perimeter of the
liquid colum
    A=beta^2*pi*ry^2-n*pi*rf^2; % area avaliable for
liquid flow
    Fcu=CalFcu1(T); % upward capillary force
    Fcd=Pl*gammaa; % downward capillary force
    Fc=Fcu-Fcd; % capillary force
    Lequ=Fc/rho/g/A; % capillary rise at equiliabrium
end


%CalEf.m, calculate fiber tensile strain
%ey,eth: tensile strain and rotational strain of yarn
%rf0: fiber helix radius before deformation
%rstrain0: within rstrain0, fibers buckle
function strainf=CalEf(ey,eth,rh,rf0)%,rstrain0)
```

```
head;

H0=1/T0;
lamday=1+ey;
lamdath=1+eth;

rf1sq=phia*rf0^5/5/ry^3+phib*rf0^4/4/ry^2+phic*rf0^3/3
/ry+phid*rf0^2/2;
rf1sq=rf1sq*2/lamday/JAM+rh*rh;
Lf0=sqrt(H0*H0+(2*pi*rf0)^2);

% if rf0<rstrain0||rf0==rstrain0
%
lamdath=(4*pi*pi*rf0.^2+H0*H0*(1-lamday*lamday))/pi/pi
/rf1sq/4;
%     lamdath=sqrt(lamdath);
%
Lf1=sqrt(H0*H0*lamday*lamday+4*pi*pi*rf1sq*lamdath*lam
dath);
% else
%
Lf1=sqrt(H0*H0*lamday*lamday+4*pi*pi*rf1sq*lamdath*lam
dath);
% end


Lf1=sqrt(H0*H0*lamday*lamday+4*pi*pi*rf1sq*lamdath*lam
dath);

lamdaf=Lf1/Lf0;
strainf=lamdaf-1;


% finding a root lies in the interval [lower,upper] by
bisection method
function root=bisection(ey,eth,rh,lower,upper)

head;

small=lower;
big=upper-0.000001;
center=(small+big)/2;
```

```
strain=CalEf(ey,eth,rh,center);

while abs(strain)>1e-6
   strainl=CalEf(ey,eth,rh,small);
   strainu=CalEf(ey,eth,rh,big);
   product1=strainl*strain;
   product2=strainu*strain;

   if (product2)<0
      small=center;
   end

   if (product1)<0
      big=center;
   end

   center=(small+big)/2;
   strain=CalEf(ey,eth,rh,center);
end

root=center;
```

```
% CalEy.m, calculate ey
% ey: tensile strain of yarn
% rA: radius which will be the boundary of the jammed region
% rAjam: radius of the jammed region
% T: twist of the yarn
% tension: applied tension on the yarn
function [ey,rA,rAjam]=CalEy(T,tension)

head;

% eth=(T-T0)/T0;
% ey=0;
% rh=0;
% dy=1E-6;
% dt=1E-6;
% H0=1/T0;
% ey0=-0.01;
% ey=fsolve(@CalDiffy1,ey0,{},T,tension);
% rA=rootrA(ey,eth,rh,H0);
```

```
eth=(T-T0)/T0;

ey=0.01;
rh=0;
dy=1E-7;
H0=1/T0;

stepy=0;

ey=ey-stepy;
rA=rootrA(ey,eth,rh,H0);
rstrain0=0;
rstrain0=TenDistri(ey,eth,rh,rA);
Utotu=CalTot(ey+dy,eth,rh,rA,rstrain0,H0);
Utotm=CalTot(ey,eth,rh,rA,rstrain0,H0);
Utotl=CalTot(ey-dy,eth,rh,rA,rstrain0,H0);

diffy1=(Utotu-Utotl)/dy/2/H0-tension;
diffy2=(Utotu-2*Utotm+Utotl)/dy/dy/H0;

stepy=diffy1/diffy2;

while abs(stepy)>1E-10
    ey=ey-stepy;
    rA=rootrA(ey,eth,rh,H0);
    rstrain0=0;
    rstrain0=TenDistri(ey,eth,rh,rA);
    Utotu=CalTot(ey+dy,eth,rh,rA,rstrain0,H0);
    Utotm=CalTot(ey,eth,rh,rA,rstrain0,H0);
    Utotl=CalTot(ey-dy,eth,rh,rA,rstrain0,H0);

    diffy1=(Utotu-Utotl)/dy/2/H0-tension;
    diffy2=(Utotu-2*Utotm+Utotl)/dy/dy/H0;

    stepy=diffy1/diffy2;
end


rstrain0=TenDistri(ey,eth,rh,rA);

tendis=fopen('tendis.dat','w+');
fprintf(tendis,'rotation=%f\n',eth);
```

```
fprintf(tendis,'        rf0            strain\n');

for rf0=0:rA/50:rA
    strain=CalEf(ey,eth,rh,rf0);
    fprintf(tendis,'%15f    %15f\n',rf0,strain*100);
end
fclose(tendis);

rAjam=CalrAjam(rA,ey);

% rAjam=(2*pi*rA)^2+H0^2-H0^2*(1+ey)^2;
% rAjam=rAjam/(1+eth)^2;
% rAjam=rAjam^0.5/pi/2;
```

```
% CalLequW.m: calculate the capillary rise at equilibrium
for wool yarn
% T: twist
% tension: applied tension

function Lequ=CalLequW(T,tension,a);

head;
if T==0 % no jammed region
    Fcu=quadl(@InterFcu,0,ry);
    Af=quadl(@InterAf,0,ry,{},{},T);
    A=pi*ry^2-Af;
else % jammed region appears in the central area of yarn
    [ey,rA,rAjam]=CalEy(T,tension);

    % upward capillary force
    Fcuj=quadl(@InterFcuj,0,rAjam,{},{},T,ey,a);
    Fcuu=quadl(@InterFcuu,rA,ry,{},{},T,ey,a);
    Fcu=Fcuj+Fcuu;

    % Af
    Afj=quadl(@InterAfj,0,rAjam,{},{},T,ey,a);
    Afu=quadl(@InterAfu,rA,ry,{},{},T,ey,a);
    Af=Afj+Afu;

    if rA<ry
        H0=1/T0;
```

```
        eth=(T-T0)/T0;
        ry1=4*pi^2*ry^2+H0^2*(1-(1+ey)^2);
        ry1=ry1/pi^2/(1+eth)^2/4;
        ry1=ry1^0.5;
    else
        ry1=CalrAjam(ry,ey);
    end

    beta=2*Af*gammaa/Fcu/ry1;

    % area available for liquid flow
    A=beta^2*pi*ry1^2-Af;

    %calculate cross-sectional perimeter of the liquid
colum, Pl
    Pl=2*pi*ry1*beta;

    %downward capillary force
    Fcd=Pl*gammaa;

    % capillary force
    Fc=Fcu-Fcd;

    Lequ=Fc/rho/g/A; % capillary rise at equilibrium
end

% calculate the intergrand of Fcu
function Intergrand=InterFcu(r);

head;

phi=phia*r.^3/ry^3+phib*r.^2/ry^2+phic*r/ry+phid;
Intergrand=4*pi*gammaa*cos(theta)*phi.*r/rhof/rf;

% calculate the upward capillary due to jammed region
function Intergrand=InterFcuj(r,T,ey,a)

head;
H0=1/T0;
eth=(T-T0)/T0;

Lf1=4*pi^2*(1+eth)^2*r.^2+H0^2*(1+ey)^2;
Lf1=Lf1.^0.5;
alpha=acos(H0*(1+ey)./Lf1);
```

```
C=4*pi*H0*(1+ey)*JAM*gammaa/rhof/rf/(1+a);
Intergrand=C*r.*cos(alpha+theta)./Lf1;

% calculate the upward capillary due to unstrained region
function Intergrand=InterFcuu(r,T,ey,a)

head;
H0=1/T0;
phi=phia*r.^3/ry^3+phib*r.^2/ry^2+phic*r/ry+phid;

Lf1=4*pi^2*r.^2+H0^2;
Lf1=Lf1.^0.5;
alpha=acos(H0*(1+ey)./Lf1);

C=4*pi*H0*gammaa/rhof/rf/(1+a);
Intergrand=C*phi.*r.*cos(alpha+theta)./Lf1;

% calculate the intergrand of Af
function Intergrand=InterAf(r,T)

head;
phi=phia*r.^3/ry^3+phib*r.^2/ry^2+phic*r/ry+phid;
Intergrand=2*pi*phi.*r/rhof;

% calculate the intergrand of Afj
function Intergrand=InterAfj(r,T,ey,a)

head;
H0=1/T0;
eth=(T-T0)/T0;
C=2*pi*JAM*H0*(1+ey)/rhof;
Intergrand=C*r./(H0^2*(1+ey)^2+4*pi^2*r.^2*(1+eth)^2).
^0.5;

% calculate the intergrand of Afu
function Intergrand=InterAfu(r,T,ey,a)

head;
H0=1/T0;
phi=phia*r.^3/ry^3+phib*r.^2/ry^2+phic*r/ry+phid;
C=2*pi*H0/rhof;
Intergrand=C*phi.*r./(H0^2+4*pi^2*r.^2).^0.5;
```

```
% CalrAjam.m, calculate rAjam
function rAjam=CalrAjam(rA,ey)

head;

rAjam=quadl(@InterrAjam,0,rA);
rAjam=rAjam*2/JAM/(1+ey);
rAjam=rAjam^0.5;

function Intergrand=InterrAjam(r)

head;

phi=phia*r.^3/ry^3+phib*r.^2/ry^2+phic*r/ry+phid;
Intergrand=r.*phi;
```

```
% CalTot.m, calculate the total energy of single yarn

function Utot=CalTot(ey,eth,rh,rA,rstrain0,H0)

head;

rh=0;
rstrain0=0;

% tensile energy
% if the integration interval is [0,rA], there is no
buckling
% if the integration interval is [rstrain0,rA], there is
buckling
% the buckling means the fibers in buckled region don't
have tensile
% energy, but still have bending and torsional energy with
the same shape
% as unbuckled
Uten=quadl(@CalTen,rstrain0,rA,{},{},ey,eth,rh,H0);


% bending and torsional energy of jammed region
Ubt1=quadl(@CalBT,1e-10,rA,{},{},ey,eth,rh,0,1,H0);
```

```
% bending  and torsional energy of unstrained region
%6-6-2007
if abs(rA-ry)<1e-10
   Ubt2=0;
else
   Ubt2=quadl(@CalBT,rA,ry,{},{},ey,eth,rh,1,1,H0);
end
% Ubt2=quadl(@CalBT,rA,1,{},{},ey,eth,rh,1,1);

Utot=Uten+Ubt1+Ubt2;

% calculate the integrand of tensile energy
function y=CalTen(rf0,ey,eth,rh,H0)

head;

lamday=1+ey;
lamdath=1+eth;

rf1sq=phia*rf0.^5/5/ry^3+phib*rf0.^4/4/ry^2+phic*rf0.^
3/3/ry+phid*rf0.^2/2;
rf1sq=rf1sq*2/lamday/JAM+rh*rh;
Lf0=sqrt(H0*H0+(2*pi*rf0).^2);
Lf1=sqrt(H0*H0*lamday*lamday+4*pi*pi*rf1sq*lamdath*lam
dath);
lamdaf=Lf1./Lf0;
ef=lamdaf-1;

phi=phia*rf0.^3/ry^3+phib*rf0.^2/ry^2+phic*rf0/ry+phid
;

%%%%%%%%%%%%%%%%%%%%%%%%%%%%%%%%%%%%%%%%%%%%
%  y=(lamdaf-1).^2.*phi.*rf0;
%  y=y*pi*H0*Ef*ry*ry*ry/RHOf;
%%%%%%%%%%%%%%%%%%%%%%%%%%%%%%%%%%%%%%%%%%%%

%%%%%%%%%%%%%%%%%%%%%%%%%%%%%%%%%%%%%%%%%%%%%
% n=length(lamdaf);
% for i=1:n
%    if (ef(i)<0.008)||(ef(i)==0.008)
%       y(i)=E1*ef(i)^2*phi(i)*rf0(i)*lamdaf(i)/2;
%       y(i)=y(i)*2*pi*H0/rhof;
%    else if (ef(i)>0.008&&ef(i)<0.022)||(ef(i)==0.022)
%
```

```
y(i)=(E1*0.008^2/2+E1*0.008*(ef(i)-0.008)+E2*(ef(i)-0.
008)^2/2)*phi(i)*rf0(i)*lamdaf(i);
%           y(i)=y(i)*2*pi*H0/rhof;
%        else if
(ef(i)>0.022&&ef(i)<0.037)||(ef(i)==0.037)
%
y(i)=E1*0.008^2/2+E1*0.008*(ef(i)-0.008)+E2*0.014^2/2+
E2*0.014*(ef(i)-0.022)+E3*(ef(i)-0.037)^2;
%              y(i)=y(i)*rf0(i)*phi(i)*lamdaf(i);
%              y(i)=y(i)*2*pi*H0/rhof;
%           else
%
y(i)=E1*0.008^2/2+E1*0.008*(ef(i)-0.008)+E2*0.014^2/2+
E2*0.014*(ef(i)-0.022)+E3*0.015^2+E3*0.015*(ef(i)-0.03
7)+E4*(ef(i)-0.037)^2/2;
%              y(i)=y(i)*rf0(i)*phi(i)*lamdaf(i);
%              y(i)=y(i)*2*pi*H0/rhof;
%           end
%        end
%     end
% end

%%%%%%%%%%%%%%%%%%%%%%%%%%%%%%%%%%%%%%%%%%%%%

%%%%%%%%%%%%%%%%%%%%%%%%%%%%%%%%%%%%%%%%%%%%%%%
n=length(lamdaf);
 for i=1:n
    if (lamdaf(i)<1.0092)||(lamdaf(i)==1.0092)

y(i)=Efi*(lamdaf(i)-1)^2*phi(i)*rf0(i)*lamdaf(i)/2;
       y(i)=y(i)*2*pi*H0/rhof;
    else if
(lamdaf(i)>1.0092&&lamdaf(i)<1.0337)||(lamdaf(i)==1.00
37)

y(i)=(Efi*0.0092^2/2+Efi*0.0092*(lamdaf(i)-1.0092)+Ef*
(lamdaf(i)-1.0092)^2/2)*phi(i)*rf0(i)*lamdaf(i);
           y(i)=y(i)*2*pi*H0/rhof;
       else

y(i)=Efi*0.0092^2/2+Efi*0.0092*(lamdaf(i)-1.0092)+Ef*0
.0245^2/2+Ef*0.0245*(lamdaf(i)-1.0337)+Efy*(lamdaf(i)-
1.0337)^2;
           y(i)=y(i)*rf0(i)*phi(i)*lamdaf(i);
```

```
            y(i)=y(i)*2*pi*H0/rhof;
        end
    end
end
%%%%%%%%%%%%%%%%%%%%%%%%%%%%%%%%%%%%%%%%%%%%%%%%%%%%


% calculate the integrand of bending energy and torsional energy
% flag=0, jammed region
% flag=1, unstrained region
% banner=0, buckling region in jammed region
% banner=1, non-buckling region in jammed region
function y=CalBT(rf0,ey,eth,rh,flag,banner,H0)

head;

lamday=1+ey;
lamdath=1+eth;

if flag==0

rf1sq=phia*rf0.^5/5/ry^3+phib*rf0.^4/4/ry^2+phic*rf0.^3/3/ry+phid*rf0.^2/2;
    rf1sq=rf1sq*2/lamday/JAM+rh*rh;
    rf1=sqrt(rf1sq);
end

if flag==1

rf1sq=(4*pi*pi*rf0.^2+H0*H0*(1-lamday*lamday))/pi/pi/lamdath/lamdath/4;
    rf1=sqrt(rf1sq);
end

alpha0=atan(2*pi*rf0/H0);

if banner==0

lamdath=(4*pi*pi*rf0.^2+H0*H0*(1-lamday*lamday))/pi/pi/rf1sq/4;
    lamdath=sqrt(lamdath);
    alpha1=atan(2*pi*rf1*lamdath/H0/lamday);
else
```

```
   alpha1=atan(2*pi*rf1*lamdath/H0/lamday);
end

kappa0=sin(alpha0).*sin(alpha0)./rf0;
kappa1=sin(alpha1).*sin(alpha1)./rf1;
tau0=sin(alpha0).*cos(alpha0)./rf0;
tau1=sin(alpha1).*cos(alpha1)./rf1;

phi=phia*rf0.^3/ry^3+phib*rf0.^2/ry^2+phic*rf0/ry+phid
;

Uben=0;
Utor=0;

Uben=(kappa1-kappa0).^2.*phi.*rf0;
Uben=Uben*pi*H0*Ef*rf^2/rhof/4;

Utor=(tau1-tau0).^2.*phi.*rf0;
Utor=Utor*pi*H0*Gfiber*rf^2/rhof/2;

y=Uben+Utor;




%rootrA.m, calculate jammed radius rA
% phia-phid: parameters defining the packing density
% ey,eth: strain
% H0: pitch
% rh: hollow radius

function y=rootrA(ey, eth, rh,H0);

head;

lamday=1+ey;
lamdath=1+eth;

a0=(H0*H0*lamday*lamday-H0*H0)*lamday*JAM/pi/pi/8/lamd
ath/lamdath+rh*rh*lamday*JAM/2;
a1=0;
a2=(phid-lamday*JAM/lamdath/lamdath)/2;

%6-6-2007
```

```
a3=phic/ry/3;
a4=phib/ry^2/4;
a5=phia/ry^3/5;

%%%%%%%%%%%%%%%%%%%%%%%%
% a3=phic/3;
% a4=phib/4;
% a5=phia/5;
%%%%%%%%%%%%%%%%%%%%%%%%


a=[a5 a4 a3 a2 a1 a0];

r=roots(a);

flag=0;
for i=1:5
   if imag(r(i))==0&&real(r(i))>0 && real(r(i))<ry
      y=r(i);
      flag=1;
   end

   if flag==1
      break;
   end
end

if flag
else y=ry;
end




% TenDistri.m, fiber tensile distribution
% rstrain0: radius where fiber tensile strain is zero
% fibers within this radius are under compression, ouside
under tension

function rstrain0=TenDistri(ey,eth,rh,rA)

head;

rf0=0;
```

```
strainf0=CalEf(ey,eth,rh,rf0); % tensile strain of fiber
at the center

strainf1=CalEf(ey,eth,rh,rA-0.000001); % tensile strain
of fiber at the surface

if (strainf0*strainf1)<0
   rstrain0=bisection(ey,eth,rh,rh,rA);
else rstrain0=0;
end


% finding a root lies in the interval [lower,upper] by
bisection method
function root=bisection(ey,eth,rh,lower,upper)

head;

small=lower;
big=upper-0.01;
center=(small+big)/2;

strain=CalEf(ey,eth,rh,center);

while abs(strain)>1e-6
   strainl=CalEf(ey,eth,rh,small);
   strainu=CalEf(ey,eth,rh,big);
   product1=strainl*strain;
   product2=strainu*strain;

   if (product2)<0
      small=center;
   end

   if (product1)<0
      big=center;
   end

   center=(small+big)/2;
   strain=CalEf(ey,eth,rh,center);
end

root=center;
```

```
% torsional.m, torsional property

function [ey,rA,rAjam]=CalEy(force)

head;

ey=0.01;
rh=0;
dy=1E-6;
dt=1E-6;

stepy=0;

ey=ey-stepy;
rA=rootrA(ey,eth,rh);
rstrain0=TenDistri(ey,eth,rh,rA);
rstrain=0;
Utotu=CalTot(ey+dy,eth,rh,rA,rstrain0);
Utotm=CalTot(ey,eth,rh,rA,rstrain0);
Utotl=CalTot(ey-dy,eth,rh,rA,rstrain0);

diffy1=(Utotu-Utotl)/dy/2/H0-force;
diffy2=(Utotu-2*Utotm+Utotl)/dy/dy/H0;

stepy=diffy1/diffy2;

while abs(stepy)>1E-8
    ey=ey-stepy;
    rA=rootrA(ey,eth,rh);
    Utotu=CalTot(ey+dy,eth,rh,rA,rstrain0);
    Utotm=CalTot(ey,eth,rh,rA,rstrain0);
    Utotl=CalTot(ey-dy,eth,rh,rA,rstrain0);

    diffy1=(Utotu-Utotl)/dy/2/H0-force;
    diffy2=(Utotu-2*Utotm+Utotl)/dy/dy/H0;

    stepy=diffy1/diffy2;
end

rAjam=(2*pi*rA)^2+H0^2-H0^2*(1+ey)^2;
rAjam=rAjam^0.5/pi/2;
```

References

1. Abbott, N. J., Temin, S. C. and Park, C., The stress-strain behavior of wool in various swelling media, Textile Research Journal, 1026-1039 (1968)

2. Aberson, G. M., The physics and chemistry of wood pulp fibers, TAPPI, 282 (1970)

3. Ackerman, B. J. and Cassidy, H. G., Anal. Chem., 26, 1874 (1954)

4. Adamson, A. W., Physical chemistry of surfaces, J. Wiley, New York (1967)

5. Adamson, A. W., Physical chemistry of surfaces, J. Wiley, New York (1990)

6. Ahumada, O., Cocca, A., Gentile, G., Martuscelli, E. and D'Orazio, L., Uniaxial tensile properties of yarns: Effects of moisture level on the shape of stress-strain curves, Textile Research Journal, 74(11), 1001-1006 (2004)

7. Amico, S. C. and Lekakou, C., Mathematical modeling of capillary micro-flow through woven fabrics, Composites: Part A, 31, 1331-1344 (2000)

8. Amico, S. C. and Lekakou, C., Axial impregnation of a fiber bundle. Part 1: Capillary experiments, Polymer Composites, 23(2), 249-263 (2002a)

9. Amico, S. C. and Lekakou, C., Axial impregnation of a fiber bundle. Part 2: Theoretical analysis, Polymer Composites, 23(2), 264-273 (2002b)

10. Ansari, N. and Haghighat, K. M., Capillary water transport in yarn, Iranian J. Polym. Sci. Technol., 8, 87-96 (1995)

11. Batch, G. L., Chen, Y. T. and Macosko, C. W., Capillary impregnation of aligned fibrous beds: Experiments and model, Journal Of Reinforced Plastics And Composites, 15(10), 1027-1051 (1996)

12. Bayramli, E. and Powell, R. L., The normal (transverse) impregnation of liquids into axially oriented fiber-bundles, Journal Of Colloid And Interface Science, 138(2), 346-353 (1990)

13. Bayramli, E. and Powell, R. L., Experimental investigation of the axial impregnation of oriented fiber bundles by capillary forces, Colloids and Surfaces, 56, 83-100 (1991)

14. Bear, J., Dynamics of fluid in porous media, Elsevier, New York (1972)

15. Bico, J. and Quere, D., Rise of liquids and bubbles in angular capillary tubes, Journal Of Colloid And Interface Science, 247(1), 162-166 (2002)

16. Bouaidat, S., Hansen, O., Bruus, H., Berendsen, C., Bau-Madsen, N. K., Thomsen, P., Wolff, A. and Jonsmann, J., Surface-directed capillary system; theory, experiments and applications, Lab On A Chip, 5(8), 827-836 (2005)

17. Brady, V., Concus, P. and Finn, R., Capillary rise in nesting cylinders, Physics Of Fluids, 15(6), 1545-1551 (2003)

18. Butt, H.-J., Graf, K. and Kappl, M., Physics and chemistry of interfaces, Second Edition, WILEY-VCH Verlag GmbH & Co. KGaA, Weinheim (2006)

19. Carman, P. C., Fluid flow through granular beds, Chemical Engineering Research and Design, 15, 150-166 (1937)

20. Carnaby, G. A. and Grosberg, P., The tensile behavior of staple-fiber yarns at small extensions, J. Text. Inst., 9, 299-308 (1976)

21. Chatterjee, P. K., Absorbency, Elsevier Scientific Pub., New York (1985)

22. Chen, X., Kornev, K. G., Kamath, Y. K. and Neimark, A. V., The kinetics of wicking of liquid droplets into yarns, Text. Res. J., 71(10), 962-869 (2001)

23. Choi, F. K. F., Shih, T. M., Carnaby, G. A. and Lo, M. T., Torsional models of two ply yarn, J. China Textile Univ. Engl. Ed., 15(1), 31-37 (1998)

24. Choi, K. F., Modeling of singles and two-ply staple-fiber yarns with special reference to warp spun yarn, PhD, The Hong Kong Polytechnic University, Hong Kong (1998)

25. Choi, K. F. and Lo, T. Y., An energy model of plain knitted fabric, Textile Research Journal, 73(8), 739-748 (2003)

26. Choi, K. F. and Tandon, S. K., An energy model of yarn bending, J. Text. Inst., 97(1), 49-56 (2005)

27. Choi, K. F. and Wong, Y. W., Modeling of two-ply yarn torsional properties, Proceedings of the Society for Experimental Mechanics Annual Conference, Ohio USA, 1999, 623-625

28. Christensen, R. M., Mechanics of composite materials, John Wiley & Sons, New York (1979)

29. Cybulska, M. and Goswami, B. C., Tensile behaviour of staple yarns, Journal Of The Textile Institute, 92, 26-37 (2001)

30. deLazzer, A., Langbein, D., Dreyer, M. and Rath, H. J., Mean curvature of liquid surfaces in cylindrical containers of arbitrary cross-section, Microgravity Science And Technology, 9(3), 208-219 (1996)

31. Deng, J. L., Zhu, Y. D., Wang, J. H. and Meng, Z. H., Numerical simulation of micro-infiltration in a fiber bundle, Composite Materials Iii, 249, 347-350 (2003)

32. Dhingra, R. C. and Postle, R., Measurement of torque in continuous-filament yarns.1. Experimental techniques, Journal Of The Textile Institute, 65(3), 126-132 (1974a)

33. Dhingra, R. C. and Postle, R., Measurement of torque in continuous-filament yarns.2. Effect of yarn tension, J. Text. Inst., 65(4), 171-181 (1974b)

34. Dhingra, R. C. and Postle, R., Torsional and recovery properties of worsted yarns, J. Text. Inst., 12, 407-412 (1975)

35. Djaja, R. G., Finite element modeling of fibrous assemblies, Master of Engineering Thesis, University of Canterbury, New Zealand, (1989)

36. Dong, M. and Chatzis, I., The imbibition and flow of a wetting liquid along the corners of a square capillary-tube, Journal Of Colloid And Interface Science, 172(2), 278-288 (1995)

37. Earland, C., Wool: Its chemestry and physics, 2, Chapman & Hall Ltd, London (1963)

38. Erickson, D., Li, D. and Park, C. B., Numerical simulations of capillary-driven flows in nonuniform cross-sectional capillaries, Journal Of Colloid And Interface Science, 250(2), 422-430 (2002)

39. Gauvin, W. H. and Katta, S., Momentum-transfer through packed-beds of various particles in turbulent-flow regime, Aiche Journal, 19(4), 775-783 (1973)

40. Gegauff, C. M., Strength and elasticity of cotton threads, Bull. Soc. Industr. Mulhouse, 77, 153-176 (1907)

41. Ghali, A., Heat and mass transfer in highly porous media, Doctoral dissertation, Kansas State University, Manhattan, KS (1992)

42. Ghali, K., Jones, B. and Tracy, J., Experimental-techniques for measuring parameters describing wetting and wicking in fabrics, Textile Research Journal, 64(2), 106-111 (1994)

43. Ghosh, A., Ishtiaque, S. and Rengasamy, S., Predictive models for strength of spun yarns: An overview, Autex Research Journal, 5(1), 20-29 (2005)

44. Gooijer, H., Warmoeskerken, M. and Wassink, J. G., Flow resistance of textile materials - part i: Monofilament fabrics, Textile Research Journal, 73(5), 437-443 (2003a)

45. Gooijer, H., Warmoeskerken, M. and Wassink, J. G., Flow resistance of textile materials part ii: Multifilament fabrics, Textile Research Journal, 73(6), 480-484 (2003b)

46. Gregory, J., Cotton yarn structure part i-macro yarn structure, J. Text. Inst., 41, T1-13 (1950a)

47. Gregory, J., Cotton yarn structure part ii-the preparation and strength testing of artificial yarn elements, J. Text. Inst., 41, T14-29 (1950b)

48. Gregory, J., Cotton yarn structure part iii-the strength of artificial yarn elements in relation to bulk and twist, J. Text. Inst., 41, T30-52 (1950c)

49. Gregory, J., Cotton yarn structure part iv-the strength of twisted yarn elements in relation to the properties of the constituent fibers, J. Text. Inst., 44, T499-514 (1953a)

50. Gregory, J., Cotton yarn structure part v-the relation between strength measurements made on fibers, fiber bundles, yarns, and cloth, J. Text. Inst., 44, T515-533 (1953b)

51. Griesser, M. T. and Taylor, P. M., The bending behaviour of fabrics: An energy approach, Mathematics And Computers In Simulation, 41(5-6), 579-586 (1996)

52. Griffin, P. R., Grove, S. M., Russell, P., Short, D., Summerscales, J., Guild, F. J. and Taylor, E., The effect of reinforcement architecture on the long-range flow in fibrous reinforcements, Composites Manufacturing, 6(3-4), 221-235 (1995)

53. Gurney, H. P., The distribution of stress in cotton products, J. Text. Inst., 16, T269 (1925)

54. Hagen, G., Ann. Phys. Chem., 46, 423-442 (1839)

55. Hamdaoui, M., Fayala, F. and Ben Nasrallah, S., Experimental apparatus and mathematical model for determination of parameters of capillary rise in fabrics, Journal Of Porous Media, 9(4), 381-392 (2006)

56. Hamdaoui, M., Fayala, F. and Ben Nasrallah, S., Dynamics of capillary rise in yarns: Influence of fiber and liquid characteristics, Journal Of Applied Polymer Science, 104(5), 3050-3056 (2007)

57. Hamraoui, A. and Nylander, T., Analytical approach for the lucas-washburn equation, Journal of Colloid and Interface Science, 250, 415-421 (2002)

58. Hearle, J. W. S., The mechanics of twisted yarns: The influence of transverse forces on tensile behavior, J. Text. Inst., 49, T389-408 (1958)

59. Hearle, J. W. S., The mechanics of twisted yarns: Tensile properties of continuous-filament yarns, J. Text. Inst., 50, T83-108 (1959)

60. Hearle, J. W. S., The mechanics of twisted yarns: Further studies of the tensile properties of continuous-filament yarns, J. Text. Inst., 51(8), T299-316 (1960)

61. Hearle, J. W. S., Theoretical analysis of the mechanics of twisted staple fiber yarns, Text. Res. J., 1060-1071 (1965)

62. Hearle, J. W. S., On the theory of the mechanics of twisted yarns, J. Text. Inst., 95-101 (1969)

63. Hearle, J. W. S. and Bose, O. N., Migration of fibers in yarns, part ii: A geometrical explanation of migration, Text. Res. J., 35, 693-699 (1965)

64. Hearle, J. W. S., El-Behery, H. M. A. E. and Thakur, V. M., The mechanics of twisted yarns: Theoretical developments, J. Text. Inst., 52(5), T197-220 (1961)

65. Hearle, J. W. S., Grosberg, P. and Backer, S., Structural mechanics of fibers, yarns, and fabrics, Wiley Interscience, New York (1969)

66. Hearle, J. W. S. and Gupta, B. S., Migration of fibers in yarns, part iii: A study of migration in a staple fiber rayon yarn, Text. Res. J., 35, 788-795 (1965)

67. Hearle, J. W. S., Gupta, B. S. and Merchant, V. B., Migration of fibers in yarns, part i: Characterization and idealization of behavior, Text. Res. J., 35, 329-334 (1965)

68. Hearle, J. W. S., Lord, R. P. and Senturk, N., Fiber migration in open end spun yarns, J. Text. Inst., 63, T605 (1972)

69. Hearle, J. W. S., Potluri, P. and Thammandra, V. S., Modelling fabric mechanics, Journal Of The Textile Institute, 92, 53-69 (2001)

70. Hearle, J. W. S. and Shanahan, W. J., Energy method for calculations in fabric mechanics.1. Principles of method, Journal Of The Textile Institute, 69(4), 81-91 (1978)

71. Hollies, N. R. S., Kaessinger, M. M. and Bogaty, H., Water transport mechanisms in textile materials part i: The role of yarn roughness in capillary-type penetration, Text. Res. J., 829-835 (1956)

72. Hollies, N. R. S., Kaessinger, M. M., Watson, B. S. and Bogaty, H., Water transport mechanisms in textile materials part ii: Capillary-type penetration in yarns and fabrics, Text. Res. J., 8-13 (1957)

73. Hsieh, Y. L., Liquid transport in fabric structures, Text. Res. J., 65(5), 299-307 (1995)

74. Hsieh, Y. L. and Yu, B. L., Liquid wetting, transport, and retention properties of fibrous assemblies.1. Water wetting properties of woven fabrics and their constituent single fibers, Textile Research Journal, 62(11), 677-685 (1992)

75. Hsieh, Y. L., Yu, B. L. and Hartzell, M. M., Liquid wetting, transport, and retention properties of fibrous assemblies.2. Water wetting and retention of 100-percent and blended woven fabrics, Textile Research Journal, 62(12), 697-704 (1992)

76. Hyvaluoma, J., Raiskinmaki, P., Jasberg, A., Koponen, A., Kataja, M. and Timonen, J., Simulation of liquid penetration in paper, Physical Review E, 73(3) (2006)

77. Ichikawa, N., Hosokawa, K. and Maeda, R., Interface motion of capillary-driven flow in rectangular microchannel, Journal Of Colloid And Interface Science, 280(1), 155-164 (2004)

78. Ichikawa, N. and Satoda, Y., Interface dynamics of capillary-flow in a tube under negligible gravity condition, Journal Of Colloid And Interface Science, 162(2), 350-355 (1994)

79. Jenkins, L. M. and Donald, A. M., Observing fibers swelling in water with an environmental scanning electron microscope, Textile Research Journal, 70(3), 269-276 (2000)

80. Jiang, X. Y., Hu, J. L. and Postle, R., A new tensile model for rotor spun yarns, Textile Research Journal, 72(10), 892-898 (2002)

81. Joos, P., Vanremoortere, P. and Bracke, M., The kinetics of wetting in a capillary, Journal Of Colloid And Interface Science, 136(1), 189-197 (1990)

82. Kamath, Y. K., Hornby, S. B., Weigmann, H.-D. and Wilde, M. F., Wicking of spin finishes and related liquids into continuous filament yarns, Text. Res. J., 64(1), 33-40 (1994)

83. Karoglou, M., Moropoulou, A., Giakoumaki, A. and Krokida, M. K., Capillary rise kinetics of some building materials, Journal of Colloid and Interface Science, 284, 260-264 (2005)

84. Kim, E. and Whitesides, G. M., Imbibition and flow of wetting liquids in noncircular capillaries, Journal Of Physical Chemistry B, 101(6), 855-863 (1997)

85. Kissa, E., Wetting and wicking, Text. Res. J., 66(10), 660-668 (1996)

86. Komori, T. and Itoh, M., Theory of the general deformation of fiber assemblies, Textile Research Journal, 61(10), 588-594 (1991)

87. Kozeny, J., Uber kapillare leitung des wassers im boden, Sitzung Akademie der Wissenschaft, 136, 271-306 (1927)

88. Lago, M. and Araujo, M., Threshold capillary pressure in capillaries with curved sides, Physica A-Statistical Mechanics And Its Applications, 319, 175-187 (2003)

89. Leaf, G. A. V., The friction couple in yarn bending, Journal Of The Textile Institute, 86(1), 45-54 (1995)

90. Levine, S., Lowndes, J., Watson, E. J. and Neale, G., Theory of capillary rise of a liquid in a vertical cylindrical tube and in a parallel-plate channel - washburn equation modified to account for the meniscus with slippage at the contact line, Journal Of Colloid And Interface Science, 73(1), 136-151 (1980)

91. Liao, K. H. and Scheideg.Ae, Statistical models of flow through porous media, Pure And Applied Geophysics, 83(6), 74-& (1970)

92. Lin, L. and Jorge, H. R., Analysis and modeling of wicking through carton liquid packaging, Analytica Chimica Acta, 552, 218-225 (2005)

93. Liu, T., Choi, K. F. and Li, Y., Capillary rise between cylinders, J. Phys. D: Appl. Phys., 40, 5006-5012 (2007a)

94. Liu, T., Choi, K. F. and Li, Y., Mechanical modeling of singles yarn, Textile Research Journal, 77(3), 123-130 (2007b)

95. Love, A. E. H., A treatise on the mathematical theory of elasticity, 4th Edition, Dover Publication, New York, NY (1944)

96. Lucas, R., Ueber das zeitgesetz des kapillaren aufstiegs von flussigkeiten, Kolloid Z., 23, 15 (1918)

97. Lukas, D. and Chaloupek, J., Wetting between parallel fibres; column-unduloid and column disintegration transitions, Proceedings Of The Institution Of Mechanical Engineers Part H-Journal Of Engineering In Medicine, 217(H4), 273-277 (2003)

98. Lukas, D., Chaloupek, J., Kost'akova, E., Pan, N. and Martinkova, I., Morphological transitions of capillary rise in a bundle of two and three solid parallel cylinders, Physica A-Statistical Mechanics And Its Applications, 371(2), 226-248 (2006)

99. Lukas, D. and Pan, N., Wetting of a fiber bundle in fibrous structures, Polymer Composites, 24(3), 314-322 (2003)

100. Lukas, D., Soukupova, V., Pan, N. and Parikh, D. V., Computer simulation of 3-d liquid transport in fibrous materials, Simulation-Transactions Of The Society For Modeling And Simulation International, 80(11), 547-557 (2004)

101. Ly, N. G. and Denby, E. F., Bending rigidity and hysteresis of wool worsted yarn, Textile Research Journal, 54(3), 180-187 (1984)

102. Marmur, A. and Cohen, R. D., Characterization of porous media by the kinetics of liquid penetration: The vertical capillaries model, Journal of Colloid and Interface Science, 189, 299-304 (1997)

103. Masliyah, J. H. and Epstein, N., Numerical study of steady flow past spheroids, Journal Of Fluid Mechanics, 44(NOV26), 493-& (1970)

104. Mason, G. and Morrow, N. R., Capillary behavior of a perfectly wetting liquid in irregular triangular tubes, Journal Of Colloid And Interface Science, 141(1), 262-274 (1991)

105. Minor, F. W., Schwartz, A. W., Wulkow, E. A. and Buckles, L. C., The migration of liquids in textile assemblies part ii: The wicking of liquids in yarns, Text. Res. J., XXIX(12), 931-939 (1959)

106. Munro, W. A., Carnaby, G. A., Carr, A. J. and Moss, P. J., Some textile applications of finite-element analysis - part i: Finite elements for aligned fibre assemblies, Journal Of The Textile Institute, 88(4), 325-338 (1997a)

107. Munro, W. A., Carnaby, G. A., Carr, A. J. and Moss, P. J., Some textile applications of finite-element analysis - part ii: Finite elements for yarn mechanics, Journal Of The Textile Institute, 88(4), 339-351 (1997b)

108. Neckar, B. and Ibrahim, S., Theoretical approach for determining pore characteristics between fibers, Textile Research Journal, 73(7), 611-619 (2003)

109. Nguyen, H. V. and Durso, D. F., Absorption of water by fiber webs: An illustration of the diffusion-type transport, TAPPI Proceeding, International Dissolving and Specially Pulps Conference, Boston, MA, 1983, 137-141

110. Nyoni, A. B. and Brook, D., Wicking mechanisms in yarns-the key to fabric wicking performance, Journal of Textile Institute, 97(2), 119-128 (2006)

111. Pan, N., Development of a constitutive theory for short fiber yarns - mechanics of staple yarn without slippage effect, Textile Research Journal, 62(12), 749-765 (1992)

112. Pan, N., Development of a constitutive theory for short-fiber yarns - mechanics of staple yarn without slippage effect (vol 62, pg 749, 1992), Textile Research Journal, 63(6), 370-370 (1993)

113. Pan, N. and Brookstein, D., Physical properties of twisted structures. Ii. Industrial yarns, cords, and ropes, Journal Of Applied Polymer Science, 83(3), 610-630 (2002)

114. Park, J. W. and Oh, A. G., Bending mechanics of ply yarns, Text. Res. J., 73(6), 473-479 (2003)

115. Patnaik, A., Rengasamy, R. S., Kothari, V. K. and Ghosh, A., Wetting and wicking in fibrous materials, Textile Progress, 1-105 (2006)

116. Patzek, T. W. and Silin, D. B., Shape factor and hydraulic conductance in noncircular capillaries i. One-phase creeping flow, Journal Of Colloid And Interface Science, 236(2), 295-304 (2001)

117. Perwuelz, A., Casetta, M. and Caze, C., Liquid organisation during capillary rise in yarns-influence of yarn torsion, Polymer Testing, 20, 553-561 (2001)

118. Perwuelz, A., Mondon, P. and Caze, C., Experimental study of capillary flow in yarns, Text. Res. J., 70(4), 333-339 (2000)

119. Pezron, I., Bourgain, G. and Quere, D., Imbibition of a fabric, Journal Of Colloid And Interface Science, 173(2), 319-327 (1995)

120. Pierlot, A. P., Water in wool, Textile Research Journal, 69(2), 97-103 (1999)

121. Pillai, K. M. and Advani, S. G., Wicking across a fiber-bank, Journal Of Colloid And Interface Science, 183(1), 100-110 (1996)

122. Platt, M. M., Mechanics of elastic performance of textile materials, part iii. Some aspects of stress analysis of textile structures-continuous-filament yarns, Text. Res. J., 20, 1-15 (1950a)

123. Platt, M. M., Mechanics of elastic performance of textile materials, part iv. Some aspects of stress analysis of textile structures-staple fiber yarns, Text. Res. J., 20, 519 (1950b)

124. Platt, M. M., Klein, W. G. and Hamburger, W. J., Mechanics of elastic performance of textile materials, part xiii, Text. Res. J., 28, 1-14 (1958)

125. Platt, M. M., Klein, W. G. and Hamburger, W. J., Mechanics of elastic performance of textile materials, part xiv. Some aspects of bending rigidity of singles yarn, Text. Res. J., 29, 611-627 (1959)

126. Poiseuille, J. L., C. R. Acad. Sci. Paris, 11, 961 (1840)

127. Postle, R., Burton, P. and Chaikin, M., The torque in twisted yarn, J. Text. Inst., 55, T448 (1964)

128. Postle, R., Carnaby, G. A. and Jong, S. d., The mechanics of wool structures, Ellis Horwood Limited, Chichester, England (1988)

129. Princen, H. M., Capillary phenomena in assemblies of parallel cylinders i. Capillary rise between two cylinders, Journal of Colloid and Interface Science, 30(1), 69-75 (1968)

130. Princen, H. M., Capillary phenomena in assemblies of parallel cylinders ii. Capillary rise in systems with more than two cylinders, Journal of Colloid and Interface Science, 30(3), 359-371 (1969)

131. Princen, H. M., Capillary phenomena in assemblies of parallel cylinders iii. Liquid columns between horizontal parallel cylinders, Journal Of Colloid And Interface Science, 34(2), 171-184 (1970)

132. Rahli, O., Tadrist, L., Miscevic, M. and Santini, R., Fluid flow through randomly packed monodisperse fibers: The kozeny-carman parameter analysis, J. Fluid Eng., Trans. ASME, 119, 188-192 (1997)

133. Rao, Y. Q. and Farris, R. J., A modeling and experimental study of the influence of twist on the mechanical properties of high-performance fiber yarns, Journal Of Applied Polymer Science, 77(9), 1938-1949 (2000)

134. Rebenfeld, L. and Miller, B., Using liquid flow to quantify the pore structure of fibrous materials, Journal Of The Textile Institute, 86(2), 241-251 (1995)

135. Reed, C. M. and Wilson, N., The fundamentals of absorbency of fibers, textile structures and polymers i: The rate of rise of a liquid in glass capillaries, J. Phys. D: Appl. Phys., 26, 1378-1381 (1993)

136. Richards, T. H., Energy methods in stress analysis: With an introduction to finite element techniques, Ellis Horwood Limited, Birmingham (1977)

137. Riding, G., An experimental study of the geometrical structure of single yarns, J. Text. Inst., 50, T425 (1959)

138. Riding, G., The stress-strain properties of multi-ply cords part ii. Experimental, J. Text. Inst., 56, T489 (1965)

139. Sagar, T. V. and Potluri, P., Computation of bending behavior of woven structures using optimization techniques, Textile Research Journal, 74(10), 879-886 (2004)

140. Scheidegger, A. E., The physics of flow through porous medis, 3rd, University of Toronto Press (1974)

141. Shanahan, W. J. and Hearle, J. W. S., Energy method for calculations in fabric mechanics.2. Examples of application of method to woven fabrics, Journal Of The Textile Institute, 69(4), 92-100 (1978)

142. Shao, X., Theoretical modeling of the tensile behavior of staple yarn, PhD Thesis, Georgia Institute of Technology, USA (2002)

143. Shao, X., Qiu, Y. and Wang, Y., Theoretical modeling of the tensile behavior of low-twist staple yarns: Part i- theoretical model, Journal of Textile Institute, 96(2), 61-68 (2005a)

144. Shao, X., Qiu, Y. and Wang, Y., Theoretical modeling of the tensile behavior of low-twist staple yarns: Part ii-theoretical and experimental results, Journal of Textile Institute, 96(2), 69-76 (2005b)

145. Siebold, A., Nardin, M., Schultz, J., Walliser, A. and Oppliger, M., Effect of dynamic contact angle on capillary rise phenomena, Colloids And Surfaces A-Physicochemical And Engineering Aspects, 161(1), 81-87 (2000)

146. Stange, M., Dreyer, M. E. and Rath, H. J., Capillary driven flow in circular cylindrical tubes, Physics Of Fluids, 15(9), 2587-2601 (2003)

147. Stansfield, G. J., The geometry of twisted multi-filament structures, British Journal of Applied Physics, 9, 133-139 (1958)

148. Staples, T. L. and Shaffer, D. G., Wicking flow in irregular capillaries, Colloids And Surfaces A-Physicochemical And Engineering Aspects, 204(1-3), 239-250 (2002)

149. Sullivan, R. R., A theoretical approach to the problem of yarn strength, J. Appl. Phys., 13, 157 (1942)

150. Tandon, S. K., Carnaby, G. A., Kim, S. J. and Choi, F. K. F., The torsional behavior of singles yarns part i: Theory, J. Text. Inst., 86(2), 185-199 (1995a)

151. Tandon, S. K., Kim, S. J. and Choi, F. K. F., The torsional behavior of singles yarns part ii: Evaluation, J. Text. Inst., 86(2), 185-199 (1995b)

152. Tao, X. M., The bending properties of multi-ply worsted yarns, International Journal of Clothing Science and Technology, 6(2/3), 65-72 (1994)

153. Treloar, L. R. G., The geometry of multi-ply yarns, J. Text. Inst., 47, T348 (1956)

154. Treloar, L. R. G., The stress-strain properties of multi-ply cords part i. Theory, J. Text. Inst., 56, T477 (1965)

155. Treloar, L. R. G., Physics of textiles, Physics Today, 30(12), 23-30 (1977)

156. Treloar, L. R. G. and Riding, G., A theory of the stress-strain properties of continuous-filament yarns, J. Text. Inst., 54, T156 (1963)

157. Turian, R. M. and Kessler, F. D., Capillary flow in a noncircular tube, Aiche Journal, 46(4), 695-706 (2000)

158. Underwood, P., Computational methods for transient analysis, T. Belytschko and T. R. Hughes, North Holland (1983)

159. Van Luijk, C. J., The structural analysis of wool yarns, PhD Thesis, University of Canterbury, New Zealand (1981)

160. Van Luijk, C. J., Carr, A. J. and Carnaby, G. A., J. Text. Inst., 75, 354-362 (1984)

161. Van Luijk, C. J., Carr, A. J. and Carnaby, G. A., J. Text. Inst., 76, 11-29 (1985)

162. van Mourik, S., Veldman, A. E. P. and Dreyer, M. E., Simulation of capillary flow with a dynamic contact angle, Microgravity Science And Technology, 17(3), 87-94 (2005)

163. VanLangenhove, L., Simulating the mechanical properties of a yarn based on the properties and arrangement of its fibers.1. The finite element model, Textile Research Journal, 67(4), 263-268 (1997a)

164. VanLangenhove, L., Simulating the mechanical properties of a yarn based on the properties and arrangement of its fibers.2. Results of simulations, Textile Research Journal, 67(5), 342-347 (1997b)

165. VanLangenhove, L., Simulating the mechanical properties of a yarn based on the properties and arrangement of its fibers.3. Practical measurements, Textile Research Journal, 67(6), 406-412 (1997c)

166. Washburn, E. W., The dynamics of capillary flow, Physical Review, 17(3), 273-283 (1921)

167. Weislogel, M. M. and Lichter, S., Capillary flow in an interior corner, Journal Of Fluid Mechanics, 373, 349-378 (1998)

168. Xiao, Y., Yang, F. Z. and Pitchumani, R., A generalized analysis of capillary flows in channels, Journal Of Colloid And Interface Science, 298(2), 880-888 (2006)

169. Young, W. B., Analysis of capillary flows in non-uniform cross-sectional capillaries, Colloids And Surfaces A-Physicochemical And Engineering Aspects, 234(1-3), 123-128 (2004a)

170. Young, W. B., Capillary impregnation into cylinder banks, Journal Of Colloid And Interface Science, 273(2), 576-580 (2004b)

171. Zhao, B., Moore, J. S. and Beebe, D. J., Surface-directed liquid flow inside microchannels, Science, 291(5506), 1023-1026 (2001)

172. Zhmud, B. V., Tiberg, F. and Hallstensson, K., Dynamics of capillary rise, Journal Of Colloid And Interface Science, 228(2), 263-269 (2000)

173. Zhong, W., Ding, X. and Tang, Z. L., Modeling and analyzing liquid wetting in fibrous assemblies, Textile Research Journal, 71(9), 762-766 (2001)

174. Zhong, W., Ding, X. and Tang, Z. L., Analysis of fluid flow through fibrous structures, Textile Research Journal, 72(9), 751-755 (2002)

175. Zhong, W. and Xing, M. Q., A stochastic model in liquid penetration through fibrous media, Journal of Colloid and Interface Science, 275, 264-269 (2004)

176. Zimliki, D. A., Kennedy, J. M., Hirt, D. E. and Reese, G. P., Determining mechanical properties of yarns and two-ply cords from single-filament data part i: Model development and predictions, Textile Research Journal, 70(11), 991-1004 (2000a)

177. Zimliki, D. A., Kennedy, J. M., Hirt, D. E. and Reese, G. P., Determining mechanical properties of yarns and two-ply cords from single-filament data part ii: Comparing model and experimental results for pet, Textile Research Journal, 70(12), 1097-1105 (2000b)